Optical methods for monitoring biological parameters of phototropic microorganisms during cultivation

A dissertation
submitted to the
Mathematics-Natural Science Faculty
of the University of Potsdam
in partial fulfillment of the
requirements for the degree of
Doctor of Natural Science

Universität Potsdam
Institut für Chemie
Physikalische Chemie

Christine Marie Frankovitch
Potsdam, June 2007

Acknowledgements

Throughout the last four years, there have been many who have helped me along the way. It is a pleasure to thank those who made this thesis possible.
It is difficult to properly express my gratitude to my Ph.D. supervisor, Prof. Dr. Hans-Gerd Löhmannsröben. The support, encouragement, scientific advice and motivation that he provided is indispensable.
I would also like to thank Dr. Oliver Reich for his attention, guidance, insight, and support during this research and the preparation of this thesis.
Many thanks to André Geßner and Sascha Eidner for always being available to answer LaTeX questions.
I am grateful to all members of the Löhmannsröben group for providing a superb working environment and for all of their support.
Thank you to The Institut für Lebensmittel- und Umweltforschung e.V., in Bergholz-Rehbrücke, Germany for the microalgae samples.
Lastly, and most importantly, I wish to thank my parents for their unconditional love and constant support. To them I dedicate this thesis.

List of Publications

C. Frankovitch, O. Reich, Hans-Gerd Löhmannsröben; "Investigation of Microalgae with Photon Density Waves" *Proceedings of SPIE - Optics for Natural Resources, Agriculture, and Foods*; **2007**; accepted for publication.

Poster Presentations

C. Frankovitch, O. Reich, Hans-Gerd Löhmannsröben; "Investigation of Microalgae with Photon Density Waves" *Tulip Summer School III*, Noordwijk, Netherlands; **2006**

C. Frankovitch, O. Reich, Hans-Gerd Löhmannsröben; "Intensity Modulated Diode Laser Spectroscopy for Bioprocess Observation" *WE-Heraeus-Summerschool "Physics of the Environment"*, Bad Honnef, Germany; **2005**

Table of Contents

Abstract

Phototropic microalgae have a large potential for producing valuable substances for the feed, food, cosmetics, pigment, bioremediation, and pharmacy industries as well as for biotechnological processes. Today it is estimated that the microalgal aquaculture worldwide production is 5000 tons of dry matter per year (not taking into account processed products) making it an approximately $1.25 billion U.S. per year industry. In this work, several spectroscopic techniques were utilized for the investigation of microalgae cells. Specifically, photondensity wave spectroscopy was applied as a technique for the on-line observation of the culture.

For effective evaluation of the photosynthetic growth processes, fast and non-invasive sensor systems that analyze the relevant biological and technical process parameters are preferred. Traditionally, the biomass in a photobioreactor is quantified with the help of turbidimetry measurements, which require extensive calibration. Another problem frequently encountered when using spectral analysis for investigating solutions is that samples of interest are often undiluted and highly scattering and do not adhere to Beer-Lambert's law.

Due to the fluorescence properties of chlorophyll, fluorescence spectroscopy techniques including fluorescence lifetime imaging and single photon counting could be applied to provide images of the cells as well as determine the effects of excitation intensity on the fluorescence lifetime, which is an indicator of the condition of the cell.

A photon density wave is a sinusoidally intensity-modulated optical wave stemming from a point-source of light, which propagates through diffuse medium and exhibits amplitude and phase variations. Light propagation though strongly scattering media can be described by the P_1 approximation to the Boltzmann transport equation. Photon density wave spectroscopy enables the ability to differentiate between scattered and absorbed light, which is desired so that an independent determination of the reduced scattering and absorption coefficients can be made. The absorption coefficient is related to the pigment content in the cells, and the reduced scattering coefficient can be used to characterize physical and morphological properties of the medium and was here applied for the determination of the average cell size.

Kurzzusammenfassung

Phototropische Mikroalgen besitzen ein großes Potential für die Herstellung von wertvollen Substanzen sowohl für die Futtermittel-, Lebensmittel-, kosmetische und pharmazeutische Industrie, als auch für die Farbstoffsynthese. Heutzutage werden schätzungsweise 5000 Tonnen Mikroalgen Trockensubstanz pro Jahr mit einem Jahresumsatz von 1,25 Mrd. US-Dollar produziert. In dieser Arbeit wurden diverse spektroskopische Untersuchungsmethoden für die Betrachtung der Zellen verwendet. Die Photonendichtewellenspektroskopie (PDW) fand dabei insbesondere bei der on-line Beobachtung der Zellen Anwendung.

Voraussetzungen für die effektive Beobachtung von photosynthetischen Wachstumsprozessen sind schnell und nicht-invasiv arbeitende Sensoren. Normalerweise wird die dabei zu untersuchende Biomasse in einem Photobioreaktor mittels Trübungsmessungen quantifiziert. Dies setzt jedoch eine sehr aufwendige Kalibration voraus. Da diese Proben zusätzlich meist in unverdünnter Form vorliegen, streuen sie stark und folgen daher nicht dem Lambert-Beer'schen Gesetz.

Aufgrund der Fluoreszenzeigenschaften des Chlorophylls können fluoreszenzspektroskopische Methoden wie fluorescence lifetime imaging microscopy (FLIM) und time correlated single photon counting (TCSPC) angwendet werden. Diese Methoden werden dabei für die visuelle Darstellung der Zellen und für die Messung der Fluoreszenzlebenszeit genutzt.

Eine Photondichtewelle ist eine sinusförmig intensitätsmodulierte optische Welle, die sich, ausgehend von einer punktförmigen Lichtquelle, durch das untersuchte Medium ausbreitet, wobei sich Phase und Amplitude der Welle verändern. Die Ausbreitung der Welle wird von der P_1-Näherung der Boltzmann-Transport-Gleichung beschrieben. Mittels PDW kann zwischen streuenden und absorbierenden Eigenschaften von trüben Probe unterschieden werden. Dies erlaubt die Absolutbestimmung des Absorptions- und reduzierten Streukoeffizienten, die für die Qualifizierung der Probe, insbesondere der Teilchengrößenbestimmung, herangezogen werden.

Chapter 1

Introduction

Fossil evidence shows that cyanobacteria have existed since the Precambrian age, about 2.5 Billion years ago [1]. They used water and hydrogen to drive photosynthesis and produced oxygen, providing the necessary component for other forms of life to develop. The first unicellular eukaryotes are thought to have arisen around 1.9 billion years ago and to have diversified greatly at around one billion years ago. With time, algae colonized the entire planet and today they can be found everywhere: primarily in marine environments such as the oceans, lakes and water tanks but also in geysers, ice, snow, high mountains, soil and in waste water. The term microalgae is the general term for all types of unicellular eukaryotic organisms belonging to several classes including Cyanophyceae, Chlorophyceae, Euglenophyceae, Xanthophyceae, Bacillariophyceae, and Rhodophyceae, and having different photosynthetic assimilatory pigments.

Interest in the phototropic microorganisms has been recently gaining momentum [2, 3, 4] leading these unicellular microorganisms to be exploited for many beneficial purposes including, but not limited to, animal feed [5], CO_2 fixation [6], pharmaceuticals [7], aquaculture [8], and human nutrition [9]. Microalgae produce various interesting metabolites such as polyunsaturated fatty acids, pigments (including chlorophyll, caroteniods, and phycobiliproteins), vitamins, and some sulfonized polysaccharides [10].

Although there is evidence that microalgae have been used as a food source for thousands of years [11], commercial cultivation success didn't follow until several decades ago in the early 1960's in Japan. Since then, there has been a rapid increase in the use of microalgae for uses including high-protein nutrition sources and supplements, antibiotic production, wastewater quality improvement, and renewable energy generation [12]. Today, it is estimated that the microalgal aquaculture worldwide production is

5000 tons of dry matter per year (not taking into account processed products) making it an approximately $1.25 billion U.S. per year industry [6].

Microalgae is the broad term used to describe all microscopic algae, cyanobacteria (also called blue-green algae) are usually considered separately because they are prokaryotic. Biotechnologically, the most important cyanobacteria include *Spirulina (Arthrospiria) platensis*, *Nostoc commune* and *Aphanizomenon flos-aquae*; likewise, *Chlorella*, *Chlamydomonas*, *Dunaliella* and *Heamatococcus* represent the best known Chlorophyta microalgae [6]. Both microalgae and cyanobacteria can be found all over the world in various ecosystems and are commercially produced in photobioreactors (PBR), which serve to supply light, required nutrients and carbon dioxide.

Since microalgae and cyanobacteria are oxygenic photoautotrophic microorganisms, they are able to metabolize carbon dioxide into carbohydrates and other organic compounds in the presence of light. This process of light driven biomass growth is called photosynthesis and can be generalized by Equation 1.1:

$$\mathrm{n\,CO_2} + 2\mathrm{n\,H_2O} \xrightarrow{h\nu} (\mathrm{CH_2O})_\mathrm{n} + \mathrm{n\,O_2} + \mathrm{n\,H_2O} \tag{1.1}$$

The biomass production process from microalgae generally requires a control action to maintain operating conditions in the optimal range, thus improving yield and productivity [13]. Biomass, or more specifically the biomass concentration, is the mass of the microorganisms per volume of cultivation broth. The real-time knowledge of relevant physical and chemical parameters is the basis of optimal process control. In bioprocesses involving cultivations, the biomass concentration is one of the most important parameters in biotechnology for both product synthesis and degradation of harmful substances [14].

The determination of biomass is usually performed via sampling of a defined volume of the cultivation broth, cell separation by centrifugation, washing the cells, and drying them at high temperatures to a constant weight. The drying process usually lasts about 24 hours, making this inappropriate for use as a real-time method. The cell concentration can also be directly measured from a cultivation broth by employing the use of a microscope and haematocytometer. In this method, the cells are directly counted under the microscope, requiring time and an experienced examiner, as there is a serious amount of subjectivity comprised in the results [15].

Process monitoring can, however, be filled by the application of an optical sensor system. Typically, simple turbidity probes are employed, which usually require exten-

sive calibration for determination of biomass because they detect light attenuation and cannot distinguish between absorbed and scattered light [16].

Visually opaque media are unusual in that some are considered opaque because they strongly absorb visible light. Others such as paint, foam, milk, and human tissue are optically opaque because the light traveling within them is highly scattered. In fact, a very small number of photons travel in straight lines through such materials. Instead, the photons incident within a thick material multiply scatter and trace out random paths until they are either absorbed, or they escape through the boundaries of the media. Media that cause photons to propagate through the material in such a manner are also referred to as turbid media.

A problem frequently encountered when using spectral analysis for investigating solutions is that samples of interest are often undiluted and highly scattering. For example, biological tissue, powders, or colloidal dispersions such as milk are all turbid. In these samples, quantification of analytes cannot rely on the Beer-Lambert relation, which is valid for media with a small concentration of dispersing material. As photons travel through the medium, they encounter scatterers and their direction of propagation is changed many times. Light can thus have a multitude of paths through the sample, making the path length term in Beer's law (see Equation 3.1) a statistical distribution instead of a known value and leading to erroneous results for media with a high concentration of scatterers. The applicability of Beer's law depends most notably on the optical path length employed, the size of the scattering and absorbing particles and on the refractive index of the solution [17]. Therefore, for the optical characterization of undiluted samples, alternate models are necessary that take both absorption and scattering into account.

Chlorophyll fluorescence has been studied since it was first observed by Hans Kautsky in 1931 [18]. Kautsky found that upon transferring photosynthetic material from the dark into the light, an increase in the yield of chlorophyll fluorescence occurred over a time period of around one second. Since then, chlorophyll fluorescence has been used as an indication of the photoactivation process [19] and to study the structure of the photosynthetic systems [20]. Many review articles have been written pertaining to chlorophyll a fluorescence, and fluorescence lifetime (for example [18, 19, 21, 22]), these articles summarize the complexity and controversy of the data interpretation. Reported fluorescence lifetimes vary between the pico-second range and 10 nano-seconds, and have been shown to depend on excitation intensity and temperature.

Because of the fluorescence characteristics of many of the pigments contained in

microalgae, fluorescence analysis has been used to discriminate microalgae [23] and as a measurement of the photosynthetic state in microalgae samples [24]. Chlorophyll fluorescence, however, provides information about the photosynthetic process, which can lead to information about culture health. Many studies have also been published on the application of culture fluorescence as it applies to biomass (for example [25, 26, 27, 28]). The problem with using culture fluorescence as an indicator of biomass is that one has to make sure that no metabolic alterations are taking place, which is only the case during the exponential growth phase [27].

The intention of this study is to provide an investigation into the optical characteristics of microalgae and to examine the prospect of using frequency domain photon density wave (PDW) spectroscopy as an on-line method for providing information about the condition of the microalgae culture in a photobioreactor during cultivation. When the intensity of a point source in a turbid medium with uniform optical properties is sinusoidally modulated, a macroscopic wave of photon density develops, and propagates outward from the source. These waves have a well-defined phase and amplitude at every point in the diffusive medium [29] and are analyzed by a phase sensitive detector system which measures the detected light intensity and phase shift of the scattered wave. Analysis with frequency domain photon density waves allows for the examination of absorption and scattering properties of turbid media [30].

Photon migration studies have been employed for non-invasive optical analysis for a variety of medical applications including the identification of tumors in turbid media [31], for monitoring the physiological state of tissue [32] and to investigate malignant tissue in humans [33]. However, little information is available on the application of PDW spectroscopy for the observation of the growth process in a bioreactor.

PDW spectroscopy consists of launching sinusoidally modulated light into a scattering medium at a single point source and detecting the modulated light at another point some distance away from the source. The photon density wave is attenuated and phase-shifted relative to the incident signal as it propagates through the scattering medium due to the scattering and absorption properties of the medium. The intensity propagation of the modulated light can be described by the P_1 approximation to the Boltzmann transport equation, which describes the transport of light in turbid media.

For PDW studies in this work, a spectrometer was constructed with an intensity modulated diode laser as the light source, quartz optic fibers serving as the source and detection fibers and a network analyzer capable of a modulation frequencies from 0.3 MHz up to 1.3 GHz. Intensity and phase data were collected at varying source and

detector separations in order to make an independent determination of the scattering and absorption properties of the microalgae culture.

Throughout this study, several different processes were applied to investigate the optical properties of microalgae, specifically unicellular photosynthetic eukaryotes *Chlorella vulgaris* and *Nannochloropsis oculata*. In the following chapter, an introduction to microalgae, microalgal cultivation, and photobioreactors is given. Subsequently, the theoretical background relevant to the processes employed here, including UV/Vis spectroscopy, fluorescence lifetime imaging spectroscopy, time correlated single photon counting, dynamic light scattering and photon density wave spectroscopy is presented. Finally the results of the optical investigations will be presented and discussed.

Chapter 2

Microalgae

Algae refers to a large and diverse group of eukaryotic organisms that contain chlorophyll and carry out photosynthesis. Traditionally included under the term algae are green, red and brown algae, charophytes, cryptophytes, chrysophytes, diatoms, dinoflagellates, and others encompassing photosynthetic prokaryotic and eukaryotic organisms [34]. Major groups of algae are classified into ten divisions on the basis of pigmentation, the chemical nature of the photosynthetic storage product, thylakoid organization and other ultrastructural features of the chloroplast, the chemistry and structure of the cell wall, the number, arrangement, and ultrastructure of the flagella (if any), and the occurrence of any special features [35]. Algae are either colonial or unicellular, the latter referred to as microalgae and are the focus of this study. Because microalgae can be cultivated in varying culture media and environments, the chemical composition can also vary over a wide range.

2.1 Chemical Composition

The chemical composition of microalgae is not always constant and can be influenced by a variety of factors including cultivation temperature, pH, illumination, minerals and nutrients present in cultivation medium and CO_2 supply [10]. Proteins, vitamins, pigments, and pharmaceutical compounds can be extracted from microalgae, and the culture medium can be manipulated in order to obtain the optimal composition of the desired product. Table 2.1 summarizes the gross chemical composition (percentage of dry matter) for various types of microalgae compared with that of some traditional food sources [10, 36].

Microalgae vary appreciably in their biological compositions, depending on species, growth conditions, culture media, and growth phase [37]. Furthermore, nutritional

Source	Protein	Carbohydrate	Lipids	Nucleic Acid
Chlorella vulgaris	51 – 58	12 – 17	14 – 22	4 – 5
Dunaliella salina	57	32	6	–
Spirulina platensis	46 – 63	8 – 14	4 – 9	2 – 5
Nannochloropsis oculata	41 – 44	2 – 4	22 – 35	–
Egg	47	4	41	–
Milk	26	38	28	–
Soya	37	30	20	–

Table 2.1: Chemical Composition (% dry matter) of traditional food sources and different microalgae [10, 36].

value of microalgae is influenced by their size, shape, digestibility and biochemical composition [38].

Some species of microalgae have also been the sources of many studies of anticancer natural products and have been shown to function in the inhibition of tumor cell growth [39, 40]. The addition of *Chlorella* species to chicken feed has also been shown to increase weight at slaughter, lower cholesterol and pose no added risk to humans [41]. Besides having a high concentration of protein, carbohydrates, lipids and nucleic acids, microalgae also contain small amounts of hydrocarbons, glycerol, and represent a valuable source of nearly all essential vitamins including A, B_1, B_2, B_6, B_{12}, C, E, biotin and folic acid. It should also be noted that microalgae can also contain toxins and heavy metal compounds and should therefore be analyzed for the presence of potentially toxic substances prior to commercialization [42].

Table 2.2 offers a summary of various products that are able to be extracted from microalgae and their applications [4, 43, 44, 45].

2.1.1 Pigment Content

All photosynthetic organisms contain one or more organic pigments capable of absorbing visible radiation that will initiate the photochemical reactions of photosynthesis. Chlorophyll and other accessory pigments that absorb energy and transfer it to the chlorophyll make up the photosynthetic unit which initiates the flow of electrons.

Although overall five different type of chlorophyll have been identified, chlorophyll-a, shown in Figure 2.1, is the primary photosynthetic pigment in all algae and the only one found in cyanobacteria. The photosynthetic unit consists of about 500 chlorophyll molecules [46]. Total chlorophyll content usually makes up approximately $0.5 - 1.5$

	Product	**Applications**
Biomass	Biomass	Health food Functional food Feed additive Aquaculture Soil Conditioner
Coloring substances & Antioxidants	Xantophylls Letein β-catorene Vitamins A & C	Food & feed additives Cosmetics
Fatty acids	Arachindonic acid Eicosapentaenoic acid Docosahexanoic acid γ-Linolenic acid Linoleic acid	Food additive
Enzymes	Superoxide dismutase Phosphoglycerate kinase Luciferace and Luciferin Restriction enzymes	Health food Research Medicine
Polymers	Polysaccharides Starch Poly-β-hydroxybutric acid	Food additive Cosmetics Medicine
Special products	Peptides Toxins Amino acids (proline, arginine, aspartic acid) Sterols	Research Medicine

Table 2.2: Microalgae products and their applications.

% of the cell's dry weight [10]. Temperature effects on the chlorophyll content per cell in *C. vulgaris* have been studied and it has been shown to vary six fold between cultivation temperatures of 5°C and 27°C [47].

Microalgae also contain carotenoids, which are yellow, orange, or red pigments that are vital to the photosynthetic process. Several of the more than 600 types of carotenoids have photoprotective functions, shielding the chlorophyll from bleaching and destruction by extreme radiation or oxygen [48]. They function both as light harvesting pigments by absorbing in regions of the visible spectrum where chlorophyll does not and funneling excitation energy to chlorophyll, and as fluorescence quenchers by dissipating excess photon energy absorbed by the chlorophyll harmlessly as heat. Carotenoids are situated in the chloroplast lamellae, bound to proteins, in close prox-

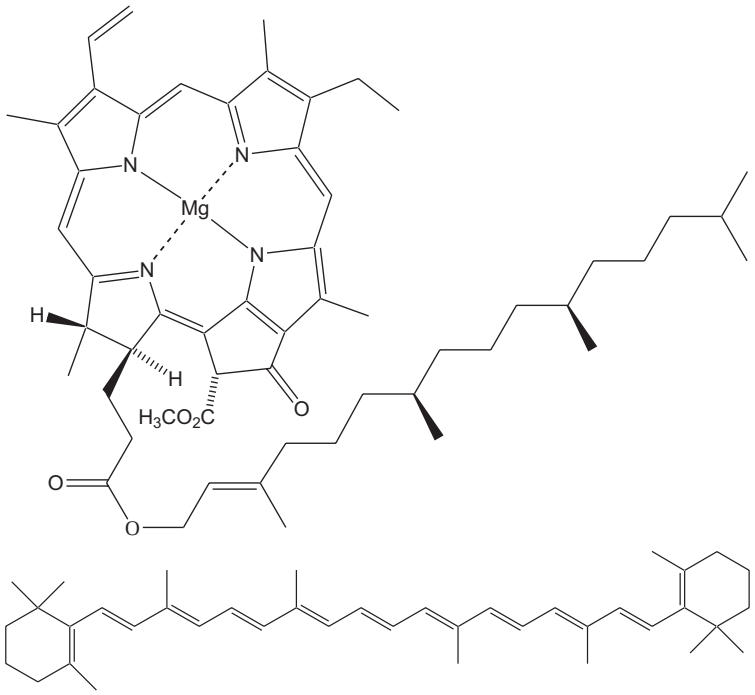

Figure 2.1: Chemical structures of Chlorophyll-*a* (top) and *trans*-β-Carotene (bottom).

imity to the chlorophyll [46].

The average concentration of all carotenoids found in algae is $0.2 - 2$ % of the dry weight [10]. β-carotene (chemical structure in Figure 2.1) has known intrinsic anti-inflammatory properties and a therapeutic anti-cancer effect is sometimes attributed to these molecules [10], however, no *in vitro* or *in vivo* investigations have demonstrated this effect [49].

Other pigments found in microalgae that have commercial importance include lycopene, zeaxanthin, astaxanthin, and lutein. These pigments are used in the cosmetic, aquaculture, health food and suntan lotion industries [6]. The absolute concentration of chlorophyll, β-carotene, and all other pigments and cell components is subject to variation depending on growth media, cultivation temperature, available photosynthetically active radiation, pH, etc...

Other components which make up microalgae cells include: waxes, hydrocarbons, glycerol, and phycobiliproteins. Phycobiliproteins are pigments which are used as natural dyes in the food, drug and cosmetic industry and as highly sensitive fluorescent reagents in diagnostic tests and for labeling antibodies. The amount present in each cell depends on the species of the cells and growth conditions.

A considerable diversity exists among the carotenoid and chlorophyll pigments. The

different divisions of microalgae are characterized in part by a specific pigment composition [50]. Figure 2.2 shows a schematic diagram of a cross-section of a *N. oculata* cell and a *C. vulgaris* cell. *N. oculata* belongs to the Heterokontophyta Eustigmatophyceae phylum and class of algae, respectively, and *C. vulgaris* belongs to the Chlorophyta Chlorophyceae phylum and class, respectively. Both types of microalgae were investigated in this study.

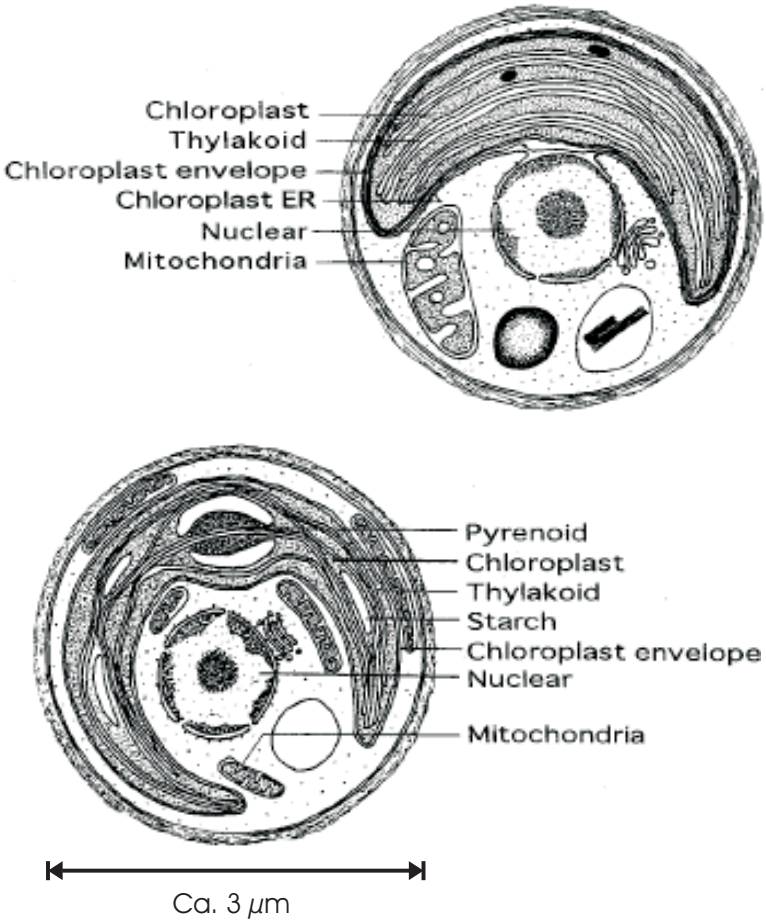

Figure 2.2: Cross-section of a *N. oculata* cell (top) and *C. vulgaris* (bottom). From [5].

Noteworthy characteristics of algae belonging to the Eustigmatophyceae class include: all species are unicellular and cocciod, chlorophyll presence is limited to chlorophyll a, and both fresh and marine water species can belong to this class. Chlorophyceae, on the other hand, includes essentially all green algae, which are found almost exclusively in fresh water. Members of this class can be uni- or multi-cellular and contain both chlorophyll a and b.

2.2 Nutrition and the Growth Cycle

The mineral nutrition requirements of algae do not differ from those of other plants. The rate of microalgal and cyanobacterial growth is dependent on light, water, nutrients, and CO_2 in the system. Nutrient requirements can broadly be classified as macronutrients and micronutrients. Macronutrients are those that are required in larger quantities such as carbon, oxygen, hydrogen, nitrogen, phosphorus, potassium and sulfur. Micronutrients (or trace elements) are those which are required in much smaller quantities but play an important role in proper cell function like chlorine, iron, boron, zinc, copper, nickel, and molybdenum. Many different combinations of macro- and micronutrients have been created, but no single medium can be said to be the best [10]. Different species of microalgae are known to have different concentration requirements for various nutrients. Table A.1 in the appendix lists the micro- and macronutrient solution composition that was used for the cultivation of *C. vulgaris* and *N. oculata* for the investigations carried out in this work.

In contrast to conventional agriculture, microalgae can not be supplied with carbon by simple diffusion from air. The natural carbon concentration in air is approximately 0.03 %, and too low to support sustained growth and productivity in microalgae cultivations, although intensive mixing may increase the assimilation of CO_2 from the air into the culture media. Hence, to cultures must be supplied with additional carbon to assure growth, usually in the form of CO_2 enriched air [10]. Nitrogen is also a very important element pertaining to algal nutrition. Algae can typically utilize nitrogen in the nitrate and ammonia forms or other organic sources of nitrogen, such as urea.

There are five reasonably well defined growth phases of microalgal growth in a batch culture when food supply is limited and no nutrients are added or taken from outside of the system [51]. The ideal shape of the phases and progression is shown in Figure 2.3.

The individual phases are not always clearly defined, and may differ in slope and length depending on the conditions in the culture. During the lag phase, the organisms are adjusting to the culture environment, as the conditions in the cultivation medium are usually different than those from the inoculation medium. After the adjustment period, the cells are dividing at a constant rate in the exponential growth phase because the light intensity is not limiting and the changes to the nutrient concentration caused by the uptake are so small that there is no effect on growth [10]. The declining growth phase is reached when the available nutrients and light intensity begin to decline and

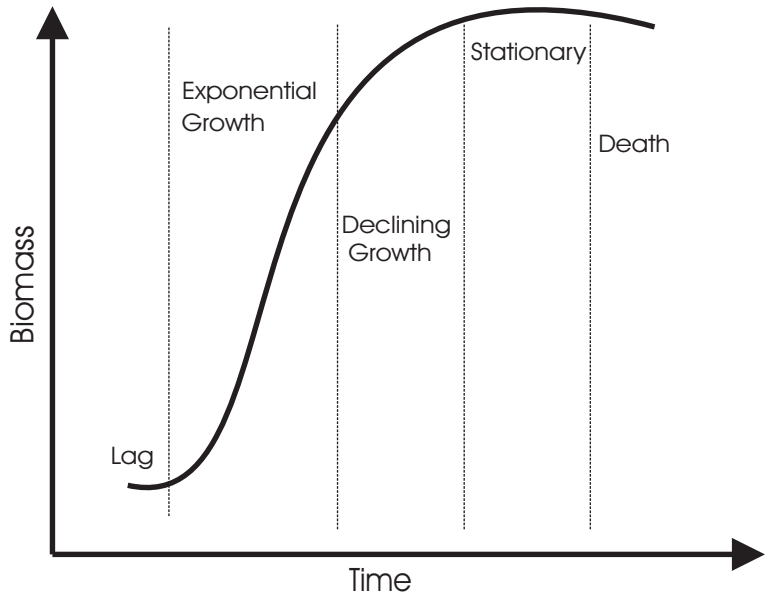

Figure 2.3: The five stages of microalgal growth in batch culture. The time and biomass scale can not be exactly defined because they largely depend on the conditions in the culture and the type of cells being cultivated.

growth slows. In the stationary phase, the growth and death rate of the algae is approximately constant. When the nutrients, CO_2 availability, and light intensity are no longer sufficient to support the population, the death phase begins.

In order to achieve the most efficient biomass yield in a PBR production system, the system should be run in the exponential growth phase. To be able to sustain such operation, nutrients and CO_2 would have to be added and biomass removed at regular intervals. It is also important to assure that sufficient light is available to all the cells throughout cultivation so that photosynthesis can be optimally achieved.

2.2.1 Photosnythesis

Photosynthesis plays in important role in the reduction of atmospheric carbon dioxide. Each year about 1×10^{11} metric tons of CO_2 is converted into organic matter by photosynthesis [52]. The basic unit of the photosynthetic apparatus is the photosystem, which is composed of a series of membrane-bound carriers which provide a pathway of electron transfer. Photosynthesis is classified as a two stage process comprised of light and dark reactions. The light reactions encompass two photon-absorbing systems in eukaryotes, photosystem I (PSI) and photosystem II (PSII); the dark reactions are also known as the Calvin cycle. The combined photosystems require the absorption of

light at two different photo-activation centers.

Chlorophyll a is the main photon-absorbing pigment in both photosystem reactions, accessory pigments include carotene, xanthophyll and phycobilins and absorb light at different wavelengths and transfer it to the chlorophyll. Both photosystems produce adenosine triphosphate (ATP) and nicotinamide adenine dinucleotide phosphate (NADPH), which are needed to produce glucose in the Calvin cycle. Photons that are absorbed by any of the pigment molecules transfer their energy within internal membrane structures called thylakoids, to nearby pigment molecules until it is eventually passed to the reaction center. In PSI the reaction center is a chlorophyll a/protein complex with an absorption peak at 700 nm, and is called P_{700}. PSII's reaction center complex has an absorbtion peak at 680 nm and is called P_{680}.

When the P_{680} chlorophyll reaction center absorbs light energy from pigments in the photosynthetic unit, it becomes excited and a non-cyclic pathway is initiated in which the electron is transferred though a series of membrane-bound electron carriers to the P_{700} chlorophyll reaction center of PSI. The synthesis of one ATP molecule is driven by the hydrogen ion gradient across the membrane which was established by the PSII to PSI electron transfer. The electron transport chain continues when a P_{700} chlorophyll absorbs light, initiating the electron transfer sequence on PSI. The transferred electron from PSII is used to balance the oxidation state of the P_{700} chlorophyll molecule. The electrons transferred though PSI are used to reduce $NADP^+$ to NADPH. The charged P_{680} molecule resulting from the unidirectional flow of electrons needed to reduce $NADP^+$ must be reduced to balance the oxidation-reduction state of this pathway [1].

This photochemical non-cyclic electron transport process (also called the Z pathway, shown in Figure 2.4 [53]) can be summarized by Equation 2.1 [54]:

$$2\,H_2O + 2\,NADP^+ + 2\,ADP + 2\,P_i \xrightarrow[P_{700}+P_{680}]{8\,h\nu} 2\,NADPH_2 + 2\,ATP + O_2 \qquad (2.1)$$

where P_i is inorganic phosphate. This equation implies that each H_2O molecule is split in the chloroplast membrane under the influence of light to give off $\frac{1}{2}O_2$ molecule. The two freed electrons are transferred to NADP along with protons to produce $NADPH_2$. Two molecules of ATP can be simultaneously formed from two adenosine diphosphate (ADP) and two P_i so that energy is stored in the form of this high-energy compound [46]. $NADPH_2$ and ATP are required to reduce CO_2 to carbohydrates in the dark

phase.

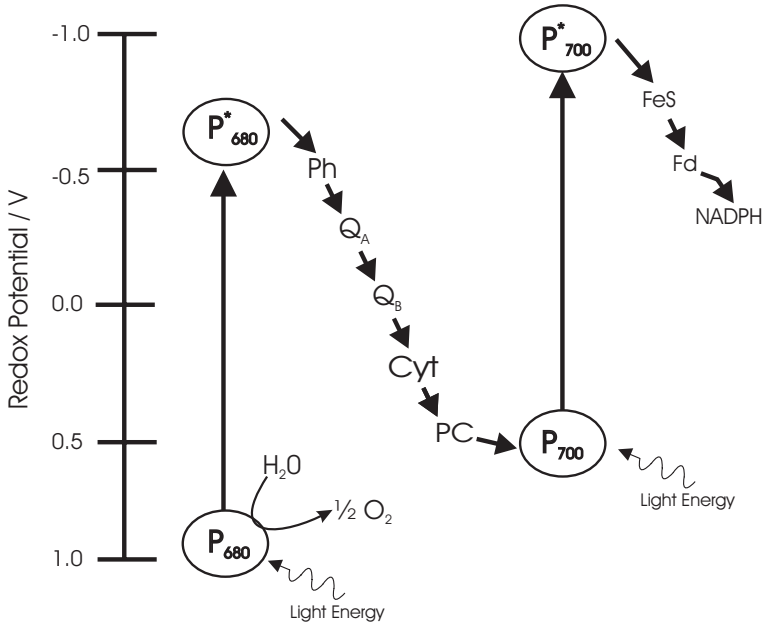

Figure 2.4: Electron flow in oxygenic photosynthesis. Ph: Pheophytin, Q: quinone, Cyt: cytochrome, PC: plastocyanin, FeS: nonheme iron-sulfur protein, Fd: ferredoxin.

The Calvin cycle consists of three phases: in the first phase, called carbon fixation, CO_2 is bound to the acceptor ribulose bisphosphate (RuBP), a five carbon sugar. This step is catalyzed by is RuBP-carboxylase (Rubisco). The reaction product is a six-carbon intermediate which immediately splits in half to form two molecules of 3-phosphoglycerate. In the second phase referred to as reduction, ATP and $NADPH_2$ from the light reactions are used to convert 3-phosphoglycerate to glyceraldehyde 3-phosphate. In phase 3, also called regeneration, ATP is used to convert some of the glyceraldehyde 3-phosphate back to RuBP, the acceptor for CO_2, thereby completing the cycle. The sum of the reactions in the Calvin cycle is given in Equation 2.2 [54]:

$$\begin{aligned} \mathrm{n\,CO_2 + 2\,nNADPH_2} \;+\; \mathrm{2\,nATP} \xrightarrow{\text{Enzyme}} & \\ \mathrm{(CH_2O)_n} \;+\; \mathrm{2\,nNADP^+ + 2\,nADP + 2\,nP_i + n\,H_2O} & \end{aligned} \tag{2.2}$$

The Calvin cycle links the almost instantaneous electronic events of the photochemical light reactions to the synthesis of the principal storage carbohydrates of the plant [55].

Photosynthetically Active Radiation

The solar energy striking the earth's atmosphere every year is equivalent to about 56 $\times$ 10^{23} joules of heat. Of this, roughly half is reflected back by the clouds and upper atmospheric gases. Of the remaining radiation that reaches the earth's surface, only approximately 50% is in the spectral region that could lead to photosynthesis [46]. The solar energy that can be utilized by plants for photosynthesis includes the wavelengths from 400 $-$ 700 nm and is termed photosynthetically active radiation (PAR). The magnitude of solar radiation that reaches the surface of the earth is dependent on the geographical position on Earth and the climatological conditions at that position. Since outdoor sunlight can not be controlled, microalgae are usually studied indoors under artificial illumination.

Photoinhibition describes the decrease in photosynthetic capacity induced when PAR exceeds levels required for saturation [56] and is often rapidly reversible (within minutes) and does not inflict permanent damage to the photosystem. However, severe photoinhibition over a long time may cause highly reactive free oxygen radicals to form (ex. H_2O_2 [57]), which degrade photosynthetic components making the damaging effects of photoinhibition only very slowly reversible. Photoinhibition in plants and algae has been shown to occur under various types of conditions [46]: when a plant or algae is exposed to irradiance higher than that under which it has been grown, when it is subjected to conditions that decrease it's rate of carbon metabolism, and for some species, by exposure to temperatures below 10°C.

The amount of light intensity available to and absorbed by an algal cell suspended in a photobioreactor varies throughout the apparatus and depends on many factors, including the specific position of the cell at a given instance, the density of the culture, and the pigmentation of the cells [58]. The simultaneous existence of complete dark, light limitation, light saturation, and photoinhibition is common within PBRs [59]. Surface illumination between 500 $-$ 1200 $\mu Em^{-2}s^{-1}$ provides for optimal photosynthesis for most species of microalgae, and intensity greater than 1200 $\mu Em^{-2}s^{-1}$ has been shown to cause a reduction in photosynthetic activity [60].

Figure 2.5 shows the effect of light intensity on photoautotrophic growth [61], the range of intensities and the growth rate depicted are relative because they both depend on the type and history of the cell since cells can acclimate fairly quickly to varying light intensities and growth conditions.

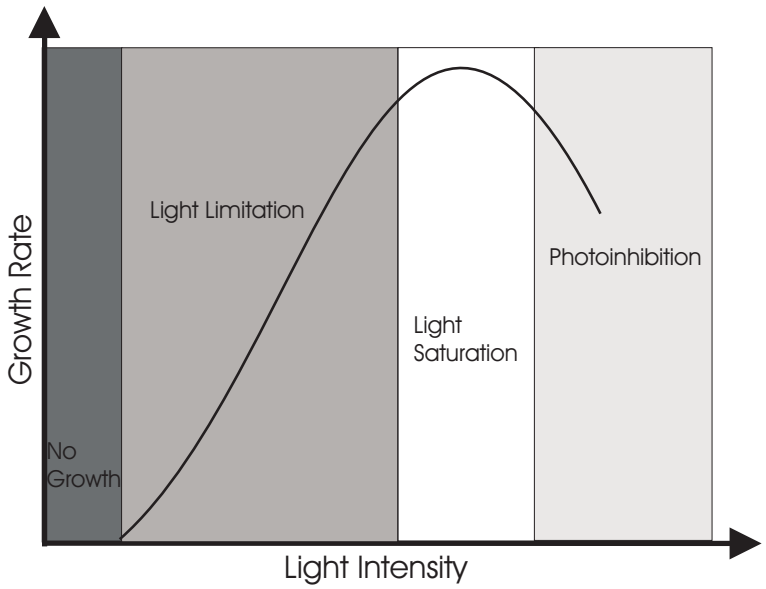

Figure 2.5: Effect of light intensity on photoautotrophic growth of photosynthetic cells. The light intensity and growth rate are relative because they vary greatly depending on the culture conditions and type of cells.

2.2.2 Photobioreactor

Bioreactors are closed systems in which microorganisms can be cultivated under defined, controllable conditions that can be optimized with regard to viability, reproducibility, and product-oriented productivity [62]. A photobioreactor is a system for the production of phototropic microorganisms, which require sunlight or artificial illumination to carry out photosynthesis [4]. Heterotrophs, on the other hand, are organisms that are incapable of making their own food from light or inorganic compounds and often lack photosynthetic pigments, and will not be considered in this study.

While almost anything in which it would be possible to grow algae could technically be called a photobioreactor, the term is more commonly used to define a closed system, as opposed to an open tank or pond. Because these systems are closed, when used to cultivate algae, everything that the algae need to grow including carbon dioxide, nutrient-rich water and light must be introduced into the system.

The inability to control the temperature and light exposure puts open cultivation systems such as ponds, raceways, and natural waters at a disadvantage over closed systems with natural or artificial light sources. Many commercially desired algal species are unlikely to be successfully cultivated in outdoor systems, which are also subjected to losses from evaporation, pollution damage and contamination threat [4]. Attempts have been made to overcome some of the limitations of open systems through the

use of plastic coverings over ponds and raceways, however, this method often proves ineffective because covering materials are not entirely transparent, and water droplets and dust on the surfaces reduce the amount of available light energy [63].

Closed PBRs, however, are faced with the challenge of supplying the cells with an effective light intensity and distribution for optimal photosynthesis. For maximum productivity, the saturation light intensity (see Figure 2.5) should be homogeneously distributed in the entire reactor, which is impossible in practical cultivation systems. Good mixing can be used to circulate the cells between the no growth, limitation, saturation and photoinhibition areas, which will serve to reduce the cell loss and damage in the no growth and inhibition areas [59].

Many different types of closed PBRs have been described, including vertical or horizontal tubular, helical (serpentine), flattened plate, and inclined or horizontal thin-panel and conical [4, 60, 64]. The critical design requirement in these photobioreactors is to supply light efficiently by maximizing the illumination surface-to-volume ratio of the reactor. As a result, tubes are often very narrow or the panels very thin. Some of the photobioreactors that work well in the laboratory may not work as well when scaled up because the surface-to-volume ratio decreases, causing poor light distribution inside the reactor [61].

Another factor that has to be taken into consideration when considering PBR designs is mixing. It has been shown that high mixing rates in some cultures may result in harmful shearing forces [65]. A balance must be achieved to obtain proper light distribution and mass transport within the PBR and mixing that doesn't result in cell damage. For all experiments in this work, a self-constructed PBR system was used (see Section 4.2).

In commercial photobioreactors, the cell density varies depending on the algae type, reactor conditions, growth stage and if it is a batch production, or if the cells are harvested continuously. The maximum attainable cell density in a PBR can vary from $1 - 8$ gL^{-1} dry weight [4], with batch systems typically reaching cell densities of between two and three gL^{-1} dry weight [66, 67, 68].

Chapter 3

Background: Light and Matter Interactions

The propagation of light inside turbid media can be described in terms of the flow of photons which can undergo a number of different processes, such as absorption, elastic scattering, inelastic scattering, and luminescence. When a photon is absorbed, it transfers its energy to the absorbing center and that energy may be transformed into other forms of electromagnetic energy. Elastic scattering involves a change in the photon's direction of propagation while it's wavelength remains essentially unchanged. By contrast, Raman scattering and luminescence processes cause larger photon wavelength changes related to the involvement of vibrational energy levels and/or stokes shift.

3.1 Extinction

The transformation of electromagnetic energy into heat, excitation energy or other forms of energy in the presence of atoms, molecules, or particles is termed absorption and the overall effect is a reduction in the intensity of the incident light beam in the medium. The term extinction refers to the combination of the energy that is lost due to scattering and absorption effects. Extinction is dependent upon the following characteristics of atoms, molecules, or particles: chemical composition, size, shape, orientation, the surrounding medium, concentration, and the polarization state and frequency of the incident beam [69].

The Beer-Lambert law (also called Beer's law) quantifies the empirical relationship relating absorption and scattering in a dilute solution:

$$E = \log \frac{I_0}{I} = \frac{1}{\ln 10} (\mu_s + \mu_a) l \tag{3.1}$$

where E is extinction, I_0 and I the light intensity before and after the sample medium, l the optical path length which is the distance the photons travel through the medium before reaching the detector, and μ_a and μ_s are the absorption and scattering coefficients, respectively and both have the units of inverse distance. The law is valid for monochromatic light sources and homogeneous solutions at low concentrations, where each absorbing center is independent of all others and only single scattering occurs.

The average photon path length depends on both the absorption and scattering coefficient; it decreases as μ_a increases and increases with increased scattering [70]. Multiple scattering effects are evident when scattered light undergoes more than one scattering event, and is re-scattered on other particles or molecules. These multiple scattering events increase with increasing optical thickness and produce deviations from Beer's law.

The scattering coefficient μ_s is the reciprocal of the scattering length. The reduced scattering coefficient μ'_s is the reciprocal of the random walk step, i.e. the average length it takes for a photon's direction to become random. The scattering coefficient and the reduced scattering coefficient are related by the single scattering anisotropy factor, g, the average cosine of the scattering angle [71].

$$\mu'_\mathrm{s} = \mu_\mathrm{s}(1 - g) = \mu_\mathrm{s}(1 - \langle \cos\theta \rangle) \tag{3.2}$$

Angular brackets are used in this work to denote average, and parenthesis signify the dependency of variables.

3.2 Fluorescence

When molecules or atoms absorb light, the equivalent of this energy has to reappear in another form. Energy absorbed by chlorophyll molecules or accessory pigments can be used to drive photosynthesis, excess energy can be emitted as heat, or it can be re-emitted as light. Fluorescence is defined as the electric dipole transition from an excited electronic state to a lower state, usually the ground state, of the same multiplicity [72].

Although chlorophyll fluorescence measurements have become a standard diagnostic tool in ecophysiology studies, the results can only provide a measure of photochemistry efficiency, not a measure of overall photosynthesis. For example, when photosynthetic

organisms are brought from darkness to constant irradiation, they undergo a change in fluorescence intensity with time known as the Kautsky effect [73], this transient reflects mainly the kinetics of electron transfer in PSII, but is also influenced by protonation events and by PSI activities [74]. The Kautsky effect has been explained as a consequence of a reduction of electron acceptors in the photosynthetic pathway. Once PSII absorbs light and quinone (Q_A in Figure 2.4) accepts an electron, it is not able to accept another one until is has passed the first onto a subsequent electron carrier (Q_B) [19].

The processes which occur between absorption and emission are typically illustrated by a Jablonski diagram (Figure 3.1). The singlet ground and first and second electronic states are depicted by S_0, S_1 and S_2, respectively and the different deactivation pathways through which an excited molecule can return to its ground-state are labeled with their corresponding rate constants k_i.

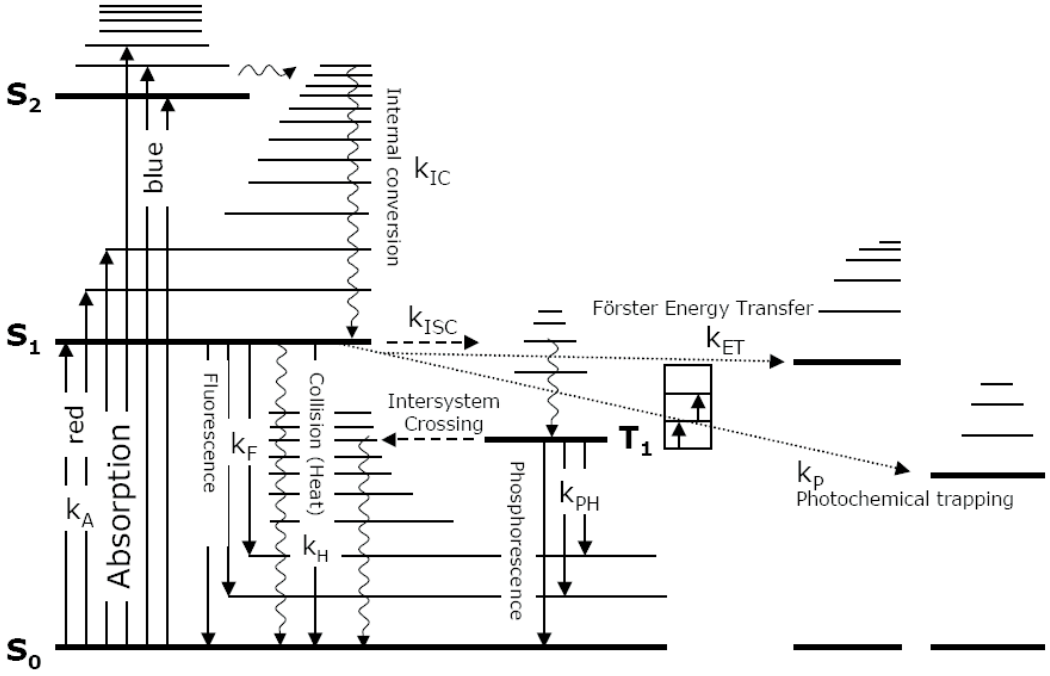

Figure 3.1: Jablonski diagram showing the deactivation pathways for an absorbed photon. The rate constants, k_i, are defined as follows: Fluorescence k_F, internal conversion k_{IC}, intersystem crossing k_{ISC}, phosphorescence k_{PH}, Förster energy transfer k_{ET}, collisional dynamic quenching k_H (heat) and photochemical trapping k_P, which occurs during photosynthesis [75].

Chlorophyll a absorbs in the blue and red regions of the spectra, but fluoresces only in the red. In isolated chloroplasts and in intact leaves and algae, the wavelength of

maximum fluorescence measured is around 685 nm and is mainly contributed by the light-harvesting complexes of PSII.

3.2.1 Fluorescence Lifetime

The fluorescence lifetime τ_{f} is the characteristic time that a molecule remains in an excited state prior to returning to the ground state and thereby a direct indicator of the energy transfer rate from the excited molecules to the local environment or to other fluorophores [76]. Since the lifetime is not dependent on the concentration of the fluorophore nor is the fluorophore concentration controllable in many applications, fluorescence lifetime analysis has become a valuable tool for obtaining quantitative information not available from standard fluorescence techniques.

For single exponential decay of fluorescence, after a brief pulse of excitation light, the fluorescence intensity as a function of time is described as:

$$I(t) = I_0\, e^{(-t/\tau_{\mathrm{f}})} \tag{3.3}$$

where I_0 is the initial intensity immediately after the excitation pulse and I(t) is the fluorescence intensity at time t. The fluorescence lifetime is defined as the time in which the fluorescence intensity decays to $1/e$ of I_0, and the inverse of the lifetime is the sum of the rates which depopulate the excited state. The average time an excited molecule remains in an excited state is determined by the number of deactivation pathways and their competing rates [74].

If all the molecules in an excited state return to the ground state by fluorescence alone, the corresponding fluorescence quantum yield is unity ($\Phi_{\mathrm{f}} = 1$). The quantum yield is defined as the ratio of emitted to absorbed quanta, and can also be described by the rates of the excited state decay.

$$\Phi_{\mathrm{f}} = \frac{\mathrm{k_f}}{\sum_i \mathrm{k}_i} \tag{3.4}$$

where k_i is the rate constant for all methods of decay (see Figure 3.1).

Chlorophyll a fluorescence lifetimes range from fractions of ns to several ns, depending on various conditions, including primarily the state of PSII and temperature [56]. The variation is for the most part due to the dynamic changes in the concentration of open reaction centers and of non-radiative excitation energy sinks.

The first event in both PSI and PSII during photosynthesis is the absorption of a

photon by chlorophyll or other light harvesting pigments and the photon's energy is then transferred to the chlorophyll molecule. A radical pair is formed in the photosystem reaction center from the chlorophyll donor and a quinone acceptor. Photochemistry can not continue until both components of the radical pair have returned to their neutral state, which is described as being open. When one or both of the components are charged the system is said to be closed. The presence of a proportion of closed reaction centers leads to an overall reduction in the efficiency of photochemistry and a corresponding increase in the yield and lifetime of fluorescence [19].

In this study, two different methods were applied for the determination of fluorescence lifetime. Fluorescence lifetime imaging microscopy provides an image of the individual cells and the localized corresponding fluorescence lifetime of each pixel. Time correlated single photon counting techniques were also employed to measure the average fluorescence lifetime of a solution of cells.

3.3 Scattering

Another process from which light is removed from an incident beam traversing a medium is scattering. The scattering of light involves the redirection of photons that takes place when an electromagnetic wave encounters a scattering particle. Interaction of light with matter depends on the electronic structure of the material as determined by its quantum mechanical properties.

When light impinges on matter, the electric field of the light induces an oscillating polarization of the electrons in the molecules called an induced dipole moment. The molecules then serve as secondary sources of light and subsequently scatter light. The frequency shifts, the angular distribution, the polarization, and the intensity of the scattered light are determined by the size, shape and molecular interactions in the scattering materials [77].

Elastic scattering of light occurs when particles in a medium are set into oscillatory motion by the electric field of the incident wave, and re-emit light of the same frequency as the primary wave. Two significant theoretical frameworks for describing elastic scattering include Rayleigh and Mie scattering, which take into account the size and shape of the scatterer. Single scattering refers to radiation that is scattered by only one scattering center and is described by Beer's law (Eqn. 3.1).

Classical light scattering experiments involve measuring the amount of light scattered by a solution at some angle relative to the incident laser beam. Figure 3.2 shows

a sketch of a scattering experiment. θ is the scattering angle, $\mathbf{k}$ and $\mathbf{k}'$ the wave vectors and $\mathbf{q}$ the scattering vector.

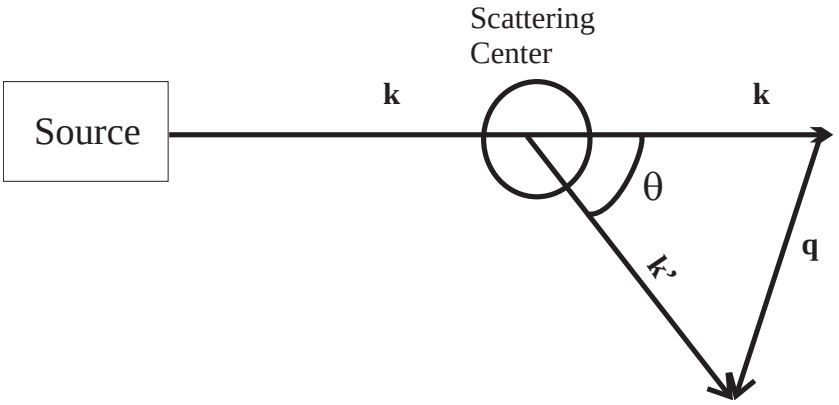

Figure 3.2: Sketch of a scattering experiment. An incident beam emitted by a source is scattered by a sample.

The scattering vector $\mathbf{q}$ is defined as:

$$\mathbf{q} = \frac{4\pi n \sin[\theta/2]}{\lambda} \tag{3.5}$$

where n describes the real part of the index of refraction. Various theories have been put forward to describe the scattering of light by particles of different shapes and sizes. In general these fall into two categories: single scattering and multiple scattering. In single scattering theory, it is assumed that the particle separation is sufficiently large, or the number of particles is sufficiently small, such that the total scattered wave due to all the particles is small compared to the incident wave [69, 78]. It is also assumed that the particles have no further interaction with light that has been scattered from neighboring particles.

3.3.1 Rayleigh Scattering

Rayleigh scattering, named after Lord Rayleigh, describes the scattering of light, or other electromagnetic radiation, by particles and molecules which are much smaller than the wavelength of light. When the particle diameter is very small compared to the wavelength, an incident electromagnetic wave is scattered elastically from a dielectrical spherical particle. Elastic scattering implies that the scattered photon has the same frequency as the incident one. The transmitted wavelength is only modified slightly by Doppler shifting due to the thermal motion of the scattering molecule or particle.

Rayleigh scattering occurs when light travels in transparent solids and liquids, and is prominently seen in gases. In this size regime, the exact shape of the scattering center is usually not very significant and can often be treated as a sphere of equivalent volume. The inherent scattering that radiation undergoes passing through a pure gas is due to microscopic density fluctuations as the gas molecules move around, which are normally small enough in scale for Rayleigh's model to apply.

Particles whose scattering properties can be described by Rayleigh scattering tend to have an isotropic angular scattering distribution and display the following relationship of scattering cross section σ_s and the wavelength:

$$\sigma_\mathrm{s} \propto \frac{1}{\lambda^4} \tag{3.6}$$

The description of scattering by Rayleigh is not valid for particles which are on the order of the wavelength of the incident light [77]. The main criteria for a Rayleigh scatterer is that the size parameter $\alpha \gg 1$ where:

$$\alpha = \frac{2\pi a}{\lambda} \tag{3.7}$$

and a is the spherical particle radius.

The scattering efficiency $\mathrm{Q_s}$ increases with decreasing wavelength, and decreases with increasing particle radius [79, 80]:

$$Q_\mathrm{s} = \frac{8}{3}\left[\frac{m^2-1}{m^2+2}\right]^2\left[\frac{2\pi n a}{\lambda}\right]^4 \tag{3.8}$$

where m is the relative index of refraction and defined as the quotient of a particles with an index of refraction n_T in a medium with an index of refraction n.

$$m = \frac{n_\mathrm{T}}{n} \tag{3.9}$$

The scattering efficiency, scattering cross section and spherical particle radius are related by:

$$Q_\mathrm{s} = \frac{\sigma_\mathrm{s}}{\pi a^2} \tag{3.10}$$

The polarization of the incident light relative to the scattering level yield the following angular distribution of the scattered light [79, 80].

$$I_{\parallel}^{s} = \frac{16\pi^4 n^4 a^6}{R^2\lambda^4}\left[\frac{m^2-1}{m^2+2}\right]^2 \cos^2[\theta] I_0 \tag{3.11}$$

$$I_{\perp}^{s} = \frac{16\pi^4 n^4 a^6}{R^2\lambda^4}\left[\frac{m^2-1}{m^2+2}\right]^2 I_0 \tag{3.12}$$

where $I_{\parallel}^{s}$ and $I_{\perp}^{s}$ are the intensity of the scattered light parallel and perpendicular, respectively, to the scattering plane polarized light. R is the distance between the detector and scattering center.

3.3.2 Mie Scattering

Mie theory describes both absorption and scattering by a spherical particle of arbitrary radius and refractive index [81]. The analysis involves the formal solution of Maxwell's electromagnetic theory for homogeneous spheres using the appropriate boundary conditions [69, 78] which in the limit of a small particle reduces to the relatively simple solution for a Rayleigh scatterer.

Scattering is most intense in the forward-direction, however due to the inclusion of absorption effects the amplitudes of the scattered waves in any direction will rarely be exactly the same, therefore the chances of complete destructive interference are minuscule. When applying Mie theory to scattering particles, the shape of the scattering center becomes much more significant and the theory applies well to spheres and provides a first.order description of optical effects in non-spherical particles [69].

Figure 3.3 shows a scattering diagram representing the scattered light distribution according to Mie's theory of a 160 nm spherical gold particle and 550 nm incident light [81].

The scattering efficiency Q_s and the angular dependency of the scattered intensity can be described with the far-field approximation [79, 80]:

$$Q_s = \frac{\lambda^2}{2\pi^2 n^2 a^2}\sum_{i=1}^{\infty}[2i+1]\left[|a_i|^2 + |b_i|^2\right] \tag{3.13}$$

$$I_{\parallel}^{s} = \frac{\lambda^2}{4\pi^2 n^2 R^2}\left\{\sum_{i=1}^{\infty}\frac{2i+1}{i[i+1]}\left[a_i\frac{\partial P_i^1(\cos\theta)}{\partial\theta} + b_i\frac{P_i^1(\cos\theta)}{\sin\theta}\right]\right\}^2 I_0 \tag{3.14}$$

$$I_{\perp}^{s} = \frac{\lambda^2}{4\pi^2 n^2 R^2}\left\{\sum_{i=1}^{\infty}\frac{2i+1}{i[i+1]}\left[a_i\frac{P_i^1(\cos\theta)}{\sin\theta} + b_i\frac{\partial P_i^1(\cos\theta)}{\partial\theta}\right]\right\}^2 I_0 \tag{3.15}$$

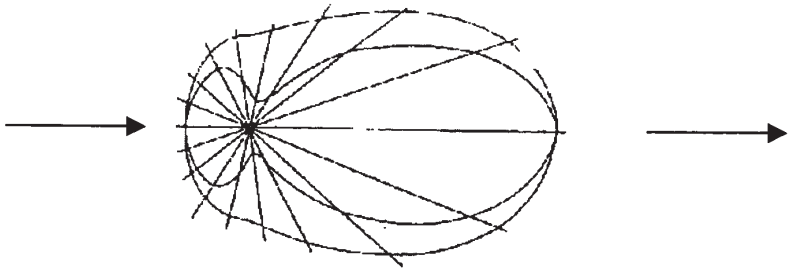

Figure 3.3: Sketch of the distribution of the scattered light intensity according to Mie's theory on a 160 nm spherical gold particle and 550 nm incident light. The direction of the arrow indicates the direction of light propagation. From [81].

In the above equations, a_i and b_i are defined as:

$$a_i = \frac{\xi_i(ka)\xi_i'(kma) - m\xi_i(kma)\xi_i'(ka)}{\zeta_i(ka)\xi_i'(kma) - m\xi_i(kma)\zeta_i'(ka)} \tag{3.16}$$

$$b_i = \frac{m\xi_i(ka)\xi_i'(kma) - \xi_i(kma)\xi_i'(ka)}{m\zeta_i(ka)\xi_i'(kma) - \xi_i(kma)\zeta_i'(ka)} \tag{3.17}$$

where k is the magnitude of the wave vector in the medium, P_i^1 is the first order Legendre polynomial, ζ_i are modified Hankel functions, ξ_i Ricatti-Bessel functions, and the slashes represent the derivative of the variables following in parenthesis.

Particle Size

In this study, Mie theory was applied to describe the relationship between the different scattering coefficients and the particle size. If inter-particle interactions are assumed to be negligible, then the particles in the suspension are considered to be independent scatterers. The specific scattering coefficient τ_s, the specific reduced scattering coefficient τ_s', the scattering coeffieient μ_s and the reduced scattering coefficient μ_s' can be used to determine the particle size [80].

The particle number density ${}^1N$ can be calculated from the ratio of the number of particles N per unit volume V_0:

$${}^1N = \frac{N}{V_0} \tag{3.18}$$

The volume fraction of the scatterer ϕ displays the following relationship to the

particle volume V:

$$\phi = \frac{NV}{V_0} \tag{3.19}$$

Applying Avogadro's number $\mathrm{N_A}$, the molar concentration $[i]$ of component i can be calculated.

$$[i] = \frac{^1N}{N_\mathrm{A}} = \frac{N}{V_0 N_\mathrm{A}} = \frac{\phi}{V N_\mathrm{A}} = \frac{3\phi}{4\pi a^3 N_\mathrm{A}} \tag{3.20}$$

τ_s is often used to describe scattering particles instead of the molar scattering coefficient ϵ_s because it takes into account the volume fraction of the scatterer. Considering Beer's law, τ_s can be defined as follows:

$$\tau_\mathrm{s} = \frac{\mu_\mathrm{s}}{\phi} = \frac{\epsilon_s[i]}{\phi} = \frac{3\pi\, a^3\, N_\mathrm{A}\, Q_\mathrm{s}\, \phi}{4\pi\, a^4 N_\mathrm{A}\, \phi} = \frac{3\, Q_\mathrm{s}}{4a} \tag{3.21}$$

where ϵ_s is the molar scattering coefficient for one type of particle with molar concentration $[i]$, Q_s is the scattering efficiency, and a is the particle radius.

For non-absorbing samples, with uniform size, Equation 3.21 becomes:

$$\mu_\mathrm{s}(\lambda) = \frac{E(\lambda)}{l} = \tau(\lambda)\, \phi = \frac{3\, Q_\mathrm{s}(\lambda)}{4a}\, \phi \tag{3.22}$$

A linear fit of extinction measurements of samples with varying volume fractions of scatterers allow for the determination $\tau_\mathrm{s}(\lambda)$. $Q_\mathrm{s}(\lambda)$ can be calculated using equation 3.13.

Since photon density wave experiments are performed in order to gain knowledge of the reduced scattering coefficient μ'_s, the specific reduced scattering coefficient τ'_s can be used for the prediction of the particle size in the solution [80].

$$\mu'_\mathrm{s} = \tau'_\mathrm{s}\, \phi = \frac{3Q_\mathrm{s}(\lambda)[1 - g(\lambda)]}{4a}\phi \tag{3.23}$$

where:

$$\phi = \sum \phi_\mathrm{i} = \sum \frac{4}{3V_0}\pi\, N_i\, a_i^3 = \frac{4}{3}\pi\, ^1N \sum f_i\, a_i^3 \tag{3.24}$$

The particle number ratio f_i is defined as the ratio of the particles with radius a_i to the total number of particles:

$$f_i = \frac{N_i}{\sum_i N_i} \tag{3.25}$$

3.3.3 Dynamic Light Scattering

Straightforward evaluation of light scattering experiments is simplest when the scattered light reaching the detector and being evaluated is singly scattered light. Contributions from multiply scattered light, which is often present even in samples with low turbidity, complicates data evaluation significantly since it usually requires such experimental information as: knowledge of the scattering geometry, intensity distribution of the incident light beam, sample dimensions and scattering cross section of the scattering particles [82].

Dynamic light scattering (DLS) is one of the most popular experimental techniques for the characterization of colloidal suspensions. DLS provides a measure of the time scale for fluctuations in the index of refraction of a complex fluid, and it probes these fluctuations on the length scale of the inverse of the scattering vector, $\mathbf{q}^{-1}$ [83].

Particles suspended in a liquid are not a static system, rather they are effected by the constant movement associated with particles in a solution called Brownian motion. As a result of this motion, the phase relations of light scattered by different particles change randomly and the number of particles found in the scattering volume changes constantly, leading to a fluctuation in scattering intensity. Analysis of the intensity fluctuations I in terms of a time correlation function can lead to information about the diffusion process [77]. A measure of the correlation is the intensity auto correlation function [84]:

$$\langle I(t_0)I(t_0+\tau)\rangle = \lim_{T\to\infty}\frac{1}{T}\int_{t_0}^{T} I(t)I(t+\tau)dt \tag{3.26}$$

where T is the transmission.

The correlation starts with a maximum value of $\langle I^2\rangle$ and decays over time t to $\langle I\rangle^2$ with the characteristic decay time τ_i

In a dynamic light scattering experiment, the intensity fluctuations are measured and the intensity correlation function is given as [84]:

$$g_2(\mathbf{q},t) = \frac{\langle I_\mathrm{s}(\mathbf{q},t)I_\mathrm{s}(\mathbf{q},t+\tau)\rangle}{\langle |I_\mathrm{s}(\mathbf{q},t)|^2\rangle} \tag{3.27}$$

Despite the fact that DLS has found widespread application to the study of many different physical systems, DLS is restricted to those systems where light is singly scattered, as a second scattering event would render the measurements of the intensity auto-correlation function meaningless.

Cross Correlation

If multiple scattering occurs in a light scattering experiment, an interpretation of the data becomes very difficult because the multiply scattered light no longer has a close association to the scattering vector $\mathbf{q}$. Another approach for particle sizing is to isolate singly scattered light and suppress undesired contributions from multiple scattering in a DLS experiment. This can be achieved by performing two scattering experiments simultaneously on the same scattering volume with two laser beams of initial wave vectors $\mathbf{k}_{i1}$ and $\mathbf{k}_{i2}$, and two detectors positioned at final wave vectors $\mathbf{k}_{f1}$ and $\mathbf{k}_{f2}$. Then, only singly scattered light will produce correlated fluctuations on the two detectors, and multiple scattered light will produce uncorrelated fluctuations which contribute only to background signal [83]. The cross correlation of the two signals from the detectors can be represented as follows:

$$G_{12}(\tau) \; = \; \langle I_1(t) I_2(t+\tau) \rangle \tag{3.28}$$

where τ is the lag time, t is the measurement time, I_1 and I_2 are the scattered intensities seen by detectors 1 and 2.

If both experiments have the same scattering vector $\mathbf{q}$, but use different scattering geometries, and the multiple scattering is suppressed, the following relationship between the dynamic structure factor $S(\mathbf{q}, \tau)$ and the measured cross correlation function $G_{12}^{(1)}(\tau)$ exists [84]:

$$G_{12}^{(1)}(\tau) = I_1^{(1)} I_2^{(1)} (1 + \beta_{12} |S(\mathbf{q}, \tau)|^2) \tag{3.29}$$

where (1) indicates singly scattered photons. The intercept of the cross correlation function $G_{12}^{(1)}(\tau)$ is given by:

$$\beta_{12} = \beta \exp \frac{-\delta q^2 R_B^2}{4} \exp \frac{-\delta x^2}{R_B^2} \tag{3.30}$$

$\delta q = |\delta \mathbf{q}|$ describes the match of the scattering vectors $\mathbf{q}_1$ and $\mathbf{q}_2$ and $\delta x = |\delta x|$ is the spatial match of the scattering volumes [83]. R_B is the incident beam radius.

In a 3-D cross correlation experiment, the multiple scattering contributes so the background and therefore reduces the intercept. This means that the maximum intercept for 3-D experiments is only one quarter of the value obtained for auto-correlation experiments, i.e. $\beta_{12,ideal} = 0.25$ [83].

Since cross correlation experiments suppress contributions from multiply scattered

light by a factor of the order of $(R\delta k_j)^{-1}$ where $\delta \mathbf{k}_j$ is the magnitude of the smallest of the two wave vector combinations $\mathbf{k}_{i2} - \mathbf{k}_{i1}$ and $\mathbf{k}_{i2} + \mathbf{k}_{i1}$ [85]. This gives the following expression for $\mathrm{G}_{12}^{(1)}(\tau)$:

$$G_{12}^{(1)}(\tau) \approx I_1 I_2 + \beta_{12} I_1^{(1)} I_2^{(1)} |S(\mathbf{q}, \tau)|^2 \tag{3.31}$$

where I_j is the average intensity of the contributions from singly and multiply scattered light measured at detector j and $S(\mathbf{q}, \tau)$ is the dynamic structure factor.

3.4 Propagation of Light in Turbid Media

The physical basis for the absorption and scattering of light radiation has already been discussed. The theories discussed describe light propagation by both large and small particles relative to the wavelength of the incident light, assuming a small enough collection of particles, or one in which the particles are far enough apart such that their individual scattered fields do not significantly perturb one other. However, in turbid media, the scattering particle density is high enough that the interaction of scattered waves between neighboring particles cannot be ignored and multiple scattering is said to occur.

It is possible to describe light transport in a multiply scattering medium using Maxwell's electromagnetic theory [78]. Such solutions are however highly complex and a more suitable description is one in which the wavelike behavior of light is not accounted for and the transport of individual photons, which can be absorbed or scattered, is considered. This treatment is known as radiative transfer theory and is formalized by the radiative transfer equation [80]:

$$\frac{d\psi(\mathbf{r}, \mathbf{\Omega}, t)}{dt} = \left[\frac{d\psi(\mathbf{r}, \mathbf{\Omega}, t)}{dt}\right]_{\text{int}} + S(\mathbf{r}, \mathbf{\Omega}, t) \tag{3.32}$$

where $\psi(\mathbf{r}, \mathbf{\Omega}, t)$ is the number of photons per volume that move in direction $\mathbf{\Omega}$ at position $\mathbf{r}$ and time t and have the units of $\mathrm{m}^{-3}\mathrm{sr}^{-1}$ (where sr is the abbreviation for steradian). During the time interval dt the intensity varies from $d\psi(\mathbf{r}, \mathbf{\Omega}, t)$ according to the radiation source $S(\mathbf{r}, \mathbf{\Omega}, t)$ (with units of $\mathrm{m}^{-3}\mathrm{s}^{-1}$) and interactions (int) with the medium.

The diffusion transport behavior of photons is commonly known as photon migration. When the intensity of the incident light wave is sinusoidally modulated, it has

veling wave disturbance of the light energy density prop-

acroscopic diagram of the

.

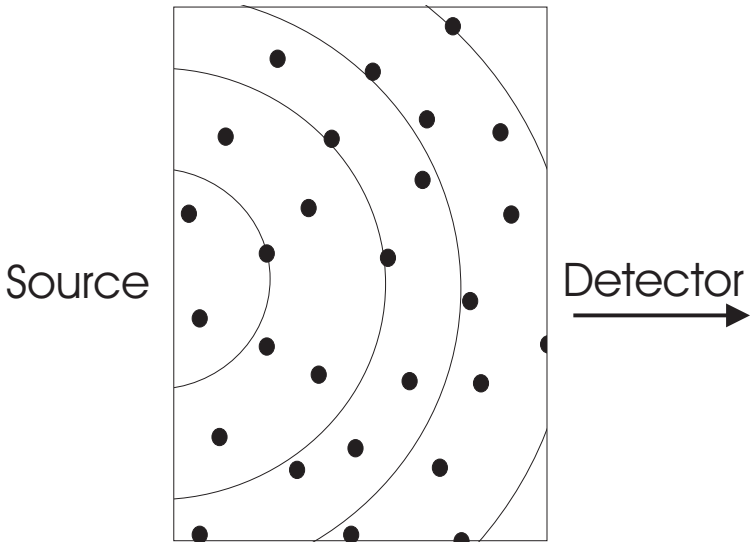

Figure 3.4: Macroscopically representative sketch of PDW propagation in a turbid solution.

When photons travel through turbid media, the transmission of light is dependent on the reflectance, scattering and absorption which occur in the media. The parameters which characterize these phenomena include scattering anisotropy g, the scattering coefficient μ_s, the absorption coefficient μ_a, and the refractive index n. The reduced scattering coefficient μ_s' can be defined as the inverse of the average distance that the photon has to travel to become random in relation to the initial direction of propagation, and g as the intensity weighted mean cosine of the scattering angle. Values of g range between -1 and +1 and depend of the refractive indexes of the scatterer and the medium and on the particle size. Ignoring interference and polarization effects, the propagation of light in turbid media can be modeled as the transport of particles which perform a random walk in the scattering media due to multiple collisions.

An intensity modulated point source of light produces a wave of light energy density which propagates spherically outwards from the source through the turbid medium, this wave is called a diffuse photon density wave (PDW) [86]. The time dependent radiative transport equation, also called the Boltzmann transport equation, treats light propagation as the transport of photons though a medium which contains particles, and gives the temporal evolution of the angular photon density in a medium where the processes of absorption and elastic scattering take place [87]:

$$\left[\mathbf{\Omega}\cdot\nabla+\frac{\partial}{c\partial t}+\left[\mu_{\mathrm{a}}+\mu_{\mathrm{s}}\right]\right]\psi\left(\mathbf{r},\,\mathbf{\Omega},\,t\right)= \\ \frac{1}{c}S\left(\mathbf{r},\,\mathbf{\Omega},\,t\right)+\mu_{\mathrm{s}}\int\psi\left(\mathbf{r},\,\mathbf{\Omega}',\,t\right)f\left(\mathbf{\Omega}',\mathbf{\Omega}\right)d\mathbf{\Omega}' \tag{3.33}$$

where $\nabla\equiv\partial/\partial\mathbf{r}$, $f(\mathbf{\Omega}',\mathbf{\Omega})$ is the probability that scattered light $\mathbf{\Omega}'$ will be scattered in the direction $\mathbf{\Omega}$ and c the speed of light in the medium.

Analytical solutions of the transport equation are difficult to obtain and numerical calculations require large amounts of computational power, however, these difficulties are reduced by considering approximate solutions. While several approximations exist, including those for planar and [88] spherical geometries [89] and the standard diffusion equation, which makes assumptions about the reduced scattering coefficient [90], the P_1 approximation has been shown to provide an accurate description of the Boltzmann transport equation even at high modulation frequencies [71].

3.4.1 The P_1 Approximation

The P_1 approximation to the Boltzmann transport equation provides a more complete approximation than the Standard Diffusion Equation (SDE). In the strongly scattering regime, the Boltzmann transport equation reduces to the SDE, which is expected to breakdown at GHz modulation frequencies [71]. The SDE is valid when the photon current density is related to the photon density by Fick's law, which is satisfied in turbid media with relatively large scattering coefficients at moderate modulation frequencies. Another condition for the validity of the SDE is that $1\gg 3\mu_{\mathrm{a}}D$, and with further help from the assumption that $\mu_{\mathrm{s}}'\gg\mu_{\mathrm{a}}$, the P_1 equation can be reduced to the SDE´[33].

The P_1 approximation is based on keeping only the terms $l=0$ and $l=1$ in the expansion of the angular photon density in the spherical harmonics and the assumption that the scattering coefficient μ_s is much larger than the absorption coefficient μ_a. Assumptions for this analysis include weak absorption, large distances to boundaries and light sources, and neglect of polarization and interference effects [30].

The following discussion provides a brief overview of the P_1 approximation to the Boltzmann transport equation, a more detailed theoretical analysis can be found in [80] and the other sources cited in this section. The Boltzmann transport equation contains both time and space derivatives and in order to provide a solution, initial and boundary conditions are required. Among the assumptions is that the sample

medium is an infinite medium, which requires that the photon flux becomes small as the distance from the source becomes large.

The P_1 approximation to the time dependent radiative transport equation for an isotropic light source yields [71, 91]:

$$s_0(\mathbf{r},t) = \left[\mathbf{\Omega}\cdot\nabla + \frac{\partial}{c\partial t} + \mu_\mathrm{a}\right] c\rho(\mathbf{r},t) + 3\left[\mathbf{\Omega}\cdot\nabla + \frac{\partial}{c\partial t} + \mu_\mathrm{a} + \mu_\mathrm{s}'\right]\mathbf{\Omega}\cdot\mathbf{J}(\mathbf{r},t) \tag{3.34}$$

where $s_0(\mathbf{r},t)$ is the source density in units of $\mathrm{m}^{-3}\mathrm{s}^{-1}$ and $\mathbf{J}(\mathbf{r},t)$ is the photon current density with units of $\mathrm{m}^{-2}\mathrm{s}^{-1}$.

Replacing $\mathbf{J}(\mathbf{r},t)$ with an expression for the photon density $\rho(\mathbf{r},t)$ yields [80]:

$$\left[\mu_\mathrm{a} + \frac{\partial}{c\partial t}\right] c\rho(\mathbf{r},t) + \nabla\cdot\mathbf{J}(\mathbf{r},t) = s_0(\mathbf{r},t) \tag{3.35}$$

In terms of the optical diffusion coefficient D:

$$D = \frac{c}{3\left[\alpha\mu_a + \mu_s'\right]} \tag{3.36}$$

where here $\alpha = 1$.

$$\begin{aligned} s_0(\mathbf{r},t) + \frac{3D\partial^2}{c^2\partial t} s_0(\mathbf{r},t) = \\ -D\nabla^2\rho(\mathbf{r},t) + (3\mu_\mathrm{a}D + c)\frac{\partial}{c\partial t}\rho(\mathbf{r},t) + \frac{3D\partial^2}{c^2\partial t^2}\rho(\mathbf{r},t) + c\mu_\mathrm{a}\rho(\mathbf{r},t) \end{aligned} \tag{3.37}$$

Intensity Modulated Light Source

For an intensity modulated point light source located within the medium, the Green's function solution to the P_1 approximation yields Equation 3.38 [71].

$$\rho_\mathrm{AC}(r,t) = \frac{C}{r}\exp\left[-k_\mathrm{I} r + i(k_\Phi r - \omega t - \Phi_0)\right] \tag{3.38}$$

$\rho_\mathrm{AC}(r,t)$ is the time dependent part of the photon density, ω is the angular modulation frequency and C depends on the power and modulation depth of the source and the optical parameters of the medium, and r is the scalar distance between source and detector. Φ_0 is the phase offset due to the overall optical pathlength outside of the sample. k_I and k_Φ represent the intensity and phase coefficients, respectively and they both have units of reciprocal length.

The komplex wave number k is composed of k_{I} and k_{Φ}:

$$k = k_{\mathrm{I}} + i\, k_{\Phi} \tag{3.39}$$

and

$$k^2 = \frac{c^3\, \mu_a\, - 3\,\omega^2\, D + i\, \left[-c^2\, \omega - 3\, c\, \omega\, \mu_a\, D\right]}{c^2\, D} \tag{3.40}$$

where $c = \mathrm{c_0/n}$, the speed of light in water. After mathematical treatment, the following equations provide the solutions for k, k_{I} and k_{Φ}, respectively (for a complete derivation, please see [80]).

$$\begin{aligned} k \;=\; & \left\{ \frac{\left[c^3\mu_{\mathrm{a}} - 3\omega^2 D\right]^2 + \left[c^2\omega + 3c\omega\mu_{\mathrm{a}} D\right]^2}{c^4 D^2} \right\}^{\frac{1}{4}} \\ & \left\{ \cos\left[\frac{1}{2}\arctan\left[\frac{c^2\omega + 3c\omega\mu_{\mathrm{a}} D}{c^3\mu_{\mathrm{a}} - 3\omega^2 D}\right]\right] - i\sin\left[\frac{1}{2}\arctan\left[\frac{c^2\omega + 3c\omega\mu_{\mathrm{a}} D}{c^3\mu_a - 3\omega^2 D}\right]\right]\right\} \end{aligned} \tag{3.41}$$

$$k_{\mathrm{I}} = \sqrt{\frac{2}{3}\left(\sqrt{\left[\left[\alpha\mu_{\mathrm{a}} + \mu'_{\mathrm{s}}\right]^2 + \frac{\omega^2}{c^2}\right]\left[\mu_{\mathrm{a}}^2 + \frac{\omega^2}{c^2}\right]} + \mu_{\mathrm{a}}\left[\alpha\mu_{\mathrm{a}} + \mu'_{\mathrm{s}}\right] - \frac{\omega^2}{c^2}\right)} \tag{3.42}$$

$$k_{\Phi} = \sqrt{\frac{2}{3}\left(\sqrt{\left[\left[\alpha\mu_{\mathrm{a}} + \mu'_{\mathrm{s}}\right]^2 + \frac{\omega^2}{c^2}\right]\left[\mu_{\mathrm{a}}^2 + \frac{\omega^2}{c^2}\right]} - \mu_{\mathrm{a}}\left[\alpha\mu_{\mathrm{a}} + \mu'_{\mathrm{s}}\right] + \frac{\omega^2}{c^2}\right)} \tag{3.43}$$

Besides using a non-linear fitting procedure, the absorption and reduced scattering coefficients μ_{a} and μ'_{s}, respectively can be determined from the measured k_{I} and k_{Φ} values [80]:

$$\mu_{\mathrm{a}} = \frac{c k_{\mathrm{I}} k_{\Phi} - \sqrt{c^2 k_{\mathrm{I}}^2 k_{\Phi}^2 - 3\omega^2\left[k_{\mathrm{I}}^2 - k_{\Phi}^2 + 3\omega^2 c^{-2}\right]}}{3\omega} \tag{3.44}$$

$$\mu'_{\mathrm{s}} = \frac{\left[1-\alpha\right] c k_{\mathrm{I}} k_{\Phi} + \left[1+\alpha\right]\sqrt{c^2 k_{\mathrm{I}}^2 k_{\Phi}^2 - 3\omega^2\left[k_{\mathrm{I}}^2 - k_{\Phi}^2 + 3\omega^2 c^{-2}\right]}}{3\omega} \tag{3.45}$$

α describes the relationship of the optical diffusion coefficient on absorption coefficient and is estimated to be 1/3 for the data analysis carried out in this work.

3.5 Experimental Data

In the PDW experiments preformed here the medium is characterized by measuring the intensity and phase of the photon density wave as a function of source and detector distance. The phase shift is described as the offset between two phases, and is detected with the network analyzer. Figure 3.5 shows the phase shift $\Delta\Phi$ and decrease in intensity as a function of time.

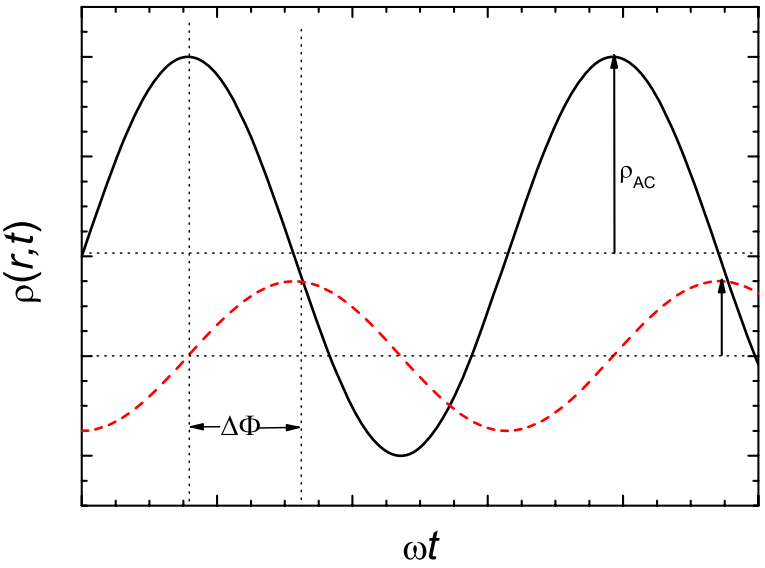

Figure 3.5: Modulated light source (solid line), phase shift $\Delta\Phi$ and decrease in intensity (dashed line). The difference in intensity is represented by the magnitudes of the arrows.

In order to calculate μ_s' and μ_a, knowledge of k_I and k_Φ as a function of the modulation frequency $f = \omega/2\pi$ is necessary. The complex amplitude $U(r, f)$ is able to be determined for different f and $r$and it's modulus $I(r, f)$, which will be referred to as intensity, is proportional to the modulus of the AC amplitude of the photon density $\rho_{AC}(r, f)$. the intensity can be defined as follows [80]:

$$I(r, f) \propto \mid \rho_{AC}(r, f) \mid = \frac{C}{r} \exp\left[-k_I(f)r\right] \tag{3.46}$$

Chapter 4

Experimental Set-up

In order to execute a thorough optical investigation of microalgae cultures, a photo-bioreactor was designed and constructed and several different optical technologies were applied for the analysis of the cells. In this chapter, an introduction to the concepts applied here and a description of the experimental set-up will be presented for each of the processes that were utilized.

4.1 Determination of Cell Concentration

C. vulgaris and *N. oculata* cells used for experiments and as inocula were provided by the Institut für Lebensmittel- und Umweltforschung e.V., in Bergholz-Rehbrücke, Germany. The dry weight of the cell solutions was determined by centrifuging 10 mL samples four times, for 10 minutes each, at approximately 3500 rpm. After each centrifugation, the sediment was re-suspended with bi-distilled water. The remaining sediment was dried at 100°C for 24 hours, and subsequently weighed to determine the dry weight cell concentration (gL^{-1}).

A Neubauer-counting chamber haematocytometer (Optik Labor, Friedrichshofen, Germany) was also used to determine the cell number density of cells in the solution. The chamber is used to count cells in a fluid environment by observing a calibrated grid through a microscope (Axiostar, Zeiss, Jena, Germany) where the exact dimensions (including depth and volume) are known. Equation 4.1 is applied for the calculation of the cell density [92].

$$^{1}N = \frac{Z \cdot F}{K \cdot A} \tag{4.1}$$

where ^{1}N is the cell number density (♯ cells mL^{-1}), Z the number of cells counted,

F the dilution factor, K the depth of the chamber and A the area of the squares containing the cells that were counted.

4.2 Cell Cultivation

When cultivating algae, several factors must be considered besides the fact that different algae have different requirements. The water must be in a temperature range that will support the specific algal species being grown. Nutrients should be controlled so they are not wasted and the algae will not starve. Light should not be too intense or weak. For microalgae cultivation in this study, a simple PBR was self-constructed from a glass vessel and illumination source. A scheme is shown in Figure 4.1. This basic, cost-effective set-up was applied in order to provide an environment where photosynthesis and cell growth could occur. Several different set-ups were tested, and this one most competently supported cell growth. While this system set-up was never tested for efficiency, it proved effective in enabling an increase in biomass and provided a platform for the on-line observation of this increase.

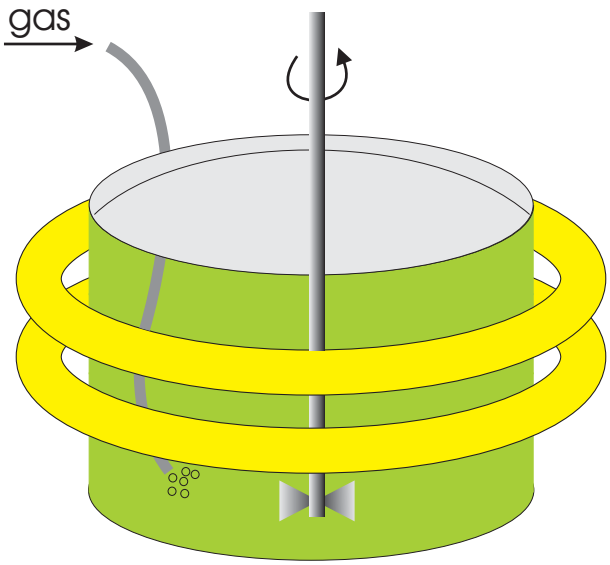

Figure 4.1: Scheme of the self-constructed photobioreactor set-up.

The light source consisted of two 60 W circular fluorescent lights (TL5 C, Philips), a circular glass tank (Diameter = 25 cm, Height = 12 cm) was used as the transparent container for cell cultivation. A KPG-stirrer was employed as the mixing source to prevent settling and flocculation. Plastic tubing with an aquarium air stone attached

at one end and submerged in the tank served as the delivery source for the 10% CO_2 (in nitrogen) gas supply. Aluminium foil was used to cover the top of the PBR to hinder evaporation and dust contamination.

4.2.1 Cultivation Conditions

A concentrated cell solution was diluted with the nutrient solution (for composition see Appendix A) to a starting concentration of approximately 0.9 gL^{-1} cell dry weight (DW). The KPG-stirrer was set to approximately 300 rpm, and the gas feed (10% CO_2 in N_2) was diffused at approximately one mL min^{-1} into the cell solution. The cultivation medium was then monitored for circa two weeks, or until an increase in dry weight was no longer observed. Water was added daily to compensate for evaporative losses, samples were collected twice a day and the dry weight was calculated as described in Section 4.1. The cell solution maintained a temperature of about 28°C throughout the cultivation cycle, with the only heat source being the radiation from the light supply. The temperature in the laboratory was maintained at approximately 22°C.

The cultivation was under constant surface illumination of approximately 350 $\mu mol/m^2s$ except for approximately one hour, twice a day. The incident light intensity on the surface of the glass vessel of the PBR was measured with a light meter (LI-250, LI-COR Biosciences GmbH, Homburg, Germany). The light source was turned off approximately 30 minutes prior to and remained off during PDW investigations.

4.3 UV/VIS Spectroscopy

Extinction measurements were performed with a commercial absorption spectrometer (Cary500Scan, Varian, Darmstadt, Germany) in a 10 mm optical glass cuvette, 1 nm bandwidth, and 0.5 s integration time per data point. All collected spectra were background corrected with the solvent in which they were suspended or dissolved. The spectrometer was turned on at least one hour prior to use.

4.4 Fluorescence Lifetime Spectroscopy

The knowledge of the fluorescence lifetime allows for the investigation of the direct molecular environment of the fluorophore, which in this case acts like a molecular

probe and can reveal valuable information in biological samples. In this study, two different methods of measuring the fluorescence lifetime of microalgae cells were applied. Fluorescence lifetime imaging involves the visualization of a sample of cells under a microscope and the collection of fluorescence intensity and lifetime data by way of pixel by pixel single photon counting analysis. The correlated single photon counting (TCSPC) experiments, on the other hand, collect no image of the cell, but provide an average lifetime of the fluorophores in a solution by means of a statistical analysis of photon emission after an excitation event. The photon counting events which are recorded in TCSPC experiments are many orders of magnitude greater than those of FLIM experiments.

4.4.1 Fluorescence Lifetime Imaging Microscopy

Fluorescence lifetime imaging microscopy (FLIM) offers many benefits, among which are that fluorescence lifetime, in contrast to fluorescence intensity, is independent of the concentration of the fluorophore and it provides visualization of the molecular environment in a single living cell [93]. In addition, many applications deal with sample geometries that prevent homogeneous illumination and/or contain a variety of inhomogeneous local environments (for example, the organelles in a cell) which can not be properly analyzed using standard fluorescence techniques.

Although FLIM has been developed for both frequency and time domain methods, only time domain methods were applied here. Using the FLIM system described below, the two dimensional images were created by the contrast of fluorescence lifetimes at each pixel.

A time-resolved confocal microscope (MicroTime 200, PicoQuant, Berlin, Germany) system was applied in these experiments, a schematic diagram is shown in Figure 4.2. A 467 nm diode laser (PicoQuant, Berlin, Germany), 80 ps full width at half maximum (FWHM), and 20 MHz repetition rate was implemented as the excitation source. An inverted microscope (IX 71, Olympus, Hamburg, Germany) with an oil immersion objective (100x, 1.4 NA, Olympus, Hamburg, Germany) was utilized for both focusing laser light onto the sample and for collecting fluorescence from the sample. The fluorescence that passed a dichroic mirror (467 nm, Picoquant, Berlin, Germany) was focused onto a 30 μm pinhole for spatial filtering to reject out of focus signals. 500 nm longpass filters (Edmund Optics, Karlsruhe, Germany) were placed before the avalanche photo diodes (APD) to further isolate single photon emission. Images were recorded

by raster scanning (E-710 digital PZT and P-733 piezo-positioner, Physik Instrumente, Karlsruhe, Germany) the sample over the focused spot of the incident laser.

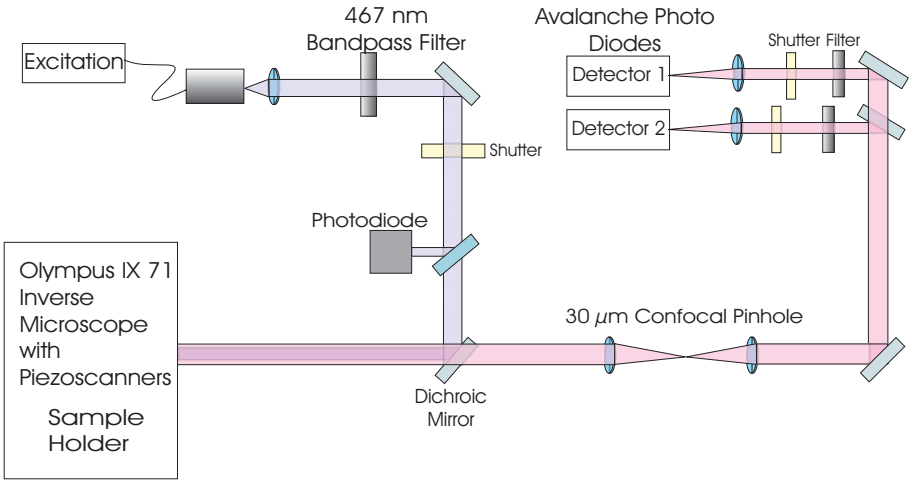

Figure 4.2: Scheme of the FLIM system.

Lifetime analysis with FLIM also has disadvantages which include the need for sample preparation and immobilization. Compared with continuous mode fluorescence lifetime imaging at video-rate [75], long data acquisition times occur when conventional FLIM systems are used. Also, measurements which are based on fluorescence intensity comparisons often do not take into consideration that molecularly identical fluorophores can have different lifetimes at different image locations, which will result in different fluorescence intensities [75].

4.4.2 Time Correlated Single Photon Counting

Time-correlated single-photon counting involves the detection of single photons emitted by a fluorescent medium. By recording the time that that fluorescence intensity takes to decay to $1/e$ of its initial value following excitation, the fluorescence lifetime can be experimentally determined. Hereby is the basis of TCSPC; the quantum nature of light enables the time distribution of individual photons within the decay profile to be recorded [94]. As opposed to FLIM measurements, where the heterogeneous fluorescence lifetime can be determined throughout one cell, TCSPC provides the average lifetime of the materials in solution. The results can be fitted to Equation 4.2.

Time correlated single photon counting (TCSPC) measurements rely on the concept that the probability distribution for emission of a single photon after an excitation event yields the actual intensity against the time distribution of all photons emitted

as a result of excitation. By sampling the single photon emission following a large number of excitation flashes, the experiment constructs this probability distribution [72]. Measurement of the decay of fluorescence by a short laser pulse can be used to study the structure and state of photosynthetic systems because the fluorescence lifetime of an excited chlorophyll depends on its surroundings [95].

In TCSPC experiments, an electrical pulse is generated at a time exactly correlated with the generation of the optical pulse. The start electrical pulse is routed to the time-to-amplitude converter (TAC), initiating the charging of a capacitor, which is stopped when the first fluorescence photon is detected. The TAC produces a voltage output with amplitude proportional to the charge in the capacitor and time between the start and stop signals. The pulse is given a numerical value in the time-to-amplitude converter and a count is stored in the data stroage device in an address corresponding to that number. Excitation and storage data is repeated in this way over many start-stop cycles until the histogram of number of counts against address number in the stroage device represents the decay curve of the sample. [72]. The evolution of the probability histogram, representing the growth and decay of the fluorescence, can be displayed in real time.

Figure 4.3 shows a block diagram of a typical single photon counting apparatus setup [94]. In this case, TCSPC measurements were made with an FLS920 fluorimeter (Edinburgh Instruments, Livingston, UK). A diode laser (PicoQuant, Berlin, Germany) with an excitation wavelength of 635 nm, 75 ps FWHM, and 10 MHz repetition rate served as the light source. 10,000 photon counts were collected in the maximum channel using 4096 channels. Emission light was detected at 680 nm and 54.8° magic angle to aviod polarization effects. A multichannel plate (ELDY EM1-132/300, Europhoton, Berlin, Germany) with a ca. 100 ps response time was applied as the fluorescence detector.

The fluorescence intensity decays were fit to the single or multiple exponential model:

$$I(t) = \sum_{i=1}^{n} \alpha_i \, e^{(-t/\tau_i)} \tag{4.2}$$

where α_i is the amplitude of the components with the fluorescence decay times τ_i. For one fluorophore localized in more than one different micro-environment, the pre-exponential factors α_i represent the fractional amount of fluorophores A_i in each environment:

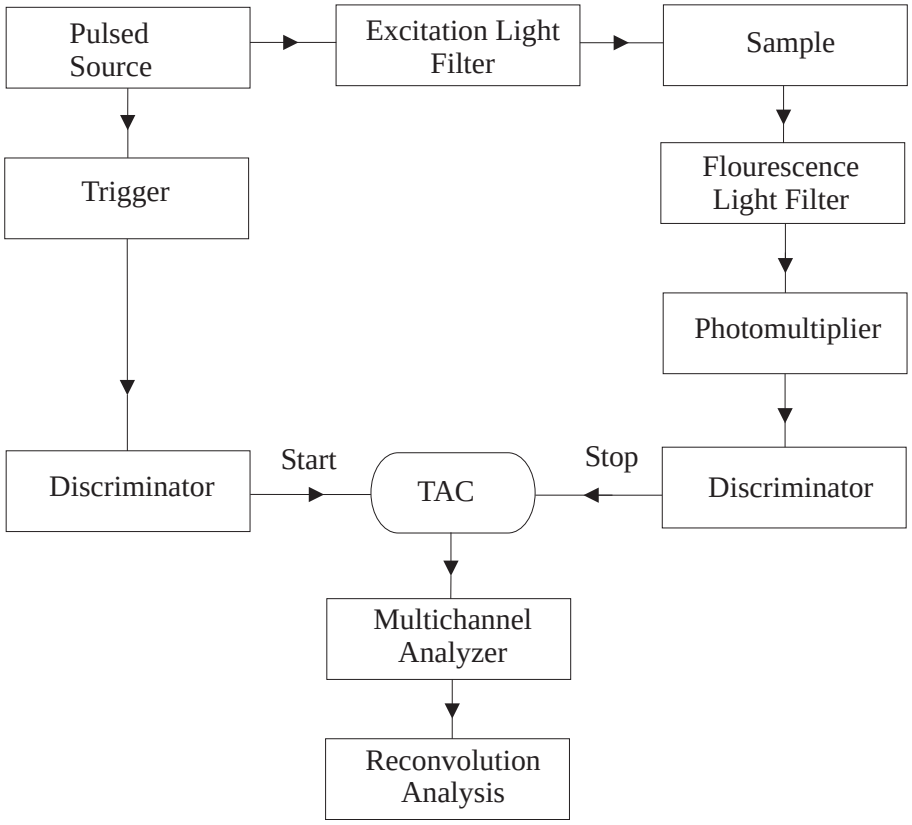

Figure 4.3: Block diagram of a typical single photon counting apparatus.

$$A_i = \frac{\alpha_i \tau_i}{\sum_{i=1}^{2} \alpha_i \tau_i} \tag{4.3}$$

The quality of the fit was assessed using the reduced χ^2_{R} values, which summarizes the discrepancy between observed values and the values expected under the model in question. The fitting function $\mathrm{Y}(\mathrm{t}_i)$ is optimal when the following expression is minimized:

$$\chi^2_{\mathrm{R}} = \frac{\sum_{i=1}^{n} \left(\frac{(I(t_i) - Y(t_i))^2}{I(t_i)} \right)}{dof} \tag{4.4}$$

where dof $= \mathrm{N} - \mathrm{p} - 1$, N is the number of observations, p the number of parameters. Values of much less than one can be a symptom of data in which the number of counts is not large enough [72].

4.5 3-D Cross Correlation DLS

3-D cross correlation dynamic light scattering experiments are based on the principle of suppressing contributions from multiple scattering and provide a measure of the time scale for the fluctuations in the index of refraction of a complex fluid. In Figure 4.4 the wave vector arrangement for a 3-D cross correlation experiment is shown. $\mathbf{k}_{i1}$ and $\mathbf{k}_{i2}$ are the initial wave vector pairs, and $\mathbf{k}_{f1}$ and $\mathbf{k}_{f2}$ are the final wave vector pairs. Signals from multiply scattered light ($\mathbf{q}_3$ and $\mathbf{q}_4$) produce different scattering vectors and therefore are not cross correlated. This scattering geometry yields matching scattering vectors $\mathbf{q}_1$ and $\mathbf{q}_2$ as a result of successful isolation of the single scattering dynamic structure factor for cross correlation measurements with overlapping measurement volumes [85].

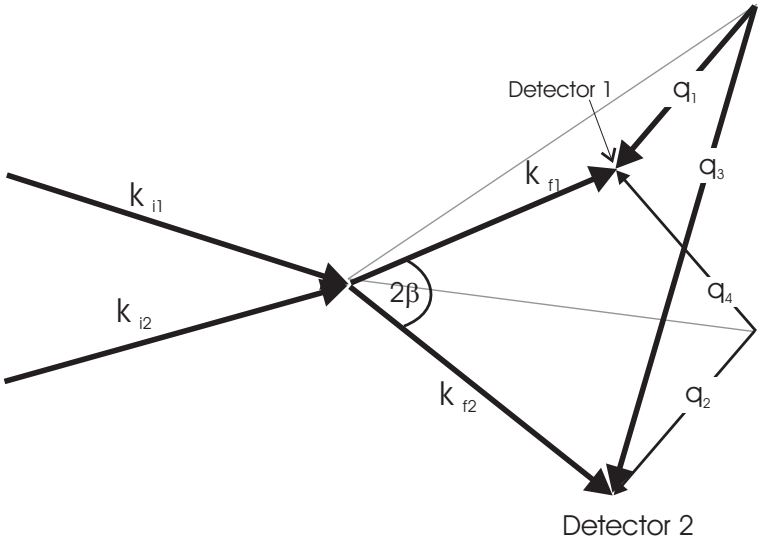

Figure 4.4: Scattering geometry in a 3-D cross correlation experiment, where $\mathbf{q}_1 = \mathbf{q}_2$ and $\mathbf{q}_3 \neq \mathbf{q}_4$.

Figure 4.5 shows a schematic set-up of a cross correlation spectrometer (LS Instruments, Switzerland, HeNe-Laser, 632.8 nm, 10-150°detection angle).

In a cross correlation experiment, the intensity originating from one incident beam is correlated with the intensity originating from the other incident beam. The scattering volume is the common volume shared by the incident and scattered light, this occurs in the area where the beams overlap. Because of the small scattering volume, 3-D cross correlation measurements provide reliable results with particle sizes up to approximately one μm.

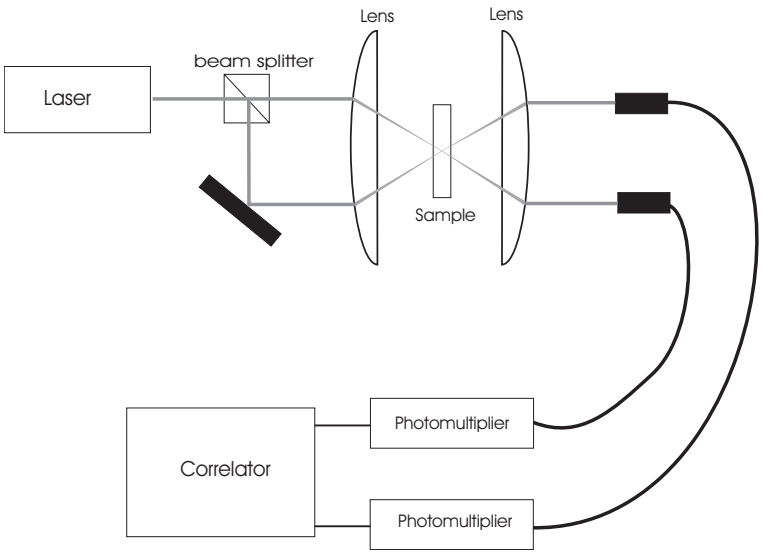

Figure 4.5: Cross Correlation Spectrometer schematic set-up. The laser beam is split into two parallel beams which are focused by a lens. The crossing point represents the scattering volume. The scattering angle θ can be varied from 15 to 150°.

4.6 Photon Density Wave Spectroscopy

The interaction of light with turbid medium is a complicated occurrence that involves both scattering and absorption of photons. Scattering is influenced by the structural characteristics of the material, such as form, density, and interferences between particles [96]. Absorption, on the other hand, is related to the chemical constituents of the medium and hence it can be used to probe the chemical properties of the particles. Since scattering and absorption are intertwined, they are difficult to independently measure. Analysis with PDW spectroscopy provides a way for the determination of absorption coefficient (μ_a) and reduced scattering coefficient (μ_s').

In order to make a thorough optical characterization of strongly scattering media, the absorption and scattering properties must be taken into consideration. A photon density wave is a modulated wave which propagates through diffuse medium and exhibits amplitude and phase variations. The P_1 approximation to the radiation transport equation, described above, can be applied for a theoretical description of photon density waves [30].

Compared to traditional lasers, diode lasers are generally compact, reliable, easy to operate, amenable to electronic high frequency modulation and temperature tuning, and are in most cases low cost. A photon density wave spectrometer, constructed

by the University of Potsdam, Physical Chemistry research group, was used for the investigations in this work.

4.6.1 Low Frequency Modulation

As a relatively simple, low cost alternative to high frequency modulation PDW spectroscopy, a low frequency intensity modulation system was developed and tested for the on-line monitoring of the development of microalgae cultures. However, when using this set-up, the phase ϕ was not measured, and therefore there could be no strict independent determination of μ_{a} and μ'_{s}. Nevertheless, the goal of analysis using this setup is to obtain information about the increase in biomass by measuring the scattered light intensity that reaches the detector as a function of the separation distance r.

The determination of μ_{a} and μ'_{s} with photon density waves measurements with variable source/detector separation and low modulation frequency can be made from a simplified form of the standard diffusion equation. Solving the transport equation for the appropriate boundary conditions yields the following dependence of light intensity on the separation distance between light source and detection point r [71]:

$$\ln(Ir) \;=\; \ln\left(\frac{const}{D}\right) \;-\; r\sqrt{3\mu'_s\mu_a} \tag{4.5}$$

D is the optical diffusion coefficient. Equation 4.5 is valid for low modulation frequencies and for infinite media.

A quadratic fit can be made once the slope m of the linear relation between $\ln(I\ r)$ and r is known.

$$m^2 \;=\; 3\mu_{\mathrm{a}}\mu'_{\mathrm{s}} \tag{4.6}$$

$$m^2 \;=\; 3\left(\mu_{\mathrm{a}}(H_20) + C_{\mathrm{c}}\mu^{\dagger}_{\mathrm{a(c)}}\right)\left(C_c\mu'^{\dagger}_{\mathrm{s(c)}}\right) \tag{4.7}$$

$\mu_{\mathrm{a}}(H_20)$ denotes the wavelength dependent absorption coefficient of water, C_c the cell concentration (gL^{-1} dry weight), and $\mu^{\dagger}_{\mathrm{a}}(c)$ and $\mu'^{\dagger}_{\mathrm{s}}(c)$ absorption and reduced scattering coefficients which are dependent on cell concentration, respectively.

The following studies employed a constant, low frequency intensity modulation of 1.0 kHz and involved no analysis of the phase lag ϕ. Regardless, a concentration dependent analysis of μ_{a} and μ'_{s} is still possible. The data collected with this method was also used to determine the experimental parameters for the variable frequency modulation

experiments.

Experimental Set-up: Low Frequency Modulation

A home-made diode laser spectrometer was assembled from photodiodes, an amplifier, and a lock-in amplifier (LIA-MVD-200-L, FEMTO Messtechnik, Berlin, Germany). The 785 nm, 70 mW laser diode (Thorlabs, Munich, Germany) was mounted in a custom built laser head which provides temperature stabilization, collimation and coupling to the fiber optics. The lock-in amplifier served as the modulation source, and the frequency was kept constant at 1.0 kHz.

For the photon migration studies, both the illumination and detection fibers (silica, 1.0 mm diameter) were immersed in the medium at the same height above the tank floor, the two fibers being separated by the distance r. The distance between the fiber-optics was increased in one or two mm steps using a linear translation stage (M410CG, PI, Karlsruhe, Germany), and the measured light intensity on the detector (Det110, Thorlabs, Munich, Germany) was recorded as voltage at each step. The intensity was amplified (98-3-70770, EG&G, Montgomeryville, PA, USA) and by means of the the lock-in-amplifier, the time-dependent intensity was read on a digital multi-meter or PC as voltage output. The movement of the linear translations stage and data collection were controlled and recorded with LabView software. The set-up is a simplified version of that shown in Figure 4.6, where a lock-in amplifier was used in place of the network analyzer.

4.6.2 High Frequency Modulation

Experimental Set-up: High Frequency Modulation

Compared to the setup described above for the low modulation frequency experiments, the system requirements for analysis with a high frequency modulated light source are more costly and advanced. Here, the network analyzer capable of frequency modulation from 0.3 MHz to 1.3 GHz provides the modulation and measures and records the phase and intensity at every source/detector separation distance measured.

Source and detector optical fibers (silica, 1.0 mm diameter) were immersed into the solution parallel to each other at the same height above the container floor, see Figure 4.6. The source light was derived from a 785 nm 70 mW laser diode (Thorlabs, Munich, Germany). The diode laser in this case was amplitude modulated from 0.3 up

to 650.15 MHz with a network analyzer (8712 ET, Agilent, Böblingen, Germany), which also serves to detect AC intensity and phase shift. The detector fiber was connected to an avalanche photodiode (S2383, Hamamatsu, Hersching, Germany) with a 0.8 mm^2 active area, and a 600 MHz cut-off frequency.

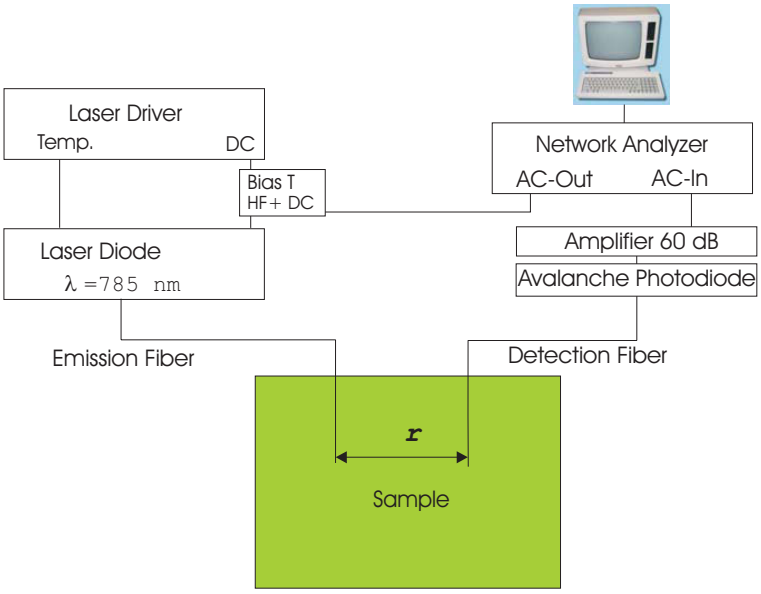

Figure 4.6: Schematic experimental set-up of the intensity modulated diode laser spectrometer.

Silica glass optical fibers were used in this case instead of plastic optical fibers, which are more flexible, durable and economical, because plastic fibers would absorb the laser source light at 785 nm (see Appendix B.1 for more information about the attenuation losses of different types of optical fibers [97]). A linear translation stage (M410CG, PI, Karlsruhe, Germany) with a repeatability of two μm was used to set the various distances between the source and detector fibers.

Avalanche photodiodes are semiconductor light sensors which utilize an internal gain mechanism that functions by applying a reverse voltage. A voltage when the PN junction of the semiconductor is illuminated, operating as a photoelectric converter. A PN junction is formed by combining N-type and P-type semiconductors together in close contact, junction referring to the overlap of the two semi-conductors. The junction between the P and N type semiconductors is a non-conductor, called the depletion zone, and occurs because the electrical charge carriers in doped N and P silicon (electrons and holes, respectively) attract and eliminate each other in a process called recombination.

Typically, the P-layer of a silicon photodiode is formed by the selective diffusion of boron to a thickness of approximately one μm or less. By varying and controlling the thickness of the various layers and doping concentrations, the spectral response and frequency range can be controlled. When electron-hole pairs are generated in the depletion layer of a photodiode with reverse voltage applied to the PN junction, the electrons drift towards the N side while the holes drift towards the P side due to the electric field developed across the PN junction [98]. When the reverse voltage is increased, electron-hole pairs collide with the crystal lattice, ionization takes place and more electron-hole pairs are formed, these pairs then create additional pairs. In this way, a single electron may result in many more being created creating an avalanche effect.

A bias-Tee (ZFBT4R2GW, MiniCircuits, Brooklyn, USA) is a three terminal circuit incorporated between the laser driver and laser head (see Figure 4.6) and serves to add the modulation signal to the DC current of the laser driver.

The laser diode was mounted on a home-made thermoelectric temperature stabilized laser head. The power and temperature control to the diode is supplied by a laser driver (LDC8002, Thorlabs, Munich, Germany).

Chapter 5

Results and Discussion

5.1 Cell Concentration

There are various ways to quantify the biomass in a cell cultivation. Cell counting using a haematocytometer is a common microscopic method that is used, but there are several problems with this method because the reproducibility of the counts is low. Because the volume analyzed is about 1 μL, the number of cells present is extremely small and does not always represent an average of the algal sample, even if the sample is mixed properly and special attention has been given to sampling, diluting and filling the chamber [10].

Figure 5.1 shows the relationship between N, calculated according to Eqn. 4.1, and the cell concentration, determined as described in Section 4.1.

The statistical error associated with N was calculated using the standard deviation of four cell counts at the same concentration and increases with increasing cell concentration. The standard deviation of the four different dried cell samples was applied as the error for the dry weight analysis and varies little with cell concentration. A linear relationship was expected between the number of cells at given concentrations, however, large deviations were observed with increasing cell concentration. In the literature, a variation of 10% has been reported with counting methods [99].

Although cell counting is a technically simple and commonly applied method, the precision associated with this method is relatively low. In the work presented here, the cell concentration in gL^{-1} dry weight (DW) is reported as the analytical method due to better data reproducibility.

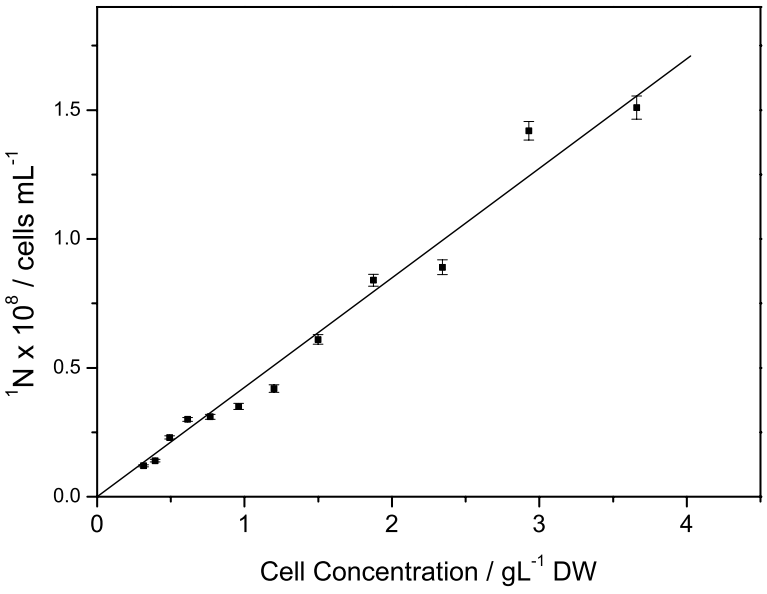

Figure 5.1: N, calculated according to Eqn. 4.1, in relation to the dry weight cell concentration. The cells were counted using a Neubauer cell haematocytometer. The solid line represents a linear fit through the origin.

5.2 UV/Vis Spectroscopic Characterization of Microalgae

A *C. vulgaris* cell solution (concentration approximately 0.2 gL^{-1} DW) suspended in the aqueous nutrient solution was analyzed and the extinction spectrum is shown in Figure 5.2. The results have been background corrected. As was discussed in Section 2.1, microalgae are composed of various pigments which absorb light at different wavelengths. The absorption peak between 650 and 740 nm is caused by the strong chlorophyll absorption in the red region, and carotenoids and chlorophyll both absorb strongly in the $400 - 500$ nm region.

Because of the contributions from multiple scattering and therefore no knowledge of the optical path length, Beer's law can not be applied to the extinction as shown on Figure 5.2 to gain knowledge of the sample concentration.

5.2.1 Pigment Characterization

In order to measure the extinction of the pigments present in *C. vulgaris*, the cells were concentrated via centrifugation and the pigments were extracted using an 80% acetone solution. The solution was filtered to remove cell debris and the extinction

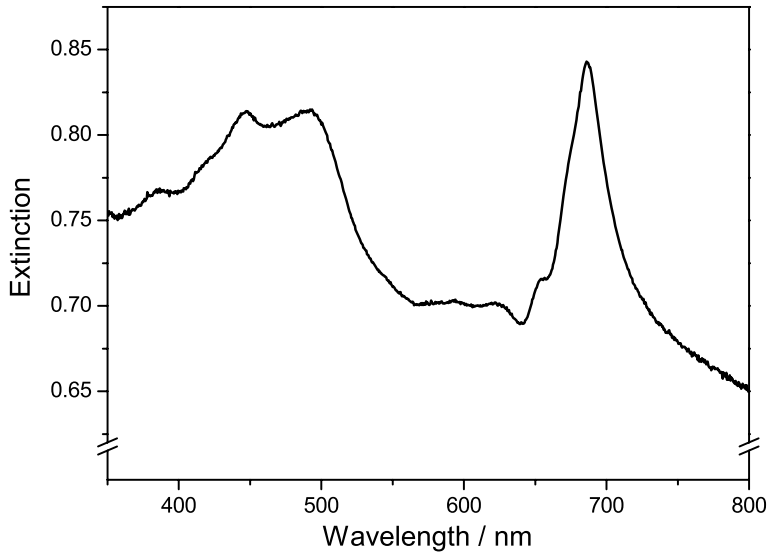

Figure 5.2: Extinction of *C. vulgaris* cells. Measurements were performed at 21°C, in an optical glass cuvette and over a 10 mm optical pathlength.

of the pigment extract and of β-carotene (Sensient Food Colors GmbH, Geesthacht, Germany) dissolved in ethanol was measured (Figure 5.3).

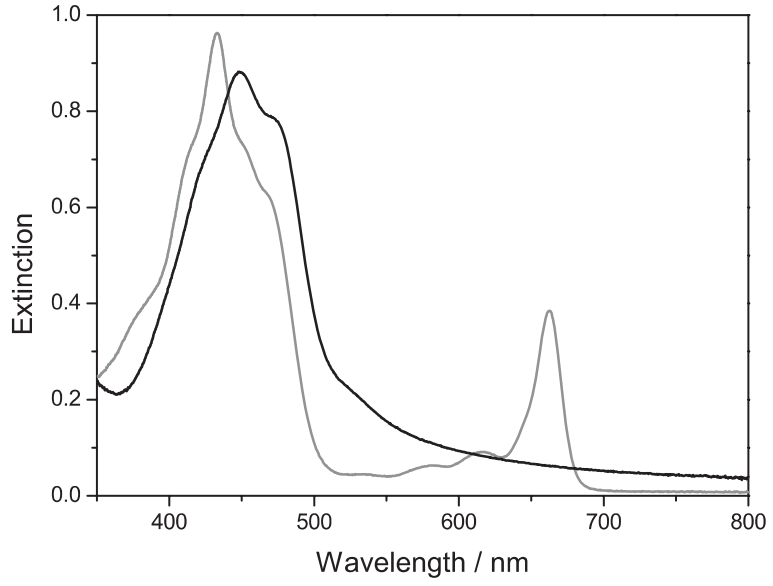

Figure 5.3: Extinction of β-carotene in ethanol (black) and pigments extracted (grey) from *C. vulgaris*. Measurements were performed at 21 °C, in an optical glass cuvette and over a 10 mm optical pathlength.

The extinction of the chlorophyll a and b (referred to here as Chl_{tot}) extract can be used to calculate the concentration of Chl_{tot} in the culture, which is often a better

indicator of microalgae biomass growth because bacteria and zooplankton, which frequently contaminate cultures, do not contain chlorophyll. The Chl_{tot} concentration in the extract can be calculated with the following equation when acetone is used as the extracting agent [10]:

$$[Chl_{tot}] = (8.02 \times A_{663}) + (20.2 \times A_{645}) \tag{5.1}$$

where Chl_{tot} is in mgL^{-1} and A is the measured extinction at 663 and 645 nm, respectively. This formula is valid for extinction measurements in a 1 cm pathlength cuvette, and was derived from the known extinction coefficients of acetone solutions of Chl_{tot} at 663 and 645 nm. The molecular masses of chlorophyll a and b are 892 and 906 Da, respectively. The extinction coefficient of chlorophyll a in 80% acetone is 16.75 $Lg^{-1}cm^{-1}$ at 645 nm and 82.04 $Lg^{-1}cm^{-1}$ at 663 nm, respectively [46, 100]

Equation 5.1 was applied to the measurements shown in Figure 5.3, where the dry weight cell concentration and dilution factor used so the extinction could be measured were known. The Chl_{tot} concentration of the extract was calculated to be 6.17 mgL^{-1}, which is 1.09% of the dry weight concentration in the original cell solution. These results are in good agreement of the literature values for the chlorophyll concentration in microalgae cells of $0.5 - 1.5$ % dry weight (see Section 2.1.1). Although the chlorophyll extraction method provides an acceptable approach for the quantification of chlorophyll present in a cell solution, the process is time consuming and not practical as an on-line analysis tool.

The multiple scattering effects present in optically dense samples are not accounted for by traditional extinction measurement, which makes an accurate interpretation of data collected in this manner inaccessible. Independent determination of absorption and scattering coefficients by traditional extinction measurements made with a standard spectrometers is theoretically quite challenging. This can be attributed to the fact that standard spectrometers are not designed to deal with the effects of multiple scattering. Because it is difficult to sufficiently characterize a multiple scattering system based on extinction measurements alone, other analysis techniques will be employed in this study.

5.3 Microalgae Fluorescence

A solution of intact *C. vulgaris* cells was analyzed at room temperature in the nutrient salt solution (see Table A.1 for composition) with a commercial fluorescence spectrometer (Fluoromax3, Yobin Yvon, Longjumeau, France). The resulting fluorescence spectrum is shown in Figure 5.4. The excitation wavelength λ_{ex} was 435 nm. *C. vulgaris* cells absorb in both the red and blue spectral regions (see Figure 5.2) and at room temperature, strong fluorescence is present in the red region.

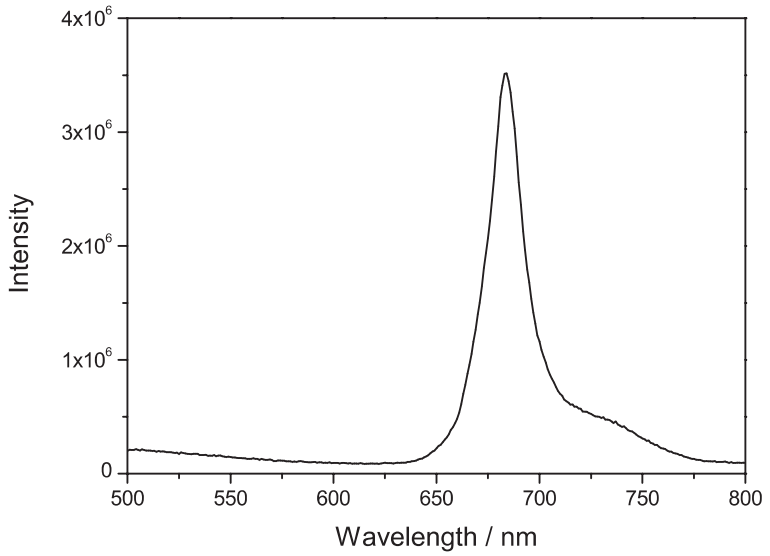

Figure 5.4: Fluorescence emission of a solution of *C. vulgaris* cells at room temperature. $\lambda_{ex} = 435$ nm.

At room temperature, chlorophyll a fluorescence is largely emitted by PSII and the attached light harvesting chlorophyll/protein complex [101]. Because there is more than one de-excitation pathway for excited molecules, the fluorescence signal of a sample is determined by the rate constants of the competing de-excitation pathways and by the fraction of open reaction centers.

5.4 FLIM

Lifetime images captured using FLIM are most commonly visualized in form of color-coded images, often called false color or pseudo color images since there is no correspondence of the color code with the physical color in the image. The scalar at each pixel of an image is replaced by a color according to its value such that regions of the

same scalar value have the same color and regions of different properties within an image can be distinguished by different colors. Fluorescence intensity images can also be recorded without the added step of calculating the lifetime. However, fluorescence intensity signals in microscopy are generally problematic to interpret because the local fluorophore concentration is not known [74]. The advantage of lifetime analysis is that it is independent of local fluorophore concentration variations.

In Figure 5.5, fluorescence intensity images of *C. vulgaris* cells in their nutrient solution environment are shown. All FLIM data presented here were collected using the setup described in Section 4.4.1 and analyzed using SymPhoTime (PicoQuandt GmbH, Berlin, Germany) software. A layer of vaseline was spread around the edges of the top and bottom microscope slides to avoid crushing the cells and causing damage.

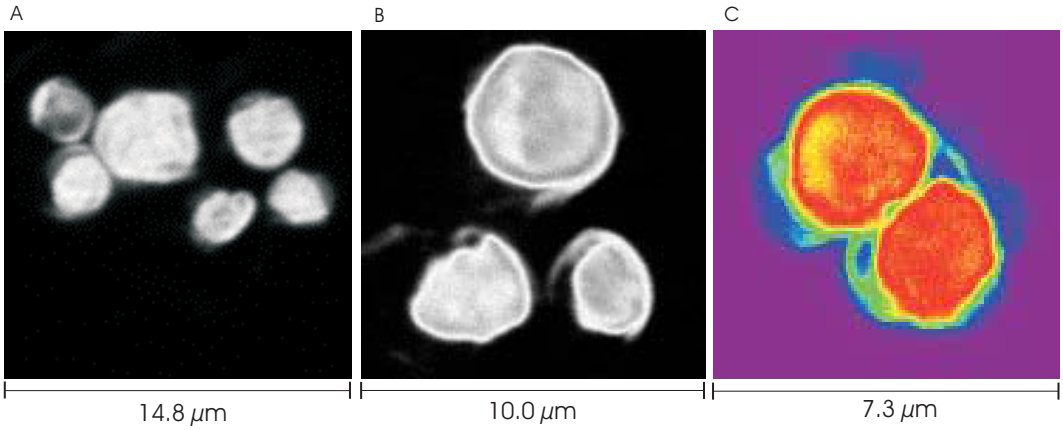

Figure 5.5: Fluorescence intensity images of *C. vulgaris* cells. A & B: unaltered. C: false color scale

Valuable information can be obtained from fluorescence intensity images for the general characterization of the culture media. For example, the cells are spherical, but not completely uniform in size and have an average cell diameter of ca $2 - 6$ μm. It can also be seen that no clusters are formed and the cells are not joined together in solution. Image C in Figure 5.5 shows the false color fluorescence intensity of two cells next to each other, here it can clearly be seen that fluorescence intensity varies little within the cell, and is related to the amount of chlorophyll in the cell because other pigments present in the cells do not contribute to fluorescence at room temperature [75].

Because the chlorophyll concentrations in the cells can not be controlled, the intensity differences between cells are impossible to interpret unless the lifetimes are measured. Due to large variable concentrations of chlorophyll in different cells, the

lifetime differences are often not correlated with fluorescence intensities. Some cells with shorter lifetimes have greater intensities than cells with lower intensities. Changes in fluorescence intensity can be caused by a change in the number of fluorophores or in the quantum yield of each fluorophore [75]. For example, during a phase change when mobile antenna move from strongly fluorescent PSII to weakly fluorescence PSI, the number of fluorophores with a certain quantum yield can decrease even though the number of molecules in the sample remains constant [102]. When this occurs, the measured fluorescence intensity changes, but the quantum yield of the remaining fluorophores remains the same.

In Figure 5.6, the fluorescence lifetime distribution of a single *C. vulgaris* cell immobilized with gelatin on a microscope slide is displayed. Image B is taken one hour after A.

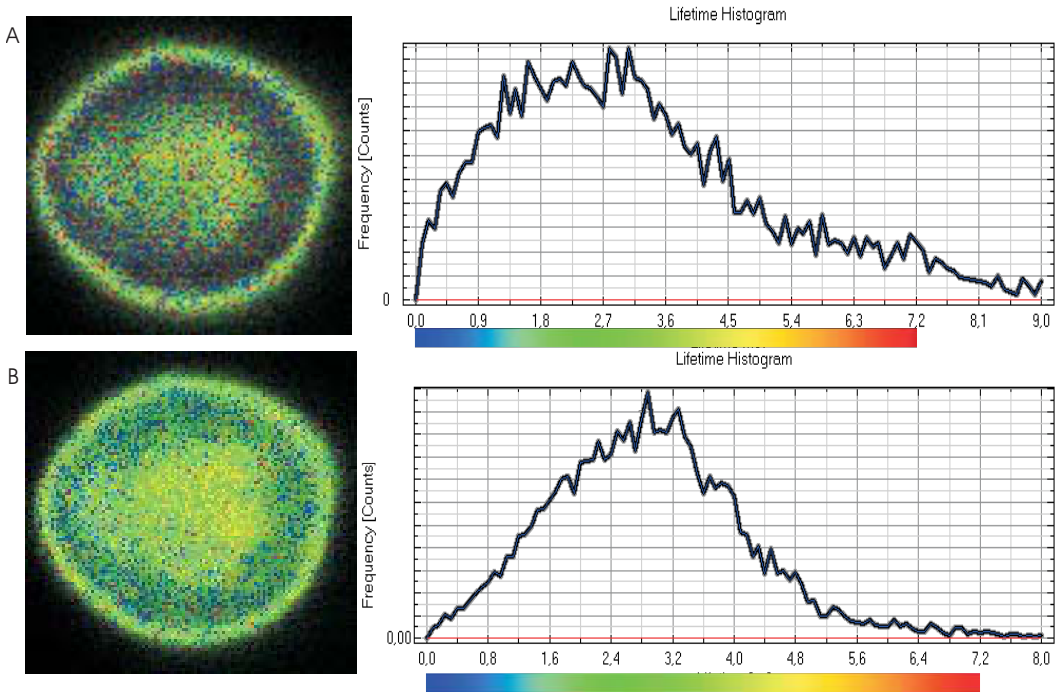

Figure 5.6: Fluorescence lifetime distribution of a *C. vulgaris* cell. B was collected one hour after A. The corresponding color scale is the same for both images, ranging from 0.0 to 7.2 ns. The lifetime distribution is shifted towards longer lifetimes in B.

In both images, a broad distribution of lifetimes between approximately 0 and 7 ns can be seen, however, in the second image, the lifetime distribution is shifted towards longer fluorescence lifetimes. The color scale corresponds to the same times for each image, increasing from blue (0.0 ns) to red (7.2 ns). The reported τ_f literature values

for in-vivo chlorophyll a and β-carotene are $0.3 - 3.2$ ns and < 1.0 ns, respectively [21, 95, 103, 104, 105]. The broad discrepancies reported in the literature values for chlorophyll a fluorescence lifetime have been attributed a number of variables including: temperature, light acclimation, excitation intensity and the presence of pigment-protein complexes [103, 104]. Fluorescence lifetime of chlorophyll is, however, independent of excitation wavelength [21].

As Figure 5.6 shows, the distribution of τ_f displays an observable shift towards longer lifetimes in the cell after it remained on the microscope slide and was re-examined one hour later. The cell looked visibly healthy, and was stored in the dark prior to the collection of the second image. The change in fluorescence lifetime over time has been associated with cell damage or stress including dehydration, photoinhibition, water stress in plants [106, 107], or in this case, possibly due to damage from the incident laser intensity. After the unnatural storage conditions provided by the microscope slide, including poor gas exchange with the environment, the increase in the fluorescence lifetime distribution can be associated with damage to the photosynthetic reaction center. Based on the quick response of chlorophyll fluorescence lifetime to changes of the cellular environment, FLIM analysis can be used as a sensitive indicator of changes in cellular metabolism and stress before any structural changes are evident.

The disadvantages of using FLIM as a tool for monitoring culture health include the long sample preparation time required and the changes in cell metabolism that occur when the cells are taken out of their growth environment and placed on the microscope slide.

5.5 TCSPC

As it has been seen in the literature [102, 107, 108] and by using FLIM methods, higher plant- and microalgae cells undergo an increase in fluorescence lifetime when under stress. Single photon counting experiments were preformed on diluted samples of *N. oculata* cells using the setup described in Section 4.4.2. Measurements were preformed at various irradiation intensities to investigate the dependency of excitation light on the fluorescence lifetime τ_f of unaltered microalgae cells.

A new cell solution was used for each different intensity measurement in order to avoid any radiation effects from previous measurement on the cells. However, the cell concentration measured at each excitation intensity remained the same. Shown in Figure 5.7 are the normalized lifetime decay curves for the lowest and highest excitation

intensities measured, 30 μW/cm^2 and 1400 μW/cm^2, respectively. The data was fitted to Equation 4.2, and only one fluorescence lifetime component was resolved for each excitation intensity. The average fluorescence lifetime was determined for the solution containing *N. oculata* cells, as opposed to FLIM measurements where the fluorescence lifetime was determined for each pixel of the cell being examined under a microscope.

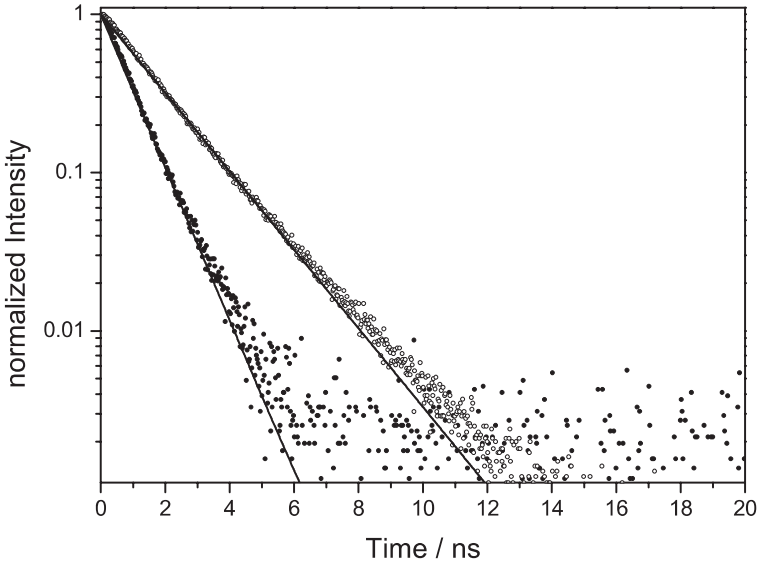

Figure 5.7: Normalized TCSPC decay results froma solution of *N. oculata* cells at excitation intensities of: 30 μW/cm^2 (full circles) and 1400 μW/cm^2 (open circles) and fit to Equation 4.2 (solid lines). λ_{textex} = 680 nm and the recorded emission wavelength is 685 nm.

As was previously discussed, an increase in fluorescence lifetime can be the result of damage or stress to the cells. Figure 5.8 shows the measured fluorescence lifetime corresponding to varying excitation intensities. Here the strong influence of the excitation intensity on the average fluorescence lifetime of *N. oculata* cells can clearly be seen. The fluorescence lifetime is an indication of the mechanisms involved in excitation light transfer and trapping. The photochemical state of reaction centers is heavily correlated with the fluorescence lifetime of the associated chlorophyll molecule [109, 110]. The open state reaction centers are capable of carrying out photosynthesis and are associated with a short fluorescence lifetime, while at the closed state reaction centers, photochemistry is not possible, and longer fluorescence lifetimes are characteristic [111].

The fluorescence lifetime of chlorophyll extracted from *N. oculata* cells with acetone was also measured at various excitation intensities. The lifetime obtained showed, as expected, no dependency on excitation intensity and at 5.12 ns was longer than the

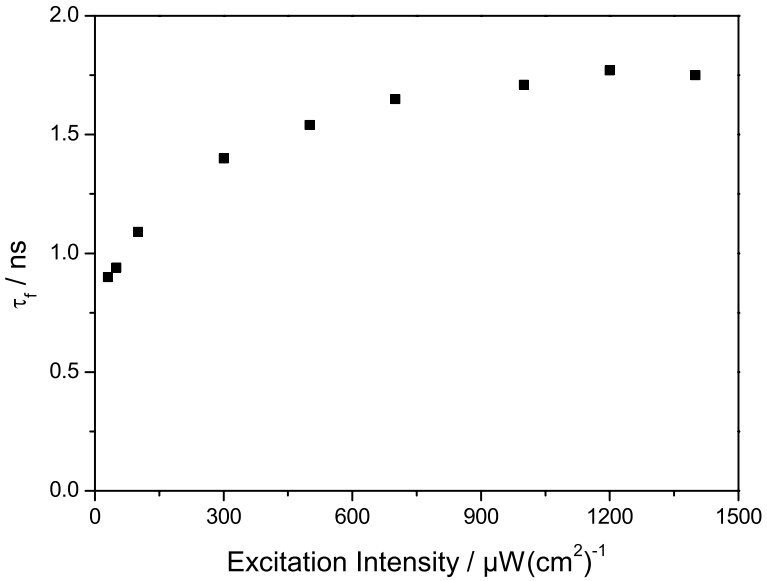

Figure 5.8: Time correlated single photon counting fluorescence lifetime results from *N. oculata* cells at varying excitation light intensity.

other average lifetimes observed with TCSPC experiments. Due to the fact that the cells and chloroplasts are no longer intact, the obtained lifetimes are not influenced by the state of photosystems, of which the structure has most likely been destroyed by the extraction process. This result agrees relatively well with the reported literature values for extracted chlorophyll a and b of approximately 6 ns [21, 112].

When seeking to optimize the growing conditions for microalgal cultures, Figure 5.8 can be used for the determination of the appropriate illumination intensity. Higher radiation intensity results in longer lifetimes, which is a result of cell stress or damage or photoinhibition and all of which lead to lower photosynthetic efficiency.

The disadvantages of using TCSPC for assessment of culture health include the need for sample dilution and preparation, and sometimes long data acquisition times. At low excitation energy intensity, data collection can take up to six hours. Fluorescence data is commonly used as a tool to relatively measure photosynthetic efficiency, but there is much disagreement in the data interpretation.

5.6 Cross Correlation DLS

3-D cross correlation DLS experiments, using the set-up described above were carried out on *C. vulgaris* cells in a cylindrical cuvette. The measurements were made 10 times at detection angles from 30 to 150°, every 15 degrees, for 300 seconds. The scattering

cell was immersed in an index matching fluid vat containing toluol. Figure 5.9 shows the cross correlation function vs. τ for milk powder (left) and *C. vulgaris* cells (right), at a detection angle of 60°.

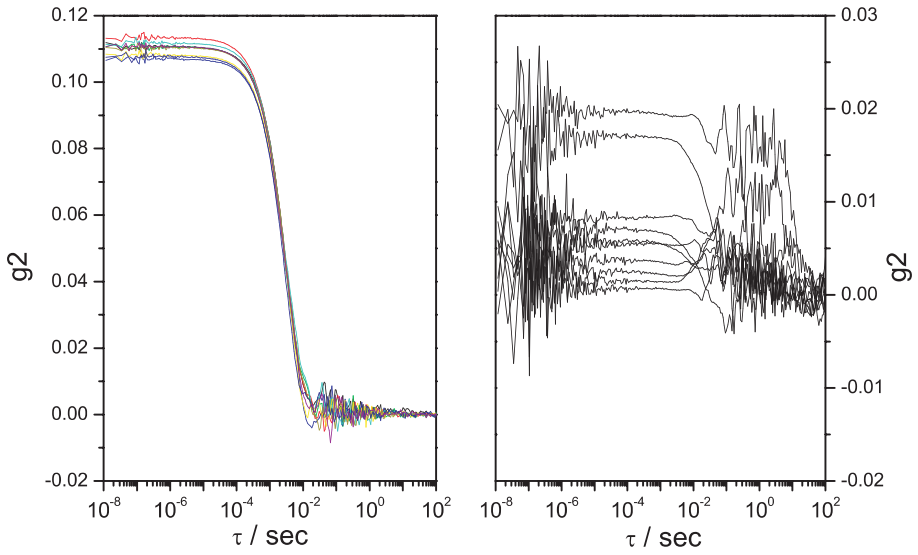

Figure 5.9: Left: Cross correlation function for milk powder at a detection angle of 60°. Right: Cross correlation function of *C. vulgaris* at a detection angle of 60°. The measurements were repeated 10 times and the cross correlation function of each measurement is shown. The smaller milk particles provide a good system for cross correlation analysis, the correlation function is reproducible and consistent. The larger *C. vulgaris* cells do not provide reproducible or consistent results, making then unsuitable for cross correlation spectroscopy.

Milk powder particles have a diameter of approximately 0.2 to 0.6 μm, display good reproducibility of the cross correlation function and are well suited for analysis with 3-D cross correlation spectroscopy. *C. vulgaris* cells, on the other hand, have a diameter of well over one μm, show no reproducible cross correlation function, and are unsuitable for such analysis. When analyzing larger particles (diameter larger than one μm) an appropriate number of particles can not be accommodated into the small scattering volume, yielding a bad cross correlation.

5.7 Modulated Diode Laser Spectroscopy

The use of photon density wave spectroscopy was applied for the on-line examination of the absorption and scattering properties of microalgae cells. The use of high frequency

modulated light allows for an independent determination of the absorption and reduced scattering coefficients, μ_a and μ_s', respectively.

For this study, two different experimental setups were implemented: a cost-efficient, simple configuration utilizing low frequency modulation, and a more sophisticated construction containing a network analyzer able to achieve modulation frequencies up to 1.3 GHz.

5.7.1 Low Frequency Intensity Modulation Results

In order to characterize the absorption and scattering properties of a liquid sample using a diode laser as the light source, the wavelength has to be appropriately chosen such that both the absorption and scattering properties can be exploited. Figure 5.2 was used to chose a wavelength where both absorption and scattering can be detected in samples of *N. oculata* cells. Because 785 nm meets the aforementioned requirements and diodes at this wavelength are readily available and inexpensive, it was selected as the light source wavelength for these studies.

A solution of *N. oculata* cells with an initial concentration of 7.0 g/L DW was analyzed using a home-made diode laser spectrometer, at 785 nm, and 1.0 kHz fixed modulation frequency. The frequency was constant throughout the duration of the data collection. The scattered light intensity was measured as voltage at each r before the translation stage moved the detector fiber to the next distance. This process was repeated nine more times and the results were averaged. The results of the linearization of the intensity as a function of r are shown in Figure 5.10.

The samples with a higher cell concentration display good linearity between $\ln(I\ r)$ and r for all measured r, which are significantly smaller than those measured at low cell concentrations. The samples containing a lower concentration of cells displayed a linear relation first at larger separation distances. It can be assumed that at low concentrations, where there is no linear relationship between $\ln(I\ r)$ and r at small r, the assumptions for the standard diffusion equation are not met, namely that the source light is not multiply scattered before reaching the detector. In this case, the lowest concentration measured corresponds to 0.77 gL^{-1} DW, which is below the usual inoculation concentration of approximately one gL^{-1} DW for cells in a PBR [113, 114].

The square of the slope of the data points in the linear region in Figure 5.10 for each concentration measured was plotted against cell concentration gL^{-1} DW and fitted using Equation 4.7. Figure 5.11 shows the results of this analysis.

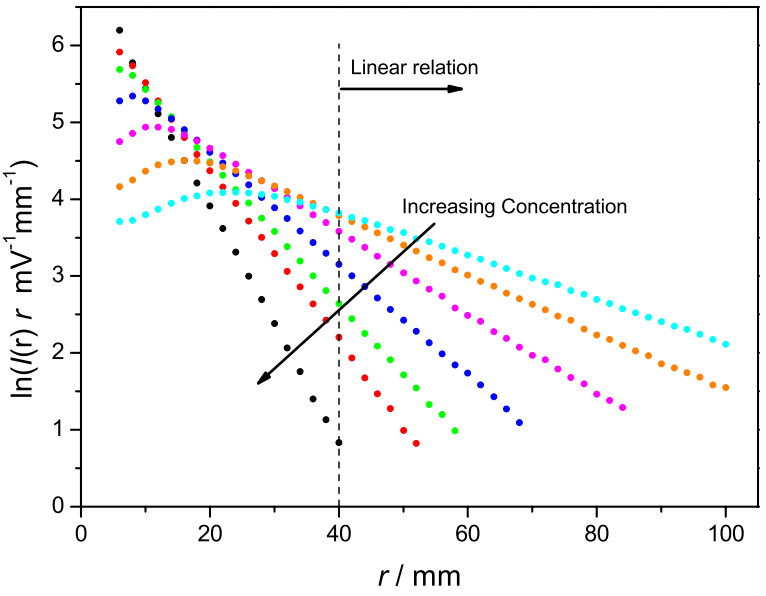

Figure 5.10: *N. oculata* cells analyzed at 735 nm. ln(Ir $mV^{-1}mm^{-1}$) vs. r for varying cell concentrations (for the sake of clarity, not all concentrations measured are shown here). The dashed line shows approximately the minimum r for a linear relationship at the lowest concentration measured.

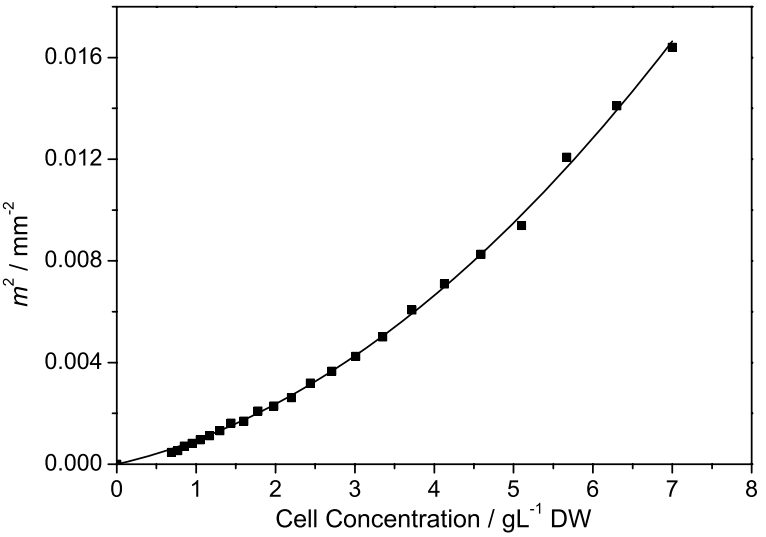

Daten: Data2_B
Modell: lowfreq fit
Gleichung: y = 3 * (0.001586 * x * P1
Gewicht:
y Keine Gewichtung.

Chi^2/DoF = 2.4667E-8
R^2 = 0.99888

P1 0.14795 ±0.00638
P2 0.00054 ±0.00004

Figure 5.11: A quadratic fit (solid line) using Equation 4.7 of m^2 of each different cell concentration measured in Figure 5.10 and known cell concentration. The concentration dependent absorption and reduced scattering coefficients were determined by the fit.

The literature value applied for the absorption coefficient of water is $1.5859 \cdot 10^{-6}$ μm^{-1} at 725 nm [115]. The concentration dependent absorption and reduced scattering

coefficients obtained from this fit were determined to be $(5.4 \pm 0.4) \times 10^{-4}$ mm^{-1}[C$_c$] and 0.148 ± 0.006 mm^{-1}[C$_c$], respectively, where [C$_c$] is the dry weight concentration of the cell solution.

5.7.2 High Frequency Intensity Modulation Results

Determination of Appropriate Modulation Frequency Range

Using the high frequency intensity modulation set-up, modulation frequencies up to and including 1.3 GHz are available. In many cases, the use of higher modulation frequencies is advantageous for a variety of reasons, including: smaller sample volume required and better resolution due to increasing phase shift at higher frequencies [71, 116]. However, a disadvantage of using high modulation frequencies is that the signal to noise ratio also increases with increasing frequency.

In Section 5.7.1 it was discussed that the results analysis takes advantage of the linear relationship between $\ln(I\ r)$ and r. And since, when dealing with dilute cultures, that relationship is first evident at larger r, the ability to carry out measurements over large source/detector separation distances is crucial.

Figure 5.12 shows the effect of modulation frequency on the detected scattered light intensity at different r in a *C. vulgaris* culture containing approximately 1.0 gL^{-1} DW. The left diagram illustrates that the signal to noise ratio becomes larger at high modulation frequencies and small r. In the diagram on the right, the modulation frequency is lower and detected intensity is clearly distinguishable from the background signal at large r.

PDW Data Analysis

The following data and error analysis methods are based on the theory developed in [80]. Although this method was tested here as an on-line analysis procedure, the sample calculations and data analysis procedure outlined in this section is for one constant cell concentration in a solution of *N. oculata* cells in the nutrient solution. Here, the cell concentration determined by the centrifugation procedure described in section 4.1 is (2.41 ± 0.02) gL^{-1} DW. Although data was collected at 51 different frequencies from 0.3 – 650.15 MHz (approximately every 13 MHz), for clarity purposes, only 11 frequencies (approximately every 65 MHz) are displayed. The results following the increase in cellular concentration with a culture will be addressed in the following section.

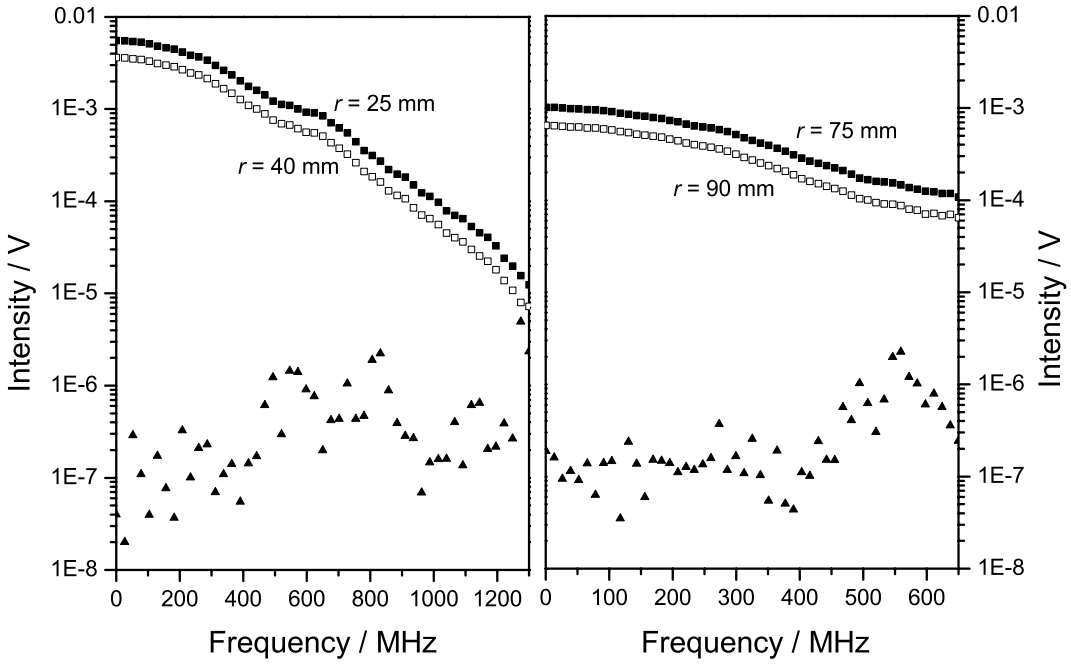

Figure 5.12: Detected intensity in relation to modulation frequency at varying r in a dilute cell culture solution. The triangles represent the background measurement. Left: 0.3 − 1300 MHz modulation frequency. Right: 0.3 − 650 MHz modulation frequency.

PDW experiments with intensity modulation at 51 frequencies f between 0.3 and 650.15 MHz and with an incident wavelength of 785 nm were conducted to independently determine the reduced scattering and absorption coefficient without the need for sample dilution. In order to achieve this, detection of the phase lag ϕ between the sinusoidally modulated laser intensity at source and detector separation distances r is necessary. The frequency was varied at each r before the translation stage moved the detector fiber to the next distance. This process was repeated nine more times, and the collected data was averaged.

The relationship between the intensity, source/detector separation distance r, and the frequency f can be described according to Equation 5.2:

$$I(r, f) = \frac{I_0(f)}{r} \exp\left[-k_{\mathrm{I}}(f)\, r\right] \tag{5.2}$$

Figure 5.13 shows a sample of the measured intensity data in relation to r at varying modulation frequencies. The measurements were linearly fitted according to Eqn. 5.2. The detected intensity decreases with increasing r at the same frequency. This is to be expected due to the influences of μ_{a} and μ_{s}' on the intensity coefficient, and the

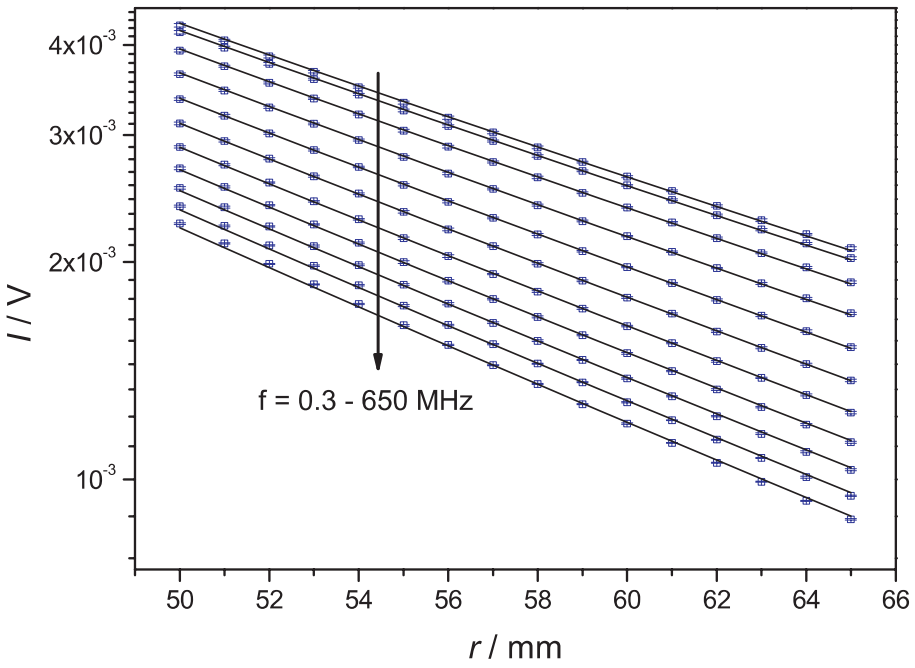

Figure 5.13: Measured intensity (squares) with error bars, and fits (lines) in relation to source and detector distances r at several different frequencies for a solution of *N. oculata* cells of concentration (2.41 ± 0.02) gL^{-1} DW. The direction of the arrow shows the increase in frequency.

properties of the diffusing wave.

A linearization of the dependency of r on the intensity I is necessary so that an analytical fit of the data is possible. Taking into consideration the standard deviation of the mean of the intensity for 10 measurements (σ_{I}), Equations 5.3 and 5.4 are applied for the linearization and treatment of the error.

$$\ln\left[I(r,f)r\right]_{r_i f_j} = \ln\left[I(r_i,f_j)r_i\right] - 0.5\frac{\sigma_I^2(r_i,f_j)}{I^2 r_i,f_j} \tag{5.3}$$

$$\sigma_{\ln Ir}(r,f)_{r_i,f_j} = \frac{\sigma_I(r_i,f_j)}{I_{r_i,f_j}} \tag{5.4}$$

The linear fit of ln[$I(r,f)r$] can be calculated by:

$$\ln[I(r,f)r] = \ln[I_0(f)] - k_i(f)r \tag{5.5}$$

The linearization of the measured intensity in dependence of r, the analytical fit and error are shown in Figure 5.14. The sample solution measured and frequencies displayed are the same as those previously described in this section. The data proved

to be compatible with linearization using Eqn. 5.5 for the whole range of frequencies applied.

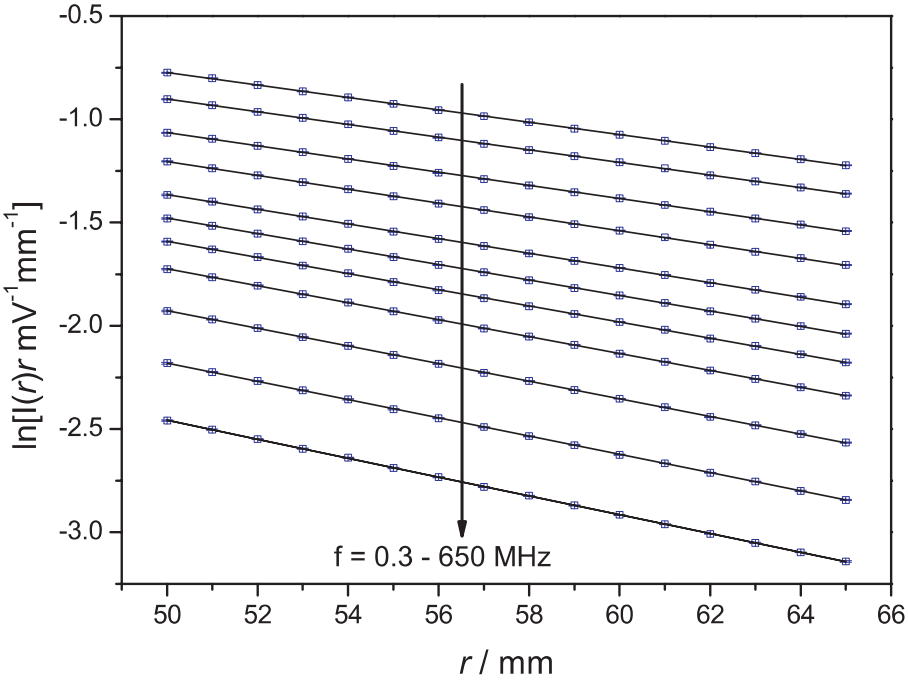

Figure 5.14: ln(*I(r,f)r*) (squares) with error bars, and linear fit according to Equation 5.5(lines) in relation to source and detector distances r at several different frequencies for a solution of *N. oculata* cells of concentration (2.41 ± 0.02) gL^{-1} DW. The direction of the arrow shows the increase in frequency.

According to Equation 5.6, a linear relation between the measured phase Φ, the phase coefficient k_Φ and r already exists. In Figure 5.15, the difference between the phase measured at r and the smallest measured distance r_0 according to Equation 5.7 is depicted.

$$\Phi(r, f) = \Phi(f) + k_\Phi(f)r \tag{5.6}$$

$$\Phi(r, f) - \Phi(r_0, f) = k_\Phi(f)\,[r - r_0] \tag{5.7}$$

Because the photon path between source and detector increases with increasing r, the phase also increases. The phase coefficient k_Φ increases as well with increasing frequency.

The rearrangement of equations 3.42 and 3.43 leads to a solution for the intensity

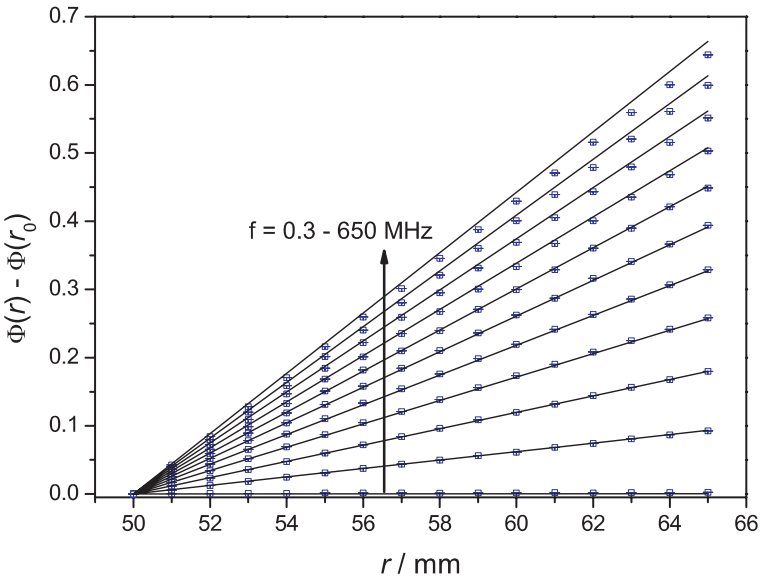

Figure 5.15: Phase difference in relation to r_0 (squares) with error bars, and fits (lines) in relation to source and detector distances r at several different frequencies for a solution of *N. oculata* cells of concentration (2.41 $\pm$ 0.02) gL^{-1} DW. The direction of the arrow shows the increase in frequency.

and phase coefficients to which a nonlinear fitting procedure can be applied to obtain information about the scattering and absorption properties of the medium.

$$k_I = \sqrt{\frac{2}{3}\left(\sqrt{\left[\left[\alpha\mu_\mathrm{a}+\mu_\mathrm{s}'\right]^2+\frac{4\pi^2f^2}{c^2}\right]\left[\mu_\mathrm{a}^2+\frac{4\pi^2f^2}{c^2}\right]}+\mu_\mathrm{a}\left[\alpha\mu_\mathrm{a}+\mu_\mathrm{s}'\right]-\frac{4\pi^2f^2}{c^2}\right)} \quad (5.8)$$

$$k_\Phi = \sqrt{\frac{2}{3}\left(\sqrt{\left[\left[\alpha\mu_\mathrm{a}+\mu_\mathrm{s}'\right]^2+\frac{4\pi^2f^2}{c^2}\right]\left[\mu_\mathrm{a}^2+\frac{4\pi^2f^2}{c^2}\right]}-\mu_\mathrm{a}\left[\alpha\mu_\mathrm{a}+\mu_\mathrm{s}'\right]+\frac{4\pi^2f^2}{c^2}\right)} \quad (5.9)$$

where $c = c_0/n$, the speed of light in water. Both k_I and k_Φ increase with increasing frequency. k_I is influenced by the demodulation of the light at higher frequencies, which is due to the different lengths of the photon paths. $k_\Phi$approaches zero at small frequencies and increases with intensity, which is also caused by the different photon path lengths.

The intensity and phase coefficients k_I and k_Φ, respectively in relation to frequency

calculated for a solution of *N. oculata* cells of concentration (2.41 ± 0.02) gL^{-1} DW are displayed in Figure 5.16.

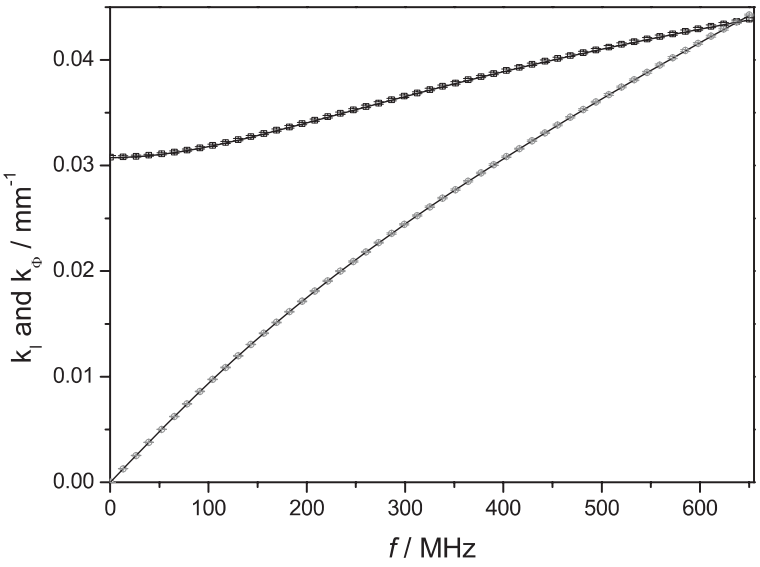

Figure 5.16: Intensity (black) and phase (grey) coefficients, with error bars and simulated values from Equations 5.8 and 5.9, respectively (lines) for a solution of *N. oculata* cells of concentration (2.41 ± 0.02) gL^{-1} DW

From k_{I} and k_{Φ} and applying Equations 3.44 and 3.45, the absorption and reduced scattering coefficients can be calculated:

$$\mu_{\mathrm{a}}(f) = \frac{ck_{\mathrm{I}}(f)k_{\Phi}(f) - \sqrt{c^2k_{\mathrm{I}}^2(f)k_{\Phi}^2(f) - 12\pi^2f^2\left[k_{\mathrm{I}}^2(f) - k_{\Phi}^2(f) + 12\pi^2f^2c^{-2}\right]}}{6\pi f} \tag{5.10}$$

$$\begin{aligned}\mu_{\mathrm{s}}'(f) &= \frac{[1-\alpha]\,ck_{\mathrm{I}}(f)k_{\Phi}(f)}{6\pi f} \\ &+ \frac{[1+\alpha]\,\sqrt{c^2k_{\mathrm{I}}^2(f)k_{\Phi}^2(f) - 12\pi^2f^2\left[k_{\mathrm{I}}^2(f) - k_{\Phi}^2(f) + 12\pi^2f^2c^{-2}\right]}}{6\pi f}\end{aligned} \tag{5.11}$$

Assuming that the error associated with $k_{\mathrm{I}}(f)$ and $k_{\Phi}(f)$ are not correlated, the error representative of μ_{a} and μ_{s}' can be calculated according to:

$$\sigma_{\mu_{\mathrm{a}}}(f_{\mathrm{i}}) = \sqrt{\left[\left.\frac{\partial\mu_{\mathrm{a}}(f)}{\partial k_{\mathrm{I}}}\right|_{\mathrm{f_I}}\sigma_{\mathrm{k_I}}(\mathrm{f_i})\right]^2 + \left[\left.\frac{\partial\mu_{\mathrm{a}}(f)}{\partial \mathrm{k}_{\Phi}}\right|_{\mathrm{f_i}}\sigma_{\mathrm{k}_{\Phi}}(f_{\mathrm{i}})\right]^2} \tag{5.12}$$

$$\sigma_{\mu'_{\mathrm{s}}}(f_{\mathrm{i}}) = \sqrt{\left[\left.\frac{\partial \mu'_{\mathrm{s}}(f)}{\partial k_{\mathrm{I}}}\right|_{\mathrm{f_I}} \sigma_{\mathrm{k_I}}(\mathrm{f_i})\right]^2 + \left[\left.\frac{\partial \mu'_{\mathrm{s}}(f)}{\partial \mathrm{k}_{\Phi}}\right|_{\mathrm{f_i}} \sigma_{\mathrm{k}_{\Phi}}(f_{\mathrm{i}})\right]^2} \tag{5.13}$$

where $\sigma_{\mu_{\mathrm{a}}}(f)$ and $\sigma_{\mu'_{\mathrm{s}}}(f)$ can be calculated with:

$$\sigma_{\mathrm{z}} = \sqrt{\left[\left.\frac{\partial z}{\partial x}\right|_{\mathrm{z}}\right]^2 \sigma_{\mathrm{x}}^2 + \left[\left.\frac{\partial z}{\partial y}\right|_{\mathrm{z}}\right]^2 \sigma_{\mathrm{y}}^2} \tag{5.14}$$

The results recovered for the solution of *N. oculata* cells of concentration (2.41 ± 0.02) gL^{-1} DW which was used in this section to demonstrate the data analysis process are: $\mu_{\mathrm{a}} = (4.743 \pm 0.009) \times 10^{-3}$ mm^{-1} and $\mu'_{\mathrm{s}} = (6.512 \pm 0.007) \times 10^{-2}$ mm^{-1}. Applications for μ_{a} and μ'_{s} will be discussed in the next section.

5.8 On-line Determination of Cellular Optical Properties

High frequency photon density wave spectroscopy was applied as an on-line technique for the observation of microalgae growth during cultivation. PDW measurements were taken twice a day and culture samples were also collected so that the cell concentration could be analytically determined via centrifugation and drying.

The corresponding increase in cell concentration with time during the cultivation process is shown in Figure 5.17. The cell concentration was determined via sample centrifugation and drying. In the culture shown here, the gas feed supply was shut off after approximately 140 hours, corresponding with the beginning of the death phase (see section 2.2). During the death phase, which is onset due to the limitation of light, minerals or nutrients, the accumulation of toxic wastes in the culture, or a combination of these factors, the algal cells die and release organic, often growth-inhibiting materials into the medium [10]. Cultures of some species will lose their pigmentation and appear washed out or cloudy, whereas cells of other species may lyse (no recognizable cells), releasing organic materials which support bacterial growth, but the culture color will be maintained. The latter is an important consideration and one reason why color should not be relied upon to gauge culture health.

In Figure 5.18, the increase in both and absorption μ_{a} and reduced scattering μ'_{s} coefficients with cultivation time can be seen. μ_{a} and μ'_{s} and their associated errors were calculated using equations 5.10 and 5.11.

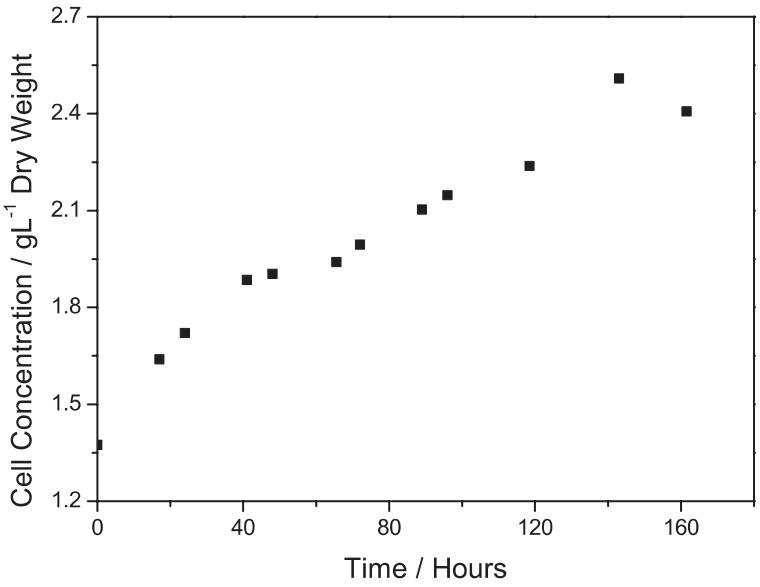

Figure 5.17: The increase in cell concentration with time for a cultivation of *N. oculata* cells.

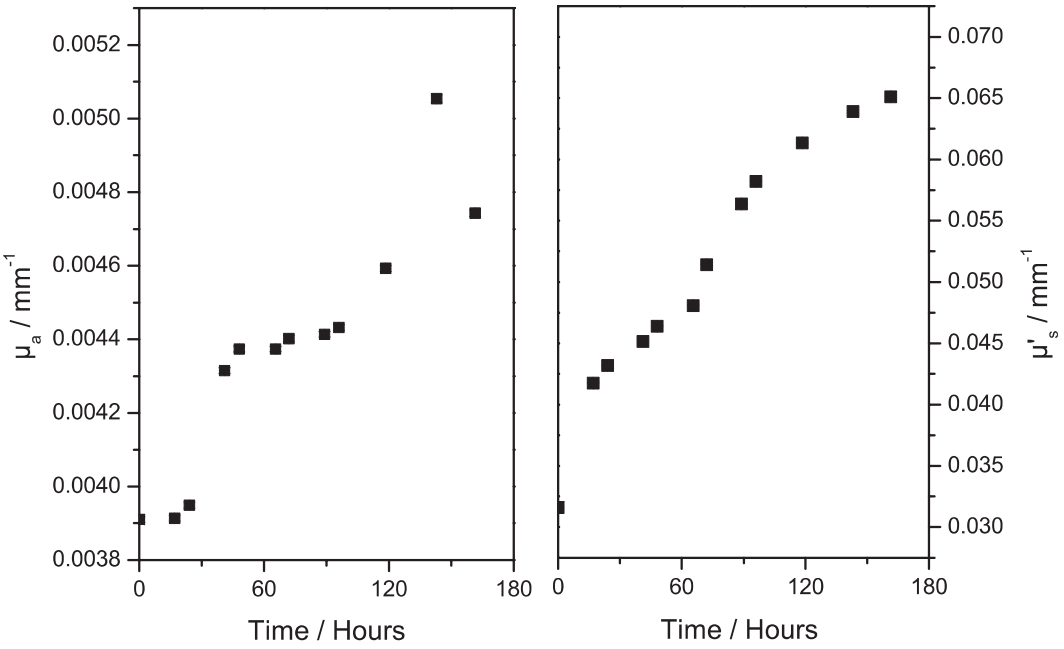

Figure 5.18: μ_a (Left) and μ_s' (Right) in relation to cultivation time for a solution of *N. oculata* cells during the cultivation process.

The calculated μ_a and μ_s' for the cell culture in relation to the cellular concentration is shown in Figure 5.19.

The optical coefficients μ_a and μ_s' of a microalgae culture can be calculated during

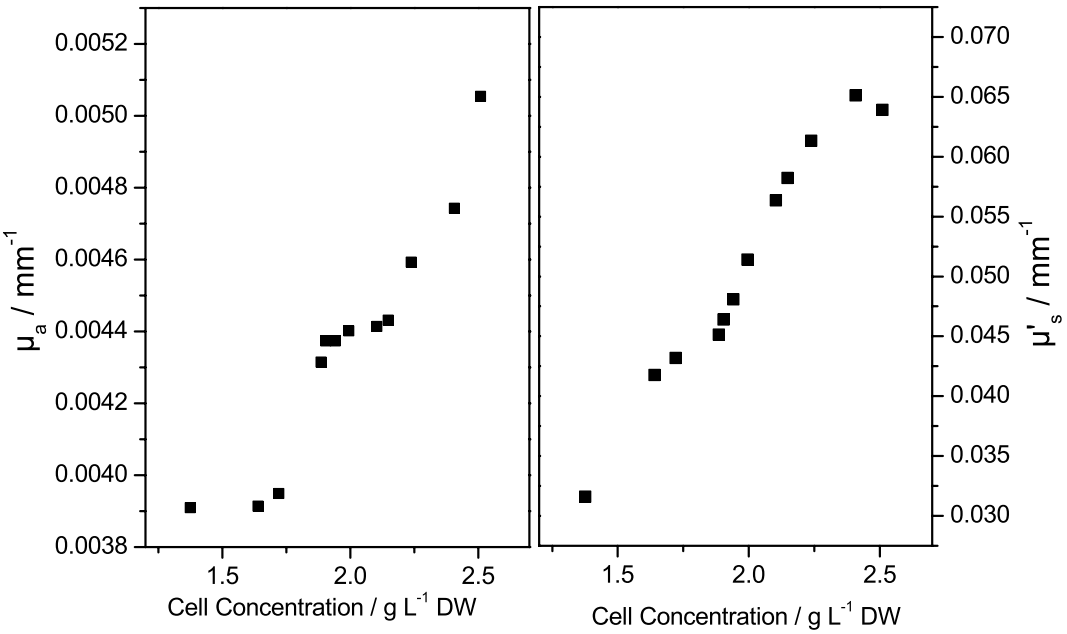

Figure 5.19: μ_a (Left) and μ_s' (Right) in relation to culture concentration for a solution of *N. oculata* cells during the cultivation process.

cultivation using high frequency PDW spectroscopy. Both parameters show an increase over time and in relation to increasing cellular concentration, which is to be expected because as the number of cells in the culture increases, more scatterers and absorbing particles are present.

The onset of the death phase, identifiable in Figure 5.17 by the decrease in concentration after approximately 140 hours, corresponds with a decrease in the absorption coefficient, but a further increase in the reduced scattering coefficient. The absorption coefficient decreases due to a loss of pigmentation or a shortage of essential minerals including iron, which causes cellular bleaching [10]. The increase in the reduced scattering coefficient may be attributed to the fact that the cells can begin to lyse but the scatterers are still present in the solution. The strong correlation between cellular concentration and the absorption and reduced scattering coefficients provides the basis for the on-line detection of the increase in microalgae biomass over time and the ability for real time determination of changes in cellular concentration in a culture.

Experiments were also performed to investigate the effect of air bubbles which form during cultivation, or the presence of beads frequently added to PBR systems to prevent flocculation or algae build up on the walls of the PBR. It was determined that the presence of both types of larger particles did not influence the calculated μ_a or μ_s'. Due

to the large set of data collected, if a foreign particle was detected, it's presence would not statistically impact the results.

Taking advantage of the linear relationship between the cell concentration and the cell number density ${}^1N$ in the culture, the reduced scattering coefficient can be applied to gain insight into the approximate cell number density in the cultivation, as shown in Figure 5.20.

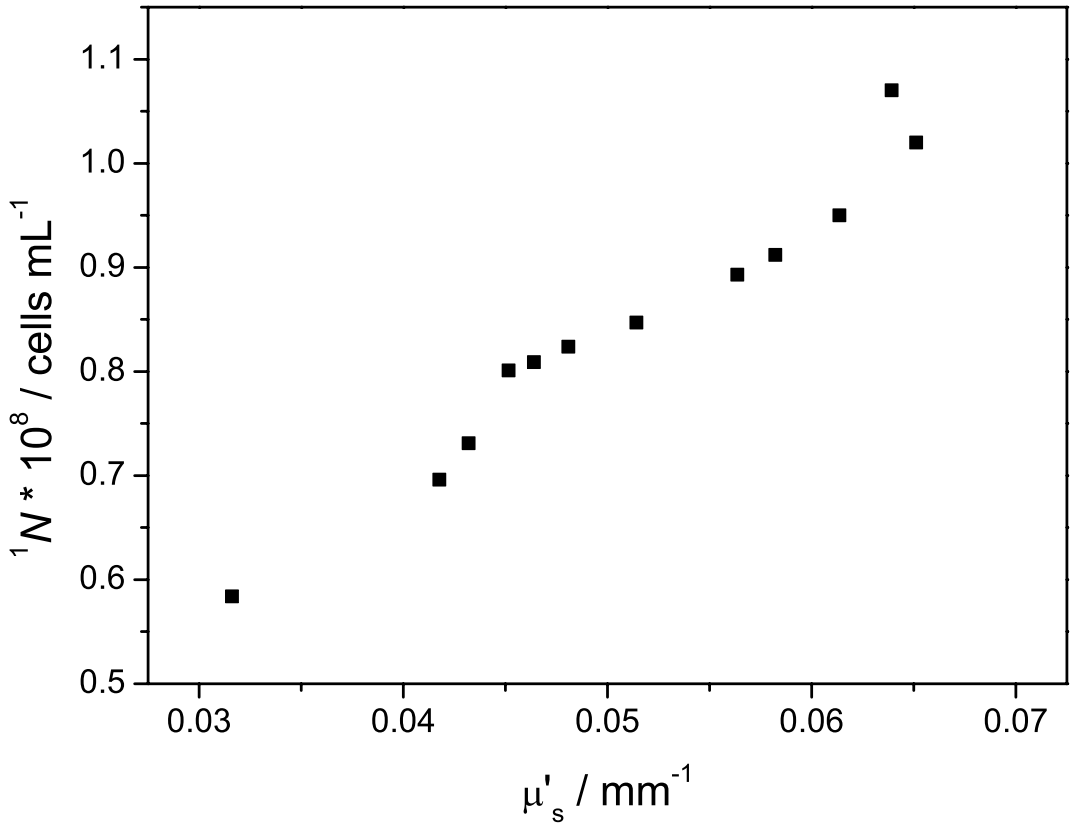

Figure 5.20: The average cell number density ${}^1N$ can be determined during cultivation with knowledge of μ'_s.

5.9 Determination of Particle Size

With the application of Mie theory, it is possible to determine the average particle size of particles in solution. Using the index of refraction of water and of the algae cells, the wavelength and the computer program MieCalc 1.0 (Simuloptics GmbH, Schwabach, Germany), the numerical solutions for the scattering efficiency Q_s and the anisotropy factor, g were obtained.

Q_s and g for a solution for algae cells is shown in Figure 5.21. The relative refractive index of microalgae cells in salt water is 1.05 [117, 118, 119].

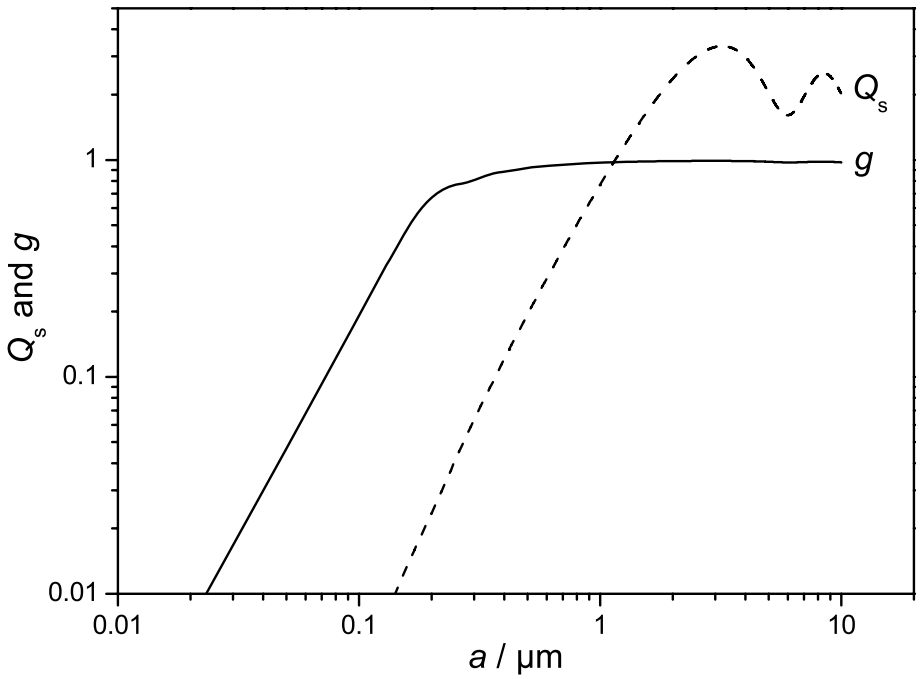

Figure 5.21: The scattering efficiency Q_s (dashed line) and anisotropy factor g (solid line) dependency on particle radius for microalgae cells in water.

Equations 3.23 and 3.24 were used to calculate the specific reduced scattering coefficient τ'_{Mie}, shown in Figure 5.22.

Using the μ'_s calculated from PDW experiments, it is possible to calculated an experimental τ'_{Exp} as a function of the cell radius a. The intersection of the τ'_{Mie} calculated from Mie theory and the experimental τ'_{Exp} leads to an estimate of the average particle size of the cells in the solution. In the inset of Figure 5.22, the various τ'_{Exp} calculated from the reduced scattering coefficients shown in Figure 5.19 are shown. The calculated average particle size increases with the reduced scattering coefficient from approximately 2.38 to 2.57 μm.

Applying τ'_{Exp} to obtain the average particle size in the cell culture, the relationship between the calculated a and cultivation time is shown in Figure 5.23. The average cell size in a cultivation has been shown to be dependent on irradiance levels [120], and to be a factor in nutrient uptake [121].

Here is has been shown that PDW spectroscopy can be used as an on-line tool for the monitoring of microalgae cell cultures. The strong correlation that exists between

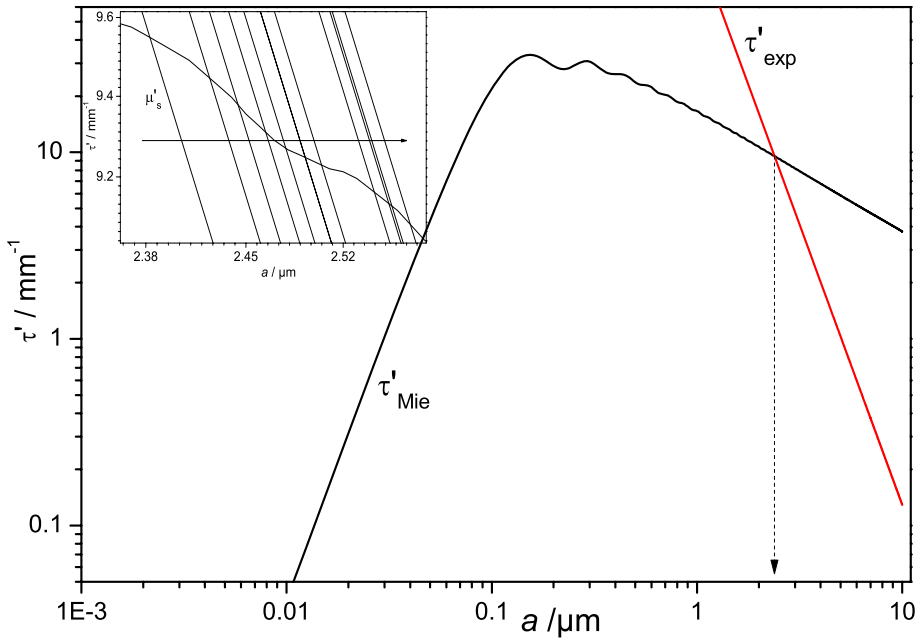

Figure 5.22: The specific reduced scattering coefficient τ' for microalgae cells in water. The dashed line indicates the average particle size for a solution of *N. oculata* cells with $\mu'_s = 0.0316$ mm^{-1}. Inset: experimental τ'_{Exp} for the various μ'_s shown in Figure 5.19. The intersection of the τ'_{Mie} obtained from Mie theory calculations and the experimental τ'_{Exp} can be used to obtain the average particle size. The arrow indicates increasing μ'_s.

cellular concentration and the absorption and reduced scattering scattering coefficients can be used as a real time indicator of changes in the concentration of microalgae cells during cultivation. The determination of the average size of the cells in the culture is also possible with the application of Mie theory and the calculated reduced scattering coefficient.

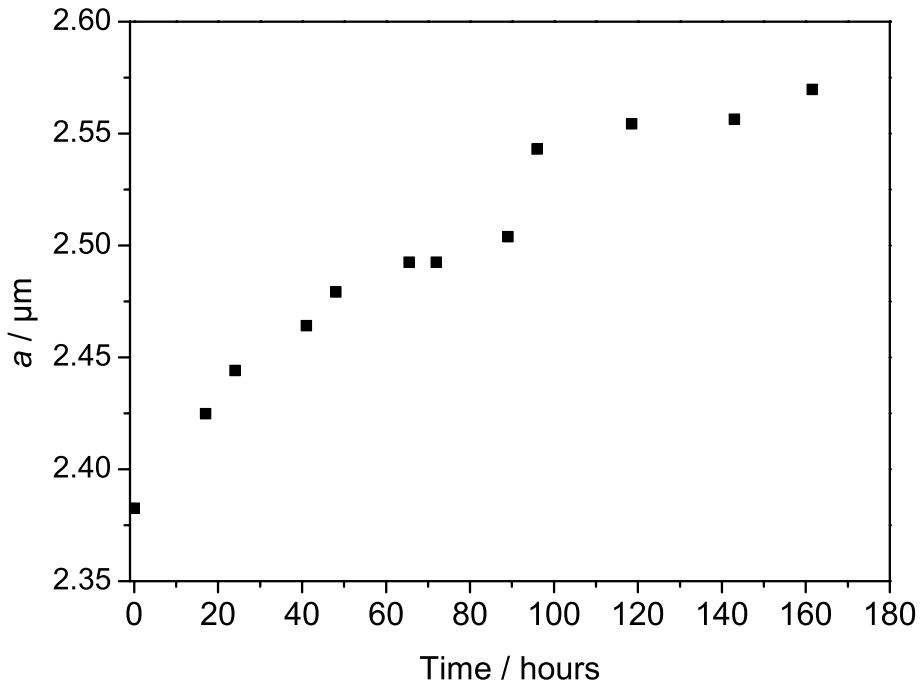

Figure 5.23: The relationship between the calculated particle size and cultivation time.

Chapter 6

Summary and Outlook

In this work several spectroscopic methods were applied for the characterization of microalgae cells, and photon density wave (PDW) spectroscopy was used as a real time analysis method for the the determination of cell size and cell number density.

Single cellular *Chlorella vulgaris* and *Nannochloropsis oculata* microalgae that were used for experiments and as inocula were provided by the Institut für Lebensmittel- und Umweltforschung e.V., in Bergholz-Rehbrücke, Germany. The composition, nutrient requirements and growth process have been described. A home made photobioreactor was constructed from an illumination source, gas feed, stirrer and glass vessel and was implemented for microalgae cultivation in these experiments.

In order to properly evaluate the increase of biomass in a photobioreactor, a real time system which analyzes the relevant biological and technical process parameters is preferred. Because many of the traditional spectroscopic methods require long sample preparation times, or the dilution of a sample, they are not suitable for real time analysis.

The fluorescence lifetime properties of microalgae cells were examined using fluorescence lifetime imaging microscopy (FLIM) and time correlated single photon counting (TCSPC). Fluorescence lifetime can be applied as an indication of the state or condition of the cell or photosystem. FLIM provides a graphic of a sample of cells under a microscope and collects fluorescence intensity and lifetime data by way of pixel by pixel single photon counting analysis. TCSPC experiments provide an average lifetime of the fluorophores in a solution by means of a statistical analysis of photon emission after an excitation event.

Both methods of fluorescence analysis provided evidence that cells under stress (ex: photoinhibition, water stress, damage) display a longer characteristic fluorescence lifetime. The effects of excitation light intensity on fluorescence lifetime were investigated

with TCSPC experiments, and it was found that the lifetime increases with increasing excitation light, indication photoinhibition. With FLIM measurements, a shift towards longer lifetimes in the measured lifetime distribution can be observed after the cell was stored on the unnatural conditions of a microscope slide.

Light scattering experiments were carried out on the cells, which can not be properly classified with extinction spectroscopy. Due to multiple scattering effects, undiluted samples do not adhere to Beer's law, which requires knowledge of the optical path-length. 3-D cross correlation dynamic light scattering experiments were carried out, which function on the basis of suppressing multiple scatting effects by performing two scattering experiments simultaneously on the same scattering volume with two incident light beams. However, due to the large diameter of the cells examined and the small scattering volume, a reproducible cross correlation function could not be observed.

Background and theory was provided for the propagation of light in turbid medium and the data analysis involved in PDW spectroscopy. A photon density wave is a sinusoidally intensity-modulated optical wave stemming from a point-source of light, which propagates through diffuse medium and exhibits amplitude and phase variations. The P_1 approximation to the Boltzmann transport equation was used as in order to make an independent determination of the reduced scattering and absorption coefficients, which is not accessible using traditional forms of spectroscopy.

Two different PDW experimental set-ups were implemented in this study, one involving low frequency modulation and the other capable of up to 1.3 GHz modulation frequencies. Both were used as real time measurement techniques and the course and detector optical fibers were submerged into the cultivation sample. Because the low frequency set-up only collected scattered light intensity and didn't involve analysis of the phase lag, the absorption and reduced scattering coefficient would not be independently determined. This set-up was used for the determination of the optical properties as a function of cell concentration and information was still gained about the increase in biomass in the cell culture.

PDW spectroscopy measurements at high modulation frequencies enabled the independent determination of the absorption and reduced scattering coefficient. The absorption coefficient is related to the pigment content in the cells, and the reduced scattering coefficient can be used to characterize physical and morphological properties of the medium. With the application of Mie theory, it is possible to determine the average particle size of particles in solution. Using the index of refraction of water and of the algae cells, the wavelength and the computer program MieCalc 1.0 (Simuloptics

GmbH, Schwabach, Germany), the numerical solutions for the scattering efficiency Q_s and the anisotropy factor, g were obtained. With the knowledge of the scattering efficiency and the reduced scattering coefficient, the specific reduced scattering coefficient could be obtained, which leads to the average particle size for the cells in the culture. The relationship between average cell size and time for a culture of *N. oculata* cells could be shown.

Since the 1960's, there has been a rapid increase in the use of microalgae for in various industries including high-protein nutrition sources and supplements, antibiotic production, wastewater quality improvement, and renewable energy generation. Since the interest in microalgae is not slowing, it is important to have a fast and effective method for the characterization of the culture. Various spectroscopic techniques which are capable of providing information about the state of the culture in a PBR have been discussed here, however, most involve sample preparation time, require that samples be taken, involve long data acquisition times or cannot properly classify the medium.

With the implementation of PDW spectroscopy as a real time monitoring device, information about the cell number density and average cell size can be obtained. This method proved to be an effective tool for the characterization of microalgae cells in a photobioreactor during cultivation.

Appendix A

Nutrient Solution Composition

Component	Amount (g)
KNO_3	25
$MgSO_4$ * $7\,H_2O$	12.5
KH_2PO_4	6.25
EDTA	0.185
$FeSO_4$ * $7\,H_2O$	0.045
Micro-Nutrient Solution	5 mL

Table A.1: Nutrient Solution for 5 L cell suspension

Component	Amount (g/L)
H_3BO_3	2.86
$MnCl_2$ * $4\,H_2O$	1.81
$ZnSO_4$	0.222
MoO_3	0.023
NH_4VO_3	0.023

Table A.2: Micro-Nutrient Solution

Appendix B

Fiber Attenuation Loss

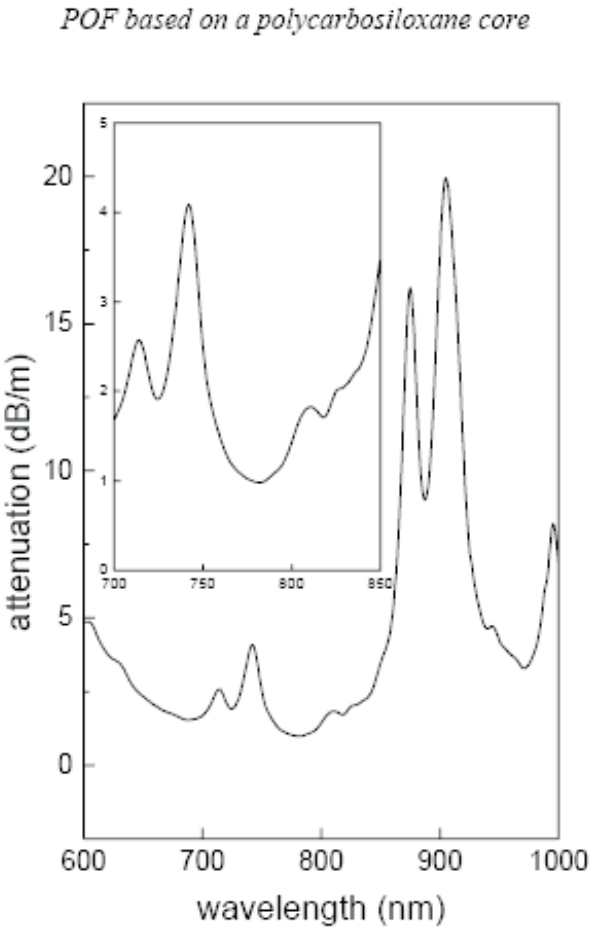

Figure 4. *The attenuation spectrum of the polycarbosiloxane based plastic optical fiber. The optical loss has been determined from 600 to 1000 nm. The lowest loss has been registered at 780 nm being 0.98 dB/m.*

Figure B.1: Attenuation loss of a plastic optical fiber [122].

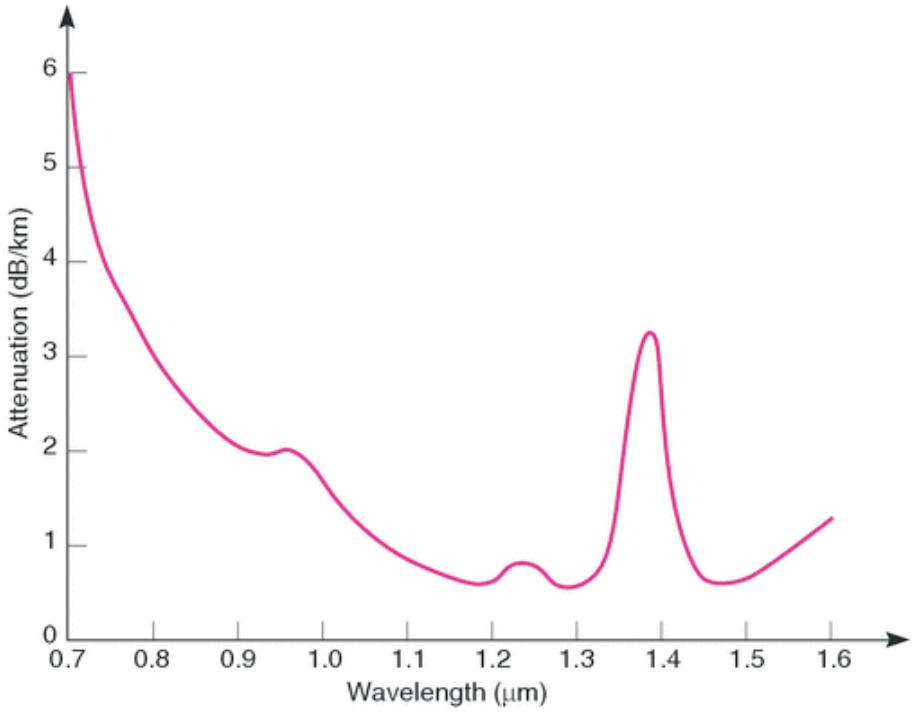

Figure B.2: Typical attenuation loss of silica optical fibers [123].

Bibliography

[1] R. Atlas. *Microbiology: fundamentals and applications.* Macmillian Publishing Company, New York, second edition, 1988.

[2] M.A. Borowitzka. Commercial production of microalgae: ponds, tanks, tubes and fermenters. *J. Biotechnol.*, 70:313–322, 1999.

[3] S. Kreitlow, S. Mundt, and U. Lindequist. Cyanobacteria - a potential source of new biologically active substances. *J. Biotechnol.*, 70:61–64, 1999.

[4] O. Pulz. Photobioreactors: production systems for phototrophic microorganisms. *Appl. Microbiol. Biotechnol.*, 57(3):287 – 293, Oct 2001.

[5] I. Maruyama, T. Nakao, I. Shigeno, Y. Ando, and K. Hirayama. Application of unicellular algae chlorella vulgaris for the massculture of marine rotifer brachionus. *Hydrobiologia*, 358:133–137, 1997.

[6] O. Pulz and W. Gross. Valuable products from biotechnology of microalgae. *Appl. Microbiol. Biotechnol.*, 65:635–648, 2004.

[7] M.A. Borowitzka. Microalgae as sources of pharmaceuticals and other biologically acitve compounds. *J. Appl. Phycol.*, 7:3–15, 1995.

[8] T.R. Sommer, W.T. Potts, and N.M Morrissy. Recent progress in the use of processed microalgae in aquaculture. *Hydrobiologia*, 204:435–443, 1990.

[9] O. Ciferri. Spirulina, the edible microorganism. *Microbiol. Rev.*, 47(4):551–578, 1983.

[10] E.W. Becker. *Microalgae; biotechnology and microbiology.* Cambridge Universtiy Press, Cambridge, 1994.

[11] G. S. Jensen, D.I. Ginsbergh, and M.S. Drapeau. Blue-green algae as an immuno-enhancer and biomodulator. *J. Am. Nutraceutical Assoc.*, 3:24–30, 2001.

[12] P. Spolaore, C. Joannis-Cassan, E. Duran, and A. Isambert. Review: commerical applications of microalgae. *J. Biosci. Bioeng.*, 101(2):87–96, 2006.

[13] P. Atanasov and E. Wilkins. Biosensors for continuous monitoring. *Biotechnol. Bioengin.*, 43:262–266, 1994.

[14] G. Janelt, N. Gerbsch, and R. Buchholz. A novel fiber optic probe for on-line monitoring of biomass concentrations. *Bioprocess. Biosyst. Eng.*, 22:275–279, 2000.

[15] C. Bittner, G. Whhnert, and T. Scheper. In situ microscopy for on-line determination of biomass. *Biotechnol. Bioeng.*, 60(1):24–35, 1998.

[16] P. Wu, S.S. Ozturk, J.D. Blackie, J.C. Thrift, C. Figueroa, and D. Naveh. Evaluation and applications of optical cell density probes in mammalian cell bioreacotrs. *Biotechnol. Bioeng.*, 45:495–502, 1995.

[17] V.P. Dick. Applicability limits of beer's law for dispersion media with a high concentration of particles. *Appl. Opt.*, 37(21):4998–5004, 1998.

[18] G.C. Govindjee. Viewpoint: sixty-three years since kautsky: chlorophyll a fluorescence. *Aust. J. Plant Physiol.*, 22:131–160, 1995.

[19] K. Maxwell and G.N. Johnson. Chlorophyll fluorescence - a practical guide. *J. Exp. Botany*, 51(345):659–668, 2000.

[20] N.R. Murty and E. Rabinowitch. Fluorescence decay studies of chlorophyll a in vivo. *Biophys. J.*, 5:655–661, 1965.

[21] J.C. Goedheer. Fluorescence in relation to photosynthesis. *Plant Physiol.*, 23:87–112, 1972.

[22] S.S. Brody. Fluorescence lifetime, yield, energy transfer, and spectrum in photosynthesis, 1950-1960. *Photosyn. Res.*, 73:127–132, 2002.

[23] D.F. Millie, O.M.E. Scjofield, G.J. Kirkpatrick, G. Johnsen, and T.J. Evens. Using absorbance and fluorescence spectra to discriminate microalgae. *Eur. J. Phycol.*, 37:313–322, 2002.

[24] J.-L. Mouget and G. Tremblin. Suitability of the fluorescence monitioring system for measurement of photosynthetic characteristics in algae. *Aquat. Bot.*, 74:219–231, 2002.

[25] S.P Srinivas and R. Mutharasan. Inner filter effects and their interferences in the interpretation of culture flourescence. *Biotechnol. Bioeng.*, 30:769–774, 1987.

[26] W.B. Armiger, J.F. Forro, L.M. Montalvo, and J.F. Lee. The interpretation of on.line process measurements of intracellular nadh in fermentation processes. *Chem. Eng. Commun*, 45:197–206, 1986.

[27] W. Beyeler, A. Einsele, and Armin Fiechter. On-line measurements of culture fluorecence: method and application. *European J. Appl. Microbiol. Biotechnol.*, 13:10–14, 1981.

[28] A. Ritzka, P. Sosnitza, R. Ulber, and T. Scheper. Fermentation monitoring and process control. *Curr. Opin. Biotechnol.*, 8:160–164, 1997.

[29] D.A. Boas, M.A. O'Leary, B. Chance, and A.G Yodh. Scattering of diffuse photon density waves by spherical inhomogeneities within turbid media: Analytic solution and applications. *Proc. Natl. Acad. Sci. USA*, 91:4887–4891, 1994.

[30] O. Reich, H.-G. Löhmannsröben, and F. Schael. Optical sensing with photon density waves: investigations of model media. *Phys. Chem. Chem. Phys*, 5:5182 – 5187, 2003.

[31] D.A. Boas, M.A. O'Leary, B. Chance, and A.G. Yodh. Scattering and wavelength transduction of diffuse photon density waves. *Phys. Rev.*, 47:2999–3002, 1993.

[32] J.P Vanhouton, D.A Benaron, S Spilman, and D.K. Stevenson. Imaging brain injuries using time-resolved near-infrared light scanning. *Pediatr. Res.*, 39(470-476), 1996.

[33] J.B. Fishkin, O. Coquoz, E.R. Anderson, M. Brenner, and B.J Tromberg. Frequency domain photon migration measurements of normal and maligannt tissue optical properties in a human subject. *Appl. Opt.*, 36:10–20, 1997.

[34] K.E. Apt and P.W. Behrens. Commercial developments in microalgal biotechnology. *J. Phycol.*, 35:215–226, 1999.

[35] Jr. F.B. Metting. Biodeversity and application of microalgae. *J. Ind. Microbiol.*, 17:477–489, 1996.

[36] S.M. Renaud, D.L. Perry, Loung-Van, Thinh, C. Kuo, A. Padovan, and N. Sammy. Effect of light intensity on the proximate biochemical and fatty acid composition of isochrysis sp. and nannochloropsis oculata for usse in tropical aquaculture. *J. Appl. Phycol.*, 3:43–53, 1991.

[37] M.R. Brown, S.W. Jeffrey, J.K Volkman, and G.A. Dunstan. Nutritional properties of microalgae for mariculture. *Aquaculture*, 151:315–331, 1997.

[38] M.R. Brown, M. Mular, I. Miller, C. Farmer, and C. Trenerry. The vitamin content of microalgae used in aquaculture. *J. Phycol.*, 11:247–255, 1999.

[39] V. Oerdoeg, W.A. Stirk, R. Lenobel, M. Bancirova, J. van Staden, J. Szigeti, and L. Nemeth. Screening microalgae for some prtentially useful agricultural and pharmaceutical secondary metabolites. *J. Appl. Phycol.*, 16:309–314, 2004.

[40] W.H. Gerwick, M.A. Roberts, P.J. Proteau, and J.-L. Chen. Screening cultured marine microalgae for anticancer-type activity. *J. Appl. Phycol.*, 6:143–149, 1994.

[41] A. Moore. Blooming prospects? *European Molecular Biology Organization Reports*, 2(6):462 – 464, 2001.

[42] M M. Rebolloso Fuentes, G.G Acien Fernandez, J.A. Sanchez Perez, and J.L Guil Guerrero. Biomass nutrient profiles of the microalgae nannochloropsis. *J. Agr. Food Chem.*, 49:2966–2972, 2001.

[43] J.R Benemann, D.M Tillett, and J.C Weissman. Microalgae biotechnology. *Trends Biotechnol.*, 5:47–53, 1987.

[44] Z. Cohen. *Products from microalgae.* Handbook of microalgal massculture. Blackwell Science Ltd., Williston, Vermont, 1999.

[45] O.M. Skulberg. Microalgae as source of bioactive molecules - experience from cyanophyte research. *J. Appl. Phycol.*, 12:341–348, 2000.

[46] D.O. Hall and K.K. Rao. *Photosynthesis.* Cambridge University Press, Cambridge, sixth edition, 1999.

[47] D.P. Maxwell, S. Falk, C.G. Trick, and N.P.A. Hunter. Growth at low temperature mimics high-light acclimation in chlorella vulgaris. *Plant Physiol.*, 150(2):535–543, 1994.

[48] T.M. Kana amd R.J Geider and C. Critchley. Regulation of photosynthetic pigments in micro-algae by multiple environmental factors: a dynamic balance hypothesis. *New Phytol.*, 137(4):629–638, 1997.

[49] G.S. Omenn, G.E. Goodman, M. D. Thornquist, J. Balmes, M.R. Cullen, A. Glass, J.P. Keogh, F.L. Meyskens, B. Valanis, J.H. Williams, S. Barnhart, and S. Hammar. Effects of a combination of beta carotene and vitamin a on lung cancer and cardiovascular disease. *N. Engl. J. Med.*, 334(18):1150–1155, 1996.

[50] C. van den Hoekand D.G. Mann and H.M Jahns. *Algae: an introduction to phycology.* Cambridge University Press, Cambridge, 1995.

[51] G.E. Fogg and B. Thake. *Algal cultures and phytoplankton ecology.* University of Wisconson Press, Madison, Wisconson, 1987.

[52] M. Yunus, U. Pathre, and P. Mohanty. *Probing photosynthesis mechanisms, regualtion and adaption.* CRC Press, Boca Raton, 2000.

[53] M.T. Madigan, J.M Martinko, and J. Parker. *Biology of microorganisms.* Prentice Hall International, Inc., New York, eighth edition, 1997.

[54] W. Larcher. *Physiological plant ecology.* Springer, New York, 3. edition, 1995.

[55] A.A. Benson and M. Calvin. Carbon dioxide fixation by green plants. *Ann. Rev. Plant Physiol.*, 1:25–40, 1950.

[56] A.S. Raghavendra. *Photosynthesis: A comprehensive treatise.* Cambridge University Press, Cambridge, 1998.

[57] M. Richter, W. Ruehle, and A. Wild. Studies on the mechanism of photosystem ii photoinhibition ii. the involvement of toxic oxygen species. *Photosyn. Res.*, 24(3):237–243, 1990.

[58] F.C. Rubio, F.G. Camacho, J.M.F. Sevilla, Y. Chisti, and E.M. Grima. A mechanistic model of photosynthesis in microalgae. *Biotechnol. Bioeng.*, 81(4):459–473, 2003.

[59] J.C. Ogbanna and H. Tanaka. Light requirement and photosynthetic cell cultivation - development of processes for efficient light utilization in photobioreactors. *J. Appl. Phycol.*, 12:207–218, 2000.

[60] M. Morita, Y. Wantanabe, and H. Saiki. Investigation of photobioreactor design for enhancing the photosynthetic productivity of microalgae. *Biotechnol. Bioeng.*, 69(6):693–698, 2000.

[61] J. Ogbonna and H. Tanaka. Industrial-size photobioreactors. *Chemtech*, 27(7):43 – 49, July 1997.

[62] R. Ulber, S. Beutel, and J.-G. Frerichs. Optical sensor systems for bioprocess monitoring. *Anal. Bioanal. Chem.*, 376:342 – 348, 2003.

[63] F. Chen. High cell density culture of microalgae in heterotrophic growth. *Trends Biotechnol.*, 14:421–426, 1996.

[64] J.C. Weissman, R.P. Goebel, and J.R Benemann. Photobioreactor design: mixing, carbon utilization, and oxygen accumulation. *Biotechnol. Bioeng.*, 31:336–344, 1988.

[65] A. Richmond. *Spirulina*, pages 85–121. Cambridge University Press, 1988.

[66] T. Sato, S. Usui, Y. Tsuchiya, and Y. Kondo. Invention of outdoor closed type photobioreactor for microalgae. *Energy Convers. Manage.*, 47(6):791–799, 2006.

[67] M. Olaizola. Commercial development of microalgal biotechnology: from the test tube to the marketplace. *Biomol. Eng.*, 20:459–466, 2003.

[68] Y. Elbahoul, K. Frey, J. Sanders, and A. Steinbuechtel. Protamylasse, a residual compound of industrial starch production, provides a suitable medium of large-scale cyanophycin production. *Appl. Environ. Microbiol.*, 71(12):7759–7767, 2005.

[69] C.F. Bohren and D.R. Huffman. *Absorption and scattering of light by small particles*. John Wiley and Sons, New York, 1983.

[70] S. Fantini, M.A. Francheschini, J.B Fishkin, B. Barbieri, and E. Gratton. Quantitative determination of the absorption spectra of chromophores in strongly scattering media: a light emitting diode based technique. *Appl. Opt.*, 33(22):5204–5213, 1994.

[71] J. Fishkin, S. Fantini, M. van de Ven, and E. Gratton. Gigahertz photon density waves in a turbid medium: theory and experiments. *Phys. Rev. E*, 53(3):2307 – 2319, March 1996.

[72] D. V. O'Connor and D. Phillips. *Time-correlated single photon counting.* Academic Press Inc. Ltd. London, 1984.

[73] H. Kautsky and A. Hirsch. Neue versuche zur kohlensäureassimilation. *Naturwissenschaften*, 19:964–989, 1931.

[74] O. Holub, M.J. Seufferheld, C Gohlke, Govindjee, and R.M. Clegg. Fluorescence lifetime imaging (fli) in real-time - a new technique in photosynthesis research. *Photosynthetica*, 34(4):581–599, 2000.

[75] O. Holub. *Fluorescence lifetime imaging at video rate: a new technique in photosynthesis research.* PhD thesis, Technischen Universität Berlin, 2003.

[76] W. Becker, A. Bergmann, G. Biscotti, and A. Rueck. Advanced time-correlated single photon counting technique for spectroscopy and imaging in biomedical systems. volume 5340 of *Proc. SPIE*, 2004.

[77] B.J Berne and R. Pecora. *Dynamic light scattering.* Dover Publications, Inc., Mineola, New York, 2000.

[78] H. C. van de Hulst. *Light scattering by small particles.* Dover Publications, Inc., New York, 1981.

[79] M. Kerker. *The scattering of light and other electromagnetic radiation.* Academic Press, New York, 1969.

[80] O. Reich. *Photonendichtewellenspektroskopie mit intensitätsmodulierten Diodenlasern.* PhD thesis, Universität Potsdam, März 2005.

[81] G. Mie. Beiträge zur optik trüber medien, speziell kolloidaler metallösungen. *Ann. Phys.*, 25:377–445, 1908.

[82] L.B. Aberle, P. Hülstede, S. Wiegand, W. Schröer, and W. Staude. Effective supression of multiply scattered light in static and dynamic light scattering. *Appl. Opt.*, 37(27):6511–6524, 1998.

[83] C. Urban and P. Schurtenberger. Characterization of turbid colliodal suspensions using light scattering techniques combined with cross-correlation methods. *J. Colloid Interface Sci.*, 207:150 – 158, 1998.

[84] C. Urban. *Development of fiber optic based dynamic light scattering for a characterization of turbid suspensions.* PhD thesis, Swiss Federal Institute of Technology Zurich, 1999.

[85] K. Schaetzel. Suppression of multiple scattering by photon cross-correlation techniques. *J. Mod. Opt.*, 38:1849–1865, 1991.

[86] B.J. Tromberg, L.O. Svaasand, T.Tsay, and R.C. Haskell. Properties of photon density waves in multiple scattering media. *Appl. Opt.*, 32:607–615, 1993.

[87] S. Fantini, M.A. Franceschini, and E. Gratton. Seim-infinite-geometry bounrdy problem for light migration in highly scattering media: a frequency-domain study in the diffusion approximation. *J. Opt. Soc. Am. B*, 11(10):2128–2138, 1994.

[88] S. Chandrasekhar. *Radiative transport.* Dover Publishers, New York, 1960.

[89] R. Aronson. Subcritical problems in spherical geometries. *Nucl. Sci. Eng.*, 86:436–449, 1984.

[90] S. Fantini, M.A. Franceschini, and E. Gratton. Effective source term in the diffusion equatrion for photon transport in turbid media. *Appl. Opt.*, 36(1):156–163, 1997.

[91] K.M Case and P.F. Zweifel. *Linear transport theory.* Addison-Wesley, Reading, MA, 1967.

[92] S. Engelhard. *Optische Vervahren zur Qualitätskontrolle von Bier und zur Zellzahlbestimmung in S. cerevisiae Kultivierungen.* PhD thesis, Universität Potsdam, März 2003.

[93] A. Periasamy, P. Wodnicki, X. Wang, S. Kwon, G. Gordon, and B. Herman. Time-resolved fluorescence lifetime imaging microscopy using a picosecond pulsed tunable dye laser system. *Rev. Sci. Instrum.*, 67(10):3722 – 3731, Oct. 1996.

[94] J.R. Lackowicz. *Topics in fluorescence spectroscopy*, volume 1 of *Techniques.* Plenum Press, New York, 1991.

[95] T.M. Nordlund and W.H. Knox. Lifetime of fluorescence from light harvesting chlorophyll a/b proteins. *Biophys. J.*, 36:193–201, 1981.

[96] F. Schael, O. Reich, and S. Engelhard. Spectroscopy in heterogeneous media and applications for bioprocess and environmental monitoring. *Int. J. Photoenergy*, 4:21 – 26, 2002.

[97] H.P.A.v.d. Boom, W. Li, and G.D. Khoe. Cwdm technology for polymer optical fiber networks. *IEEE J. Quantum Electron.*, 17(3):461–470, 2001.

[98] Hamamatsu Photonics K.K. *Characteristics and use of Si APD*, 1995.

[99] C. Butterwick, S.I Heaney, and J.F. Talling. A comparison of eight methods for estimating the biomass and growth of planktonic algae. *Br. Phycol. J.*, 17:69–79, 1982.

[100] W. Inskeep and P. Bloom. Extinction coefficients of chlorophyll a and b in n,n-dimethylformamide and 80 percent acetone. *Plant Physiol.*, 77:483–485, 1985.

[101] G.H Krause and E. Wiess. Chlorophyll fluorescence as a tool in plant physiology ii. interpretation of fluorescence signals. *Photosyn. Res.*, 5:139–157, 1984.

[102] J.F. Allen and J. Forsberg. Molecular recognition in thylakoid structure and function. *Trends Plant Sci.*, 6(7):317–326, 2001.

[103] P. Falkowski and D.A. Kiefer. Chlorophyll a fluorescence in phytoplankton: relationship to photosynthesis and biomass. *J. Plankton Res.*, 7(5):715–731, 1985.

[104] T. Mar, Govindjee, G.S. Singhal, and H. Merkelo. Lifetime of the excited state in vivo i. *Biophys. J.*, 12:797–808, 1972.

[105] G.H Krause and E. Weis. Chlorophyll fluorescence and photosynthesis: the basics. *Physiol. Plant. Mol. Biol.*, 42(313-349), 1991.

[106] Z.G. Cerovica, Y. Goulasa, M. Gorbunova, J.M. Briantaisb, L. Camenena, and I. Moyaa. Fluorosensing of water stress in plants: Diurnal changes of the mean lifetime and yield of chlorophyll fluorescence, measured simultaneously and at distance with a tau-lidar and a modified pam-fluorimeter, in maize, sugar beet, and kalanchoe. *Remote Sens. Environ.*, 58:311–321, 1996.

[107] G. Cox and A. Salih. Fluorescence lifetime of symbionts and fluorescent proteins in reef corals. volume 5700 of *Multiphoton microscopy in the Biomedical Sciences V*, 2005.

[108] J.M. Briantais, J. Dacosta, Y. Goulas, J.-M. Ducruet, and I. Moya. Heat stress induces in leaves an increase of the minimum level of chlorophyll fluorescence, fo: A time-resolved analysis. *Photosyn. Res.*, 48:189–196, 1996.

[109] L.N.M. Duysens and H.E. Sweers. In "studies on microalgae and photosynthetic bacteria". *Janan Soc Plant Physiol*, pages 353–372, 1963.

[110] A. Mueller, R. Lumry, and M.S. Walker. Light-intensity dependence of the in vivo fluorescence lifetime of chlorophyll. *Photochem. Photobiol.*, 9:113–126, 1969.

[111] K.K. Karukstis and K. Sauer. Fluorescence decay kinetics of chlorophyll in photosynthetic membranes. *J. Cell. Biochem.*, 23:131–158, 1983.

[112] A.B. Rubin, L.E Minchenkova, A.A. Krasnovsky, and L.A. Tummerman. Investigation of average protochlorophyll fluorescence continuance in the process of etiolated leaves greening. *Biofizika*, 7:571–577, 1962.

[113] J.E. Keffer and G.T Kleinheinz. Use of chlorella vulgaris for co2 mitigation in a photobioreactor. *J. Ind. Microbiol. Biotechnol.*, 29:275–280, 2002.

[114] F. Chen and M.R. Johns. A strategy for high cell density culture of heterotrophic microalgae with inhibitory substrates. *J. Appl. Phycol.*, 7:43–46, 1995.

[115] G. M. Hale and M. R. Querry. Optical constants of water in the 200 - nm to 200 - μm wavelength region. *Appl. Opt.*, 12(3):555 – 563, March 1973.

[116] U.J. Netz, A.H Hielscher, A.K. Scheel, and J. Beuthan. Experimental results for propagation of diffuse photon-density waves up to 1 ghz in a tissue like medium containing an absorbing edge. *Laser Physics*, 16(5):765–773, 2006.

[117] A Morel and S. Maritorena. Bio-optical properties of oceanic waters: A reappraisal. *J. Geophys. Res.*, 106:7163–7180, 2001.

[118] E. Aas. *Some aspects of light scattering by marine particles.* PhD thesis, University of Bergen, 1984.

[119] E. Aas. Refractive index of phytoplankton derived from its metabolite composition. *J. Plankton Res.*, 18(12):2223–2249, 1996.

[120] H. Claustre and J. Gostan. Adaptation of biochemical composition and cell cize to irradiance in two microalgae: possible ecological implications. *Mar. Ecol. Prog. Ser.*, 40:167–174, 1987.

[121] M. Hein, M. F. Pedersen, and K. Sand-Jensen. Size dependent nitrogen uptake in micro- and macroalgae. *Mar. Ecol. Prog. Ser.*, 118:247–253, 1995.

[122] T. A. C. Flipsen, A. J. Pennings, and G. Hadziioannou. Polymer optical fiber with high thermal stability and low optical losses based on novel densely crosslinked polycarbosiloxanes. *J. Appl. Poly. Sci.*, 67(13):2223–2230, 1998.

[123] http://www.newport.com/tutorial/139687/1033/catalog.aspx. Accessed 14 June 2007.